

# Estimating Heterogeneous Treatment Effects for Spatio-Temporal Causal Inference\*

Lingxiao Zhou<sup>†</sup> Kosuke Imai<sup>‡</sup> Jason Lyall<sup>§</sup> Georgia Papadogeorgou<sup>¶</sup>

November 3, 2025

## Abstract

Scholars from diverse fields increasingly rely on high-frequency spatio-temporal data. Yet, causal inference with these data remains challenging due to spatial spillover and temporal carryover effects. We develop methods to estimate heterogeneous treatment effects by allowing for arbitrary spatial and temporal causal dependencies. We focus on common settings where the treatment and outcomes are time-varying spatial point patterns and where moderators are either spatial or spatio-temporal variables. We define causal estimands based on stochastic interventions where researchers specify counterfactual distributions of treatment events. We propose the Hájek-type estimator of the conditional average treatment effect (CATE) as a function of spatio-temporal moderator variables, and establish its asymptotic normality as the number of time periods increases. We then introduce a statistical test of no heterogeneous treatment effects. Through simulations, we evaluate the finite-sample performance of the proposed CATE estimator and its inferential properties. Our motivating application examines the heterogeneous effects of US airstrikes on insurgent violence in Iraq. Drawing on declassified spatio-temporal data, we examine how prior aid distributions moderate airstrike effects. Contrary to expectations from counterinsurgency theories, we find that prior aid distribution, along with greater amounts of aid per capita, is associated with increased insurgent attacks following airstrikes.

*Keywords:* causal inference, point process, spatial-temporal data, stochastic intervention, unstructured interference

---

\*We thank the anonymous reviewer from the Magaro Peer Pre-Review Program at the Institute for Quantitative Social Science, Harvard University, for their valuable feedback. This material is based upon work partially supported by the National Science Foundation under Grant No. 2124124, 2124463, and 2124323.

<sup>†</sup>Department of Statistics, University of Florida

<sup>‡</sup>Department of Government and Department of Statistics, Harvard University

<sup>§</sup>Department of Government, Dartmouth College

<sup>¶</sup>Department of Statistics, University of Florida

# 1 Introduction

Estimation of causal effects based on spatio-temporal data is important in many disciplines, including public health, ecology, environment, and social sciences (e.g., [Meierrieks and Gries, 2013](#); [Brunello et al., 2016](#); [Bind, 2019](#); [Christiansen et al., 2022](#); [Wang et al., 2022](#)). Recent examples include the effects of air pollution on child cognitive development ([Wodtke et al., 2022](#)), and the use of Call Detail Records to track population mobility during war ([Christia et al., 2022](#)).

Yet valid causal inference with spatio-temporal data remains a challenge due to the potential existence of spatial spillover and temporal carryover effects. Indeed, much of the existing causal inference literature has not directly dealt with spatio-temporal data. In particular, prior studies on estimating heterogeneous treatment effects—the focus of this paper—have primarily considered settings with i.i.d. observations (e.g., [Imai and Ratkovic, 2013](#); [Wager and Athey, 2018](#); [Fan et al., 2022](#); [Kennedy, 2023](#)). While a few methods account for spatial spillover effects (but not temporal carryover effects), they typically impose a specific interference structure that may not hold in practice (e.g., [Giffin et al., 2023](#); [Tchetgen Tchetgen et al., 2021](#)).

We develop a statistical methodology for analyzing treatment effect heterogeneity in spatio-temporal data with arbitrary spillover and carryover effects. In our setting, the treatment and outcome variables are time-varying spatial point patterns, while the moderator of interest is either spatial or spatio-temporal variables. We begin by defining the conditional average treatment effect (CATE) in the presence of arbitrary spillover and carryover effects. Our definition employs a stochastic intervention, which specifies a counterfactual probability distribution of treatment assignment across space and time. This intervention can be specified to alter the spatial and temporal distribution of treatment assignment, its

overall intensity, and other features. It can also be adaptive and depend on the values of past variables, including intermediate variables affected by previous treatments.

We propose a two-step estimation procedure. We first use the stabilized IPW weights to estimate the treatment effect for each time period and in each small geographical area, which we refer to as “pixel.” A pixel can be any geographical unit of choice, including a fine spatial grid cell and an administrative unit. In the second step, we characterize treatment effect heterogeneity by fitting pixel-on-pixel regression of the effect estimate on a low-dimensional function of moderators for each time period, and then aggregating these regression results across time.

Leveraging the martingale theory, we establish that the proposed CATE estimator based on stabilized weights is consistent and asymptotically normal, provided that the propensity score model is correctly specified. Although our asymptotic variance is not identifiable, we derive a variance upper bound and propose a consistent estimator. Our simulation studies indicate that the empirical coverage of the resulting confidence intervals based on the variance bound is close to the nominal level, even in complex data-generating scenarios. Furthermore, we develop an asymptotically valid statistical test of no heterogeneous treatment effect. Rejection of this null hypothesis implies the existence of heterogeneous treatment effects as a function of the moderator. The proposed statistical tests contrast with the existing tests that are only applicable to i.i.d. data and do not allow for spatial or temporal interference (e.g., [Crump et al., 2008](#); [Sant’Anna, 2021](#)).

Lastly, we show that the asymptotic variance of the proposed estimator with stabilized IPW weights is no greater when the propensity score is estimated than when it is known. A similar result has been obtained for the standard IPW estimator in the i.i.d. ([Hirano et al., 2003](#)) and spatio-temporal settings ([Papadogeorgou et al., 2022](#)). We generalize these

results to the stabilized IPW estimator in both i.i.d. and spatio-temporal settings.

Our work builds on the spatio-temporal causal inference framework of [Papadogeorgou et al. \(2022\)](#), but makes a number of methodological contributions. First, we propose methodology for estimating the CATE in complex spatio-temporal settings. While doing so, we address theoretical complications that arise from the pixel-on-pixel regression within the martingale theory framework. In particular, we find that a pixel-on-pixel regression that pools data across all time periods would lead to invalid asymptotic results except under strong assumptions on correct model specification and constant effect heterogeneity across time. We address this problem by using time-specific regressions, and show that this procedure leads to valid estimation and inference.

Second, while the use of stabilized weights substantially improves the efficiency of the estimators in the spatio-temporal settings, the existing asymptotic results are obtained for the standard IPW estimator and do not apply to the stabilized IPW estimator. Thus, our theoretical results for stabilized IPW estimators are new in both i.i.d. and spatio-temporal settings. Lastly, we introduce a new variance bound estimator that is consistent and has a much improved finite-sample performance. These methodological and theoretical advancements are essential in developing reliable causal inference methods for settings with complex dependencies and high-dimensionality.

Our application comes from the Iraq War (2003–2011), where the United States (US) used both economic aid and airstrikes as part of the “hearts and minds” counterinsurgency campaign. Drawing on newly declassified geolocated data, we examine how prior aid programs moderated the effects of US airstrikes on insurgent violence. We find that districts receiving aid tend to experience increased insurgent attacks following intensified airstrikes, and these effects grow as aid per capita rises, even when the amounts are relatively small.

Our findings challenge the prevailing expectations that economic aid and airstrikes work together to reduce short-term insurgent attacks.

**Related Literature.** The literature on spatio-temporal causal inference remains sparse due to the challenges of complex confounding and interference across both space and time (Wang, 2021). Only a few studies consider causal heterogeneity in such settings, and address different aspects of the problem. For example, Christiansen et al. (2022) propose a latent spatial model to adjust for confounders that vary across either time or space, but not both, while assuming a specific graphical structure relating treatment, outcome, and latent confounders. Zhang and Ning (2023) introduce a spatially interrupted time-series design to estimate heterogeneous treatment effects of a fixed intervention during a specific period, while Jerzak et al. (2023) explore heterogeneity by incorporating image-based moderators, such as satellite imagery, to capture geographic variation in randomized controlled trials. In contrast, we build on the spatio-temporal causal inference framework of Papadogeorgou et al. (2022), and develop a methodology to estimate heterogeneous treatment effects while accounting for arbitrary spatial spillover and temporal carryover effects. In addition, under our framework, moderators can be either spatial or spatio-temporal variables.

A greater number of studies focus on spatial causal inference problems but without the temporal dimension. These works rely on design-based inference with randomized experiments (e.g., Wang et al., 2020) or impose structures on the patterns of spatial spillover effects (e.g., Bardaka et al., 2018; Kolak and Anselin, 2020; Zigler et al., 2013; Papadogeorgou et al., 2019; Barkley et al., 2020; Tchetgen Tchetgen et al., 2021; Giffin et al., 2023). Unlike these studies, we leverage the temporal dimension to avoid structural assumptions about spillover and carryover effects under both experimental and observational settings.

Our work also contributes to the broader causal inference literature on CATE estimation

by considering spatio-temporal settings. Much of the existing literature on CATE has focused on i.i.d. settings without interference (e.g., [Imai and Ratkovic, 2013](#); [Abrevaya et al., 2015](#); [Athey et al., 2019](#); [Hahn et al., 2020](#); [Fan et al., 2022](#)). Many existing approaches, such as the DR-learner ([Kennedy, 2023](#)) and FW-learner ([Yang et al., 2023](#)), employ a two-step estimation procedure using pseudo-outcomes. However, these methods assume i.i.d. data with unit-specific covariates. Existing approaches to CATE estimation for spatial data typically lack a temporal dimension, assume finitely many spatial units, and rely on structural assumptions about spillover effects, such as clustered network interference (e.g., [Credit and Lehnert, 2023](#); [Bargagli-Stoffi et al., 2020](#)).

The remainder of this paper is organized as follows. In [Section 2](#), after introducing our causal estimand, we present our assumptions, propose the new CATE estimator, and derive the theoretical results. In [Section 3](#), we evaluate the empirical performance of the proposed estimator through simulation studies. [Section 4](#) introduces our empirical analysis and presents the main findings. Finally, we conclude with a discussion of future research directions in [Section 5](#).

## 2 The Proposed Methodology

In this section, we describe the proposed methodology for estimating the CATE based on spatio-temporal data. We begin by defining the causal estimands and then introduce the new CATE estimator. Finally, we derive the asymptotic properties of the proposed estimator, develop an inferential procedure, and formalize a test for the null hypothesis of no heterogeneity.

## 2.1 Setup

We adopt the framework of [Papadogeorgou et al. \(2022\)](#) for causal inference with spatio-temporal treatment and outcome processes. Suppose that we observe the data over  $T$  discrete time periods,  $t \in \mathcal{T} = \{1, 2, \dots, T\}$ . Let  $\Omega$  denote the entire space under consideration that contains a potentially infinite number of possible treatment and outcome locations. We use  $W_t(s) \in \{1, 0\}$  to indicate whether or not location  $s \in \Omega$  receives the treatment at time  $t$ , whereas  $W_t = W_t(\Omega) \in \mathcal{W}$  denotes the treatment point pattern at time  $t$  with  $\mathcal{W}$  representing the set of all possible point patterns. For simplicity, this set is assumed to be identical across time periods. In addition, we assume that the number of treated locations at each time period is finite. We use  $\overline{\mathbf{W}}_t = (W_1, W_2, \dots, W_t)$  to denote the collection of treatment history up to time  $t$ , and  $\overline{\mathbf{w}}_t = (w_1, w_2, \dots, w_t)$  for its realization.

Let  $Y_t(\overline{\mathbf{w}}_t)$  represent the potential outcome for the space  $\Omega$  at time  $t \in \mathcal{T}$  for any given treatment sequence  $\overline{\mathbf{w}}_t \in \mathcal{W}^t = \mathcal{W} \times \dots \times \mathcal{W}$ . We do not restrict the form of  $Y_t(\overline{\mathbf{w}}_t)$  so that it can depend on the entire treatment path  $\overline{\mathbf{w}}_t$  in an arbitrary way. This allows for unrestricted spatial spillover effects based on all treated locations at time  $t$  as well as temporal carryover effects of past treatment patterns. We only observe the outcome point pattern at time  $t$  corresponding to the observed treatment sequence, and thus the observed outcome point pattern is given by  $Y_t = Y_t(\overline{\mathbf{W}}_t)$ . We use  $\overline{\mathbf{Y}}_t = \{Y_1, Y_2, \dots, Y_t\}$  to represent the collection of observed outcomes up to and including time period  $t$ . Lastly, we use  $\overline{\mathcal{Y}}_T = \{Y_t(\overline{\mathbf{w}}_t) : \overline{\mathbf{w}}_t \in \mathcal{W}^t, t \in \mathcal{T}\}$  to denote the collection of potential outcomes for all treatment sequences and all time periods.

Furthermore,  $\mathbf{X}_t$  denotes the set of possibly time-varying confounders that are realized prior to  $W_t$  but after  $W_{t-1}$ , where  $\overline{\mathbf{X}}_t = (\mathbf{X}_1, \mathbf{X}_2, \dots, \mathbf{X}_t)$  denotes the collection of observed covariates over the time periods  $1, 2, \dots, t$ . We use  $\overline{\mathcal{X}}_T = \{\mathbf{X}_t(\overline{\mathbf{w}}_{t-1}) : \overline{\mathbf{w}}_{t-1} \in \mathcal{W}^{t-1}, t \in \mathcal{T}\}$

to denote the set of potential values for the covariates under all treatment sequences and all time periods. Then, the observed covariates are given by  $\mathbf{X}_t = \mathbf{X}_t(\overline{\mathbf{W}}_{t-1})$ .

Finally, we use  $\overline{H}_t = \{\overline{\mathbf{W}}_t, \overline{\mathbf{Y}}_t, \overline{\mathbf{X}}_{t+1}\}$  to present the observed history preceding the treatment at time  $t + 1$ . Since our statistical inference is based on a single time series, the randomness comes only from the treatment assignment  $W_t$  given the complete history that includes all factual and counterfactual values  $\overline{H}_{t-1}^* = \{\overline{\mathbf{W}}_t, \overline{\mathcal{Y}}_T, \overline{\mathcal{X}}_T\}$ .

## 2.2 Causal estimands

Our goal is to investigate treatment effect heterogeneity under stochastic interventions. We consider a stochastic intervention  $F_h$  that defines a counterfactual distribution over the treatment point pattern. To begin, we consider stochastic interventions that are fixed and do not depend on  $\mathbf{X}_t$  and  $Y_t$ , both of which can be affected by the treatment. In Section 2.7, we extend the proposed framework to adaptive interventions that may depend on the observed history. For concreteness, we consider the Poisson process, which is specified by its intensity function  $h : \Omega \rightarrow [0, \infty)$ , though our methodology can accommodate alternative stochastic intervention distributions.

We study how the causal effects of a change in the stochastic intervention vary across regions based on their characteristics, which may be spatial or spatio-temporal variables. These characteristics are potential moderators for the treatment effect under study. Formally, we partition the space  $\Omega$  into a total of  $p$  regions or “pixels” in  $\mathcal{S} = \{S_1, S_2, \dots, S_p\}$ , where  $\Omega = \bigcup_{i=1}^p S_i$  with  $S_i \cap S_{i'} = \emptyset$  for  $i \neq i'$ . For each pixel, we measure the moderator using either its original value (if constant within the pixel) or a summary statistic within the pixel (e.g., mean). We use  $\mathbf{R}_{it} \in \mathcal{R}$  to denote the value of the potential moderator for pixel  $S_i$  at time  $t$  where  $\mathcal{R}$  is the support of the variable. The discretization of space for the moderator enables us to analyze effect heterogeneity at the pixel level without any

restrictions on the structure of spatial spillover or temporal carryover effects.

In our application, pixels are equally sized small geographical areas, while the moderator is the humanitarian aid provided during the previous month within the district to which each pixel belongs. The choice of pixel resolution should be guided by the data resolution and the variability of the moderator across space. Since our method does not capture intra-pixel heterogeneity, finer partitions may be needed if the treatment assignment or the effect modifiers vary substantially within pixels. If pixels are of unequal size, this effectively assigns equal weight to regions of different sizes when defining the estimand.

**Intervention over a single time period.** Let us define the expected number of outcome events within pixel  $S_i$  at time  $t$  under stochastic intervention  $F_h$  as:

$$N_{it}(F_h) = \int_{\mathcal{W}} N_{S_i}(Y_t(\overline{\mathbf{W}}_{t-1}, w_t)) dF_h(w_t)$$

where  $N_{S_i}(Y_t(\overline{\mathbf{W}}_{t-1}, w_t))$  is the number of outcome events that fall within pixel  $S_i$  at time  $t$  based on the treatment path  $(\overline{\mathbf{W}}_{t-1}, w_t)$ . Then, the treatment effect of  $F_{h'}$  versus  $F_{h''}$  for time period  $t$  and pixel  $S_i$  is defined as the contrast in the expected number of outcome events between the two stochastic intervention regimes:  $\tau_{it}(F_{h'}, F_{h''}) = N_{it}(F_{h''}) - N_{it}(F_{h'})$ .

We are interested in estimating how this pixel-level treatment effect varies as a function of the moderator  $\mathbf{R}_{it}$ . We define the conditional average treatment effect (CATE) at time  $t$  when the moderator takes a specific value  $\mathbf{r} \in \mathcal{R}$  as:

$$\tau_t(\mathbf{r}; F_{h'}, F_{h''}) = \frac{1}{\sum_{i=1}^p I(\mathbf{R}_{it} = \mathbf{r})} \sum_{i=1}^p \tau_{it}(F_{h'}, F_{h''}) I(\mathbf{R}_{it} = \mathbf{r}) \quad (1)$$

where  $I$  represents the indicator function. For notational simplicity, we instead write the CATE as  $\tau_{t,h',h''}(\mathbf{r})$ . In our application, if we use the receipt of aid in the previous month

as the dichotomous moderator, then  $\tau_{t,h',h''}(1)$  represents the average effect on the expected number of insurgent attacks for a district that received aid, when changing the distribution of airstrikes from  $F_{h'}$  to  $F_{h''}$ .

Since the moderator can take many values, we characterize the CATE by projecting the pixel-level treatment effect  $\tau_{t,h',h''}(\mathbf{r})$  onto a space of  $\mathbf{R}_{it}$  using an interpretable model  $\tau_{t,h',h''}^{\text{Proj.}}(\mathbf{r}; \boldsymbol{\beta}_t)$ , which is indexed by a low-dimensional vector  $\boldsymbol{\beta}_t$ . For example, one may choose a linear model with  $\mathbf{R}_{it}$  as predictors and  $\boldsymbol{\beta}_t$  as their coefficients (see [Kennedy et al., 2019](#); [van der Laan et al., 2011](#); [Ding et al., 2019](#), for similar estimands). Formally, we focus on the projection estimand defined as:

$$\tau_{t,h',h''}^{\text{Proj.}}(\mathbf{r}; \boldsymbol{\beta}_t^*) \quad \text{where} \quad \boldsymbol{\beta}_t^* = \arg \min_{\boldsymbol{\beta}_t} \sum_{i=1}^p \left[ \tau_{t,h',h''}(\mathbf{R}_{it}) - \tau_{t,h',h''}^{\text{Proj.}}(\mathbf{R}_{it}; \boldsymbol{\beta}_t) \right]^2.$$

This estimand represents the best approximation to the true CATE curve that can be achieved with the selected parametric model  $\tau_{t,h',h''}^{\text{Proj.}}(\mathbf{r}; \boldsymbol{\beta}_t)$ .

Finally, we average the time-specific projected CATEs over all time periods to define the following overall projected CATE:

$$\tau_{h',h''}^{\text{Proj.}}(\mathbf{r}; \boldsymbol{\beta}_1^*, \dots, \boldsymbol{\beta}_T^*) = \frac{1}{T} \sum_{t=1}^T \tau_{t,h',h''}^{\text{Proj.}}(\mathbf{r}; \boldsymbol{\beta}_t^*).$$

When the moderator takes a finite number of values,  $\tau_{t,h',h''}(\mathbf{r})$  defined in Equation (1) can be represented exactly based on a saturated parametric model, and the projection estimand coincides with the true CATE. For a continuous moderator, projecting this estimand onto a lower-dimensional space helps us understand how the CATE varies with the moderator. Our inferential target is  $\tau_{h',h''}^{\text{Proj.}}(\mathbf{r}; \boldsymbol{\beta}_1^*, \dots, \boldsymbol{\beta}_T^*)$ , which represents the projection of the CATE onto the working model class. Even if the working model is misspecified, our estimation

and inference are still valid with respect to this projection parameter.

**Intervention over multiple time periods.** We generalize our estimand to stochastic interventions defined over multiple consecutive time periods. Consider a stochastic intervention over  $M$  time periods, denoted by  $F_{\mathbf{h}} = F_{h_1} \times F_{h_2} \times \dots \times F_{h_M}$ , where the treatment is assigned according to  $F_{h_1}$  at time  $t$ ,  $F_{h_2}$  at time  $t - 1$ , and so on until time  $t - M + 1$ .

Formally, we define the expected number of outcome events in pixel  $S_i$  at time  $t$  under this multi-period stochastic intervention as follows:

$$N_{it}(F_{\mathbf{h}}) = \int_{\mathcal{W}^M} N_{S_i}(Y_t(\overline{\mathbf{W}}_{t-M}, w_{t-M+1}, \dots, w_t)) dF_{\mathbf{h}}(w_{t-M+1}, \dots, w_t). \quad (2)$$

As before, we define the CATE with respect to  $F_{\mathbf{h}'}$  and  $F_{\mathbf{h}''}$  for time  $t$  as

$$\tau_{t, \mathbf{h}', \mathbf{h}''}(\mathbf{r}) = \frac{1}{\sum_{i=1}^p I(\mathbf{R}_{i, t-M+1} = \mathbf{r})} \sum_{i=1}^p \tau_{it}(F_{\mathbf{h}'}, F_{\mathbf{h}''}) I(\mathbf{R}_{i, t-M+1} = \mathbf{r}),$$

where  $\tau_{it}(F_{\mathbf{h}'}, F_{\mathbf{h}''}) = N_{it}(F_{\mathbf{h}''}) - N_{it}(F_{\mathbf{h}'})$  is the pixel-specific effect and  $\mathbf{R}_{t-M+1}$  denotes the moderator that immediately precedes the intervention time periods and hence is a pretreatment variable, avoiding post-treatment bias.

Finally, the projection estimand for this multi-period case is defined as

$$\tau_{t, \mathbf{h}', \mathbf{h}''}^{\text{Proj.}}(\mathbf{R}_{i, t-M+1}; \boldsymbol{\beta}_t^*) \quad \text{where} \quad \boldsymbol{\beta}_t^* = \arg \min_{\boldsymbol{\beta}_t} \sum_{i=1}^p \left( \tau_{t, \mathbf{h}', \mathbf{h}''}(\mathbf{R}_{i, t-M+1}) - \tau_{t, \mathbf{h}', \mathbf{h}''}^{\text{Proj.}}(\mathbf{R}_{i, t-M+1}; \boldsymbol{\beta}_t) \right)^2.$$

Averaging this quantity over time, we have the overall CATE, which is defined as

$$\tau_{\mathbf{h}', \mathbf{h}''}^{\text{Proj.}}(\mathbf{r}; \boldsymbol{\beta}_M^*, \dots, \boldsymbol{\beta}_T^*) = \frac{1}{T - M + 1} \sum_{t=M}^T \tau_{t, \mathbf{h}', \mathbf{h}''}^{\text{Proj.}}(\mathbf{r}; \boldsymbol{\beta}_t^*).$$

**Working model.** When the moderator is continuous or takes a large number of distinct values, the working model  $\tau_{t,h',h''}^{\text{Proj.}}(\mathbf{r}; \boldsymbol{\beta}_t)$  can be viewed as an approximation to the true CATE curve. Since the working model does not have to be correctly specified, different model specifications can be chosen under different goals. Here, for simplicity and interpretability, we consider the following model for each time period:

$$\tau_{t,h',h''}^{\text{Proj.}}(\mathbf{r}; \boldsymbol{\beta}_t) = \sum_{l=1}^L \beta_{t,l} z_l(\mathbf{r}) = \mathbf{z}(\mathbf{r})^\top \boldsymbol{\beta}_t, \quad (3)$$

where  $\mathbf{z}(\mathbf{r}) = (z_1(\mathbf{r}), \dots, z_L(\mathbf{r}))^\top$  are, for example, the basis functions of splines.

Although we focus on a working model that is linear in the pre-specified  $z_l(\mathbf{r})$  functions, future work could consider semi-parametric models, such as series estimators discussed in [Kennedy \(2023\)](#). While these semi-parametric models are effective with independent and identically distributed data, extending them to spatio-temporal data is beyond the scope of this paper. In addition, determining the optimal number of bases in a series expansion is typically achieved through cross-validation, which is challenging in the spatio-temporal setting due to dependence across space and time. We leave these extensions to future work.

## 2.3 Assumptions

We require two assumptions about the treatment assignment mechanism. Here, we focus on the scenario, in which the intervention distribution is identical and independent over  $M$  time periods,  $F_{\mathbf{h}} = F_h \times \dots \times F_h$ , though it is straightforward to extend our theory to different and/or dependent intervention distributions across time periods (see [Section F](#)). Adaptive interventions that depend on the observed history are discussed in [Section 2.7](#).

**Assumption 1.**  $f(W_t \mid \overline{\mathbf{W}}_{t-1}, \overline{\mathcal{Y}}_T, \overline{\mathcal{X}}_T) = f(W_t \mid \overline{H}_{t-1})$ .

**Assumption 2.** *There exists  $\delta_W > 0$  such that  $e_t(w) > \delta_W f_h(w)$  for all  $w \in \mathcal{W}$  for which  $f_h(w) > 0$ , where  $e_t(w) = f(W_t = w \mid \overline{H}_{t-1})$ .*

Since our framework focuses on a single unit observed over time, Assumption 1 is more restrictive than the standard sequential ignorability assumption (e.g., Robins et al., 2000) because the independence is assumed for all potential outcomes and potential confounders across all time periods, past or future, i.e.,  $\bar{\mathcal{Y}}_T$  and  $\bar{\mathcal{X}}_T$ . Assumption 2 ensures that all treatment patterns that are feasible under the stochastic intervention are observable under the treatment assignment mechanism.

## 2.4 Two-step estimation procedure

We develop a two-step estimation procedure by building on methodology for estimating the CATE with i.i.d. data (e.g., Kennedy, 2023; Fan et al., 2022; Yang et al., 2023). We first construct a pseudo-outcome based on the estimated propensity score, and then regress contrasts of pseudo-outcomes on the moderators of interest. This procedure maintains a simple CATE analysis regardless of the complexity of the propensity score estimation.

We construct a pseudo-outcome by weighting the observed number of events in each pixel at each time period using the estimated propensity score and the density of the stochastic intervention. The (IPW) pseudo-outcome in pixel  $S_i$  at time  $t$  is given by

$$\tilde{Y}_{it}^I(F_h; \hat{\gamma}) = \rho_{th}(\hat{\gamma}) N_{S_i}(Y_t), \quad \text{where} \quad \rho_{th}(\hat{\gamma}) = \prod_{j=t-M+1}^t \frac{f_h(W_j)}{e_j(W_j; \hat{\gamma})} \quad (4)$$

for any  $i = 1, 2, \dots, p$  and  $t = M, M + 1, \dots, T$ , where  $f_h$  is the density corresponding to the stochastic intervention  $F_h$ ,  $e_t(W_t; \gamma)$  is a propensity score model with a  $K$ -dimensional vector of parameters  $\gamma \in \mathbb{R}^K$ , and  $\hat{\gamma}$  is an estimate of  $\gamma$ . To ensure computational tractability, the propensity score model incorporates prior values of variables from a finite temporal lag, chosen based on one's domain-specific knowledge of treatment assignment persistence.

The above IPW-based weighting scheme can produce large weights for some time pe-

riods when the estimated propensity score is much smaller than the intervention density. Therefore, we consider the following Hájek-type pseudo-outcome with stabilized weights,

$$\tilde{Y}_{it}^H(F_{\mathbf{h}}; \hat{\gamma}) = \frac{\rho_{t\mathbf{h}}(\hat{\gamma})}{\sum_{t=M}^T \rho_{t\mathbf{h}}(\hat{\gamma}) / (T - M + 1)} N_{S_i}(Y_t). \quad (5)$$

We then compare the outcome under two intervention distributions,  $F_{\mathbf{h}''}$  and  $F_{\mathbf{h}'}$ , at each pixel using  $\tilde{\tau}_{it}^H(F_{\mathbf{h}'}, F_{\mathbf{h}''}; \hat{\gamma}) = \tilde{Y}_{it}^H(F_{\mathbf{h}''}; \hat{\gamma}) - \tilde{Y}_{it}^H(F_{\mathbf{h}'}; \hat{\gamma})$ . Below, for notational simplicity, we denote  $\tilde{\tau}_{it}^H(F_{\mathbf{h}'}, F_{\mathbf{h}''}; \hat{\gamma})$  as  $\tilde{\tau}_{it, \mathbf{h}', \mathbf{h}''}^H(\hat{\gamma})$ , and let  $\tilde{\boldsymbol{\tau}}_t^H(\hat{\gamma}) = (\tilde{\tau}_{1t, \mathbf{h}', \mathbf{h}''}^H(\hat{\gamma}), \dots, \tilde{\tau}_{pt, \mathbf{h}', \mathbf{h}''}^H(\hat{\gamma}))^\top$  represent the vector of pseudo-outcome contrasts for the  $p$  pixels at time period  $t$ .

We regress the pseudo-outcome contrast at time  $t$ ,  $\tilde{\boldsymbol{\tau}}_t^H(\hat{\gamma})$ , on the moderator as shown in Equation (3). This gives the following Hájek estimator of  $\boldsymbol{\beta}_t$ ,

$$\hat{\boldsymbol{\beta}}_t^H = \arg \min_{\boldsymbol{\beta}_t} (\tilde{\boldsymbol{\tau}}_t^H(\hat{\gamma}) - \mathbf{Z}_t \boldsymbol{\beta}_t)^\top (\tilde{\boldsymbol{\tau}}_t^H(\hat{\gamma}) - \mathbf{Z}_t \boldsymbol{\beta}_t), \quad (6)$$

where  $\mathbf{Z}_t = [\mathbf{z}(\mathbf{R}_{1, t-M+1}) \dots \mathbf{z}(\mathbf{R}_{p, t-M+1})]^\top$ . Finally, we obtain the projected CATE estimator by averaging across time periods,

$$\hat{\tau}_{\mathbf{h}', \mathbf{h}''}(\mathbf{r}) = \tau_{\mathbf{h}', \mathbf{h}''}^{\text{Proj.}}(\mathbf{r}; \hat{\boldsymbol{\beta}}_M^H, \dots, \hat{\boldsymbol{\beta}}_T^H) = \mathbf{z}(\mathbf{r})^\top \left( \frac{1}{T - M + 1} \sum_{t=M}^T \hat{\boldsymbol{\beta}}_t^H \right). \quad (7)$$

As evident in (6), the time-specific estimates  $\hat{\boldsymbol{\beta}}_t^H$  are obtained by fitting a separate regression model for each time period rather than a pooled regression using data across all time periods. With separate regressions, the resulting estimating equations have a conditional mean of zero for any given time period, forming a martingale difference sequence with respect to the history filtration. This allows us to derive the asymptotic properties of the estimator, as shown below.

## 2.5 Asymptotic properties

We now show that the proposed Hájek-type CATE estimator is consistent and asymptotically normal. Unfortunately, the asymptotic variance is unidentifiable because we only observe a single time series. Nevertheless, we derive a variance upper bound and propose a consistent estimator of this bound. All proofs are presented in the appendix. Our results are new in the spatio-temporal causal inference literature. [Papadogeorgou et al. \(2022\)](#) derive asymptotic properties for the IPW estimator, and leave studying the asymptotic behavior of stabilized weighting estimators to future work. We also show that when the propensity score is estimated, the asymptotic variance of the Hájek estimator is no greater than when the propensity score is known. This extends the analogous result of [Hirano et al. \(2003\)](#), which was applicable only to the IPW estimator of the ATE in i.i.d. settings, to CATE estimation with stabilized weights in spatio-temporal settings.

We formally state the asymptotic normality of the Hájek estimator based on the estimated propensity score. Besides the two assumptions introduced in [Section 2.3](#), we require standard regularity conditions, which are formally stated in the appendix.

**Theorem 1.** *Suppose that Assumptions 1 and 2 hold, along with the regularity conditions specified in Assumptions A.1, A.2, A.4 and A.5. Let  $\hat{\gamma}$  be the estimate of the propensity score parameters obtained by solving the estimating equation  $\sum_{t=M}^T \psi(W_t, \bar{H}_{t-1}; \gamma) = 0$ , where  $\psi(W_t, \bar{H}_{t-1}; \gamma)$  is specified in Assumption A.2. Then as  $T \rightarrow \infty$ , we have that*

$$\frac{1}{\sqrt{T-M+1}} \sum_{t=M}^T (\hat{\beta}_t^H - \beta_t^*) \xrightarrow{d} N(\mathbf{0}, \mathbf{J} \mathbf{V}^H \mathbf{J}^\top),$$

where  $\mathbf{V}^H = \tilde{\mathbf{V}}^H - \mathbf{U}^\top \mathbf{V}_{ps}^{-1} \mathbf{U}$ , matrices  $\mathbf{J}$ ,  $\tilde{\mathbf{V}}^H$  that are defined in [Theorem A.4](#), matrix  $\mathbf{V}_{ps}$  defined in [Assumption A.2](#), and matrix  $\mathbf{U}$  defined in [Assumption A.5](#).

In [Theorem A.4](#) of [Section C](#), we establish that the estimator based on the true propensity score is asymptotically normal with variance  $\mathbf{J} \tilde{\mathbf{V}}^H \mathbf{J}^\top$ . Thus, the difference between the

asymptotic variance based on the true and the estimated propensity score is  $\mathbf{J}\mathbf{U}^\top \mathbf{V}_{ps}^{-1} \mathbf{U}\mathbf{J}^\top$ . This quantity is large when the estimating equation corresponding to the causal effect estimator based on the true propensity score is strongly correlated with the score function of the propensity score model. By showing that this difference is a positive semidefinite matrix, we establish that using the estimated propensity score leads to a more efficient estimator.

**Theorem 2.** *If the propensity score model is correctly specified, the estimator  $\frac{1}{T-M+1} \sum_{t=M}^T \hat{\beta}_t^H$  based on the estimated propensity score has asymptotic variance that is no larger than the asymptotic variance of the same estimator using the known propensity score. That is, for  $\mathbf{J}\tilde{\mathbf{V}}^H \mathbf{J}^\top$  in Theorem A.4, and  $\mathbf{J}\mathbf{V}^H \mathbf{J}^\top$  in Theorem 1,  $\mathbf{J}(\tilde{\mathbf{V}}^H - \mathbf{V}^H)\mathbf{J}^\top$  is a positive semidefinite matrix.*

The matrix  $\mathbf{V}^H$  is based on the covariance matrix of the estimating equations conditional on the complete history, i.e.,  $\mathbf{V}^H = \text{plim}_{T \rightarrow \infty} \frac{1}{T-M+1} \sum_{t=M}^T \mathbb{V}[\mathbf{A}_t(\gamma^*) \mid \bar{H}_{t-M}^*]$  for vector  $\mathbf{A}_t(\gamma)$  defined in Section C.1. As mentioned earlier,  $\mathbb{V}[\mathbf{A}_t(\gamma^*) \mid \bar{H}_{t-M}^*]$  cannot be consistently estimated without further assumptions due to the fact that we only observe a single time series. However, since  $\mathbf{V}^{H*} = \text{plim}_{T \rightarrow \infty} \frac{1}{T-M+1} \sum_{t=M}^T \mathbb{E}[\mathbf{A}_t(\gamma^*) \mathbf{A}_t(\gamma^*)^\top \mid \bar{H}_{t-M}^*]$  is an upper bound of  $\mathbf{V}^H$ , the asymptotic variance  $\mathbf{J}\mathbf{V}^H \mathbf{J}^\top$  is bounded above by  $\mathbf{J}\mathbf{V}^{H*} \mathbf{J}^\top$ . Moreover, the following proposition shows that we can consistently estimate the upper bound of the asymptotic variance.

**Proposition 1.** *Suppose that the conditions of Theorem 1 hold. For  $\mathbf{A}_t(\gamma)$  defined in Assumption A.4, define  $\hat{\mathbf{V}}^H = \frac{1}{T-M+1} \sum_{t=M}^T \hat{\mathbf{V}}_t^H$  where  $\hat{\mathbf{V}}_t^H = \mathbf{A}_t(\hat{\gamma}) \mathbf{A}_t(\hat{\gamma})^\top$ , and*

$$\hat{\mathbf{J}} = \left[ \mathbf{I} \quad -\mathbf{I} \quad -\frac{1}{T-M+1} \sum_{t=M}^T (\mathbf{Z}_t^\top \mathbf{Z}_t)^{-1} \mathbf{Z}_t^\top \tilde{\mathbf{Y}}_t^H(F_{\mathbf{h}'}; \hat{\gamma}) \quad \frac{1}{T-M+1} \sum_{t=M}^T (\mathbf{Z}_t^\top \mathbf{Z}_t)^{-1} \mathbf{Z}_t^\top \tilde{\mathbf{Y}}_t^H(F_{\mathbf{h}''}; \hat{\gamma}) \right],$$

where  $\tilde{\mathbf{Y}}_t^H(F_{\mathbf{h}}; \hat{\gamma}) = \left( \tilde{Y}_{1t}^H(F_{\mathbf{h}}; \hat{\gamma}), \dots, \tilde{Y}_{pt}^H(F_{\mathbf{h}}; \hat{\gamma}) \right)^\top$ . Then, for any matrix  $\mathbf{Q}$  that depends on  $T$  and converges to the identity matrix  $\mathbf{I}$  in probability as  $T \rightarrow \infty$ ,  $\hat{\mathbf{J}}\mathbf{Q}\hat{\mathbf{V}}^H\mathbf{Q}^\top\hat{\mathbf{J}}^\top$  is a consistent estimator for  $\mathbf{J}\mathbf{V}^{H*} \mathbf{J}^\top$ .

We use the estimated variance bound to construct confidence intervals whose coverage

will be at least as large as the nominal level.

The choice of the matrix  $\mathbf{Q}$  affects the performance of our inferential procedure. Even though setting  $\mathbf{Q} = \mathbf{I}$  returns a consistent estimator for the variance upper bound according to Proposition 1, it often performs poorly in finite samples. Building on the same idea as the Hájek estimator for the causal effect,  $\mathbf{Q}$  is chosen to stabilize the variance bound estimator.

First, we consider  $F_{h'}$  and  $F_{h''}$ , the simplifications of  $F_{\mathbf{h}'}$  and  $F_{\mathbf{h}''}$  to one time period interventions,  $M = 1$ . Then, we define the mean IPW weights for  $F_{h'}$  and  $F_{h''}$  as  $\xi_{h'} = \frac{1}{T} \sum_{t=1}^T \frac{f_{h'}(W_t)}{e_t(W_t; \hat{\gamma})}$  and  $\xi_{h''} = \frac{1}{T} \sum_{t=1}^T \frac{f_{h''}(W_t)}{e_t(W_t; \hat{\gamma})}$ , respectively. We set

$$\mathbf{Q} = \text{diag}(\rho_{h'}^{-1} \mathbf{1}_L, \rho_{h''}^{-1} \mathbf{1}_L, \xi_{h'}^{-M}, \xi_{h''}^{-M}),$$

where  $\text{diag}(\cdot)$  denotes a diagonal matrix with diagonal entries specified as its argument,  $\mathbf{1}_L$  is a  $L \times 1$  vector of ones, and  $\rho_{h'} = \frac{1}{T-M+1} \sum_{t=M}^T \rho_{th'}$  and  $\rho_{h''} = \frac{1}{T-M+1} \sum_{t=M}^T \rho_{th''}$  are the mean IPW weights for  $F_{h'}$  and  $F_{h''}$ , respectively. Since  $\rho_{h'}$ ,  $\rho_{h''}$ ,  $\xi_{h'}$ , and  $\xi_{h''}$  converge to 1 in probability as  $T \rightarrow \infty$ ,  $\mathbf{Q}$  converges to  $\mathbf{I}$  in probability as  $T \rightarrow \infty$ . Here,  $\rho_{h'}^{-1} \mathbf{1}_L$  and  $\rho_{h''}^{-1} \mathbf{1}_L$  stabilize the pseudo-outcomes, while  $\xi_{h'}^{-M}$  and  $\xi_{h''}^{-M}$  stabilize the IPW weights, which take a product form across  $M$  time periods, using the mean of the one-period weights. This choice of  $\mathbf{Q}$  provides stabilization of the variance upper bound estimator. For stochastic interventions that are dependent across the  $M$  time periods, we discuss the choice of  $\mathbf{Q}$  in Section F.

Our simulation study in Section 3 demonstrates a good empirical coverage rate for the constructed confidence interval, even when  $M$  is relatively large. Thus, our methodology provides significantly improved inference compared to a heuristic variance bound used in Papadogeorgou et al. (2022), where the coverage rate deteriorates quickly as  $M$  increases.

Section C presents additional theoretical results and detailed proofs for the Hájek esti-

mator, and Section B establishes that the IPW estimators are also consistent and asymptotically normal, with consistently estimable variance bounds. In simulations, the IPW estimators show larger variance than the stabilized Hájek estimator, consistent with the i.i.d. case (see Section J.5). Moreover, the mean estimated variance bound across simulations closely matches the Monte Carlo variance when the number of time periods is large (Section D).

## 2.6 Statistical test of no heterogeneous treatment effect

We develop a statistical test for treatment effect heterogeneity with the null hypothesis that all coefficients of  $\mathbf{z}(\mathbf{r})$  in Equation (7), other than the intercept, are equal to zero. For notational simplicity, we describe the proposed test in a setting in which  $\mathbf{z}(\mathbf{r})$  does not include an intercept. The test, however, can be easily adopted in models with an intercept.

Let  $\bar{\boldsymbol{\beta}} = \frac{1}{T-M+1} \sum_{t=M}^T \hat{\boldsymbol{\beta}}_t^H$  and  $\bar{\boldsymbol{\beta}}^* = \frac{1}{T-M+1} \sum_{t=M}^T \boldsymbol{\beta}_t^*$ . We are interested in testing the null hypothesis that  $H_0 : \bar{\boldsymbol{\beta}}^* = \mathbf{0}$ , which holds if the treatment effect is not heterogeneous with respect to  $\mathbf{z}(\mathbf{r})$ . The alternative is  $H_A : \bar{\boldsymbol{\beta}}^* \neq \mathbf{0}$ . We propose the test statistic

$$T_c = (T - M + 1) \bar{\boldsymbol{\beta}}^\top (\hat{\mathbf{J}} \mathbf{Q} \hat{\mathbf{V}}^H \mathbf{Q}^\top \hat{\mathbf{J}}^\top)^{-1} \bar{\boldsymbol{\beta}},$$

and calculate the  $p$ -value as  $\mathbb{P}(\chi_L^2 > T_c)$ , where  $\chi_L^2$  denotes the chi-square distribution with  $L$  degrees of freedom. The following theorem shows that the limiting rejection probability under the null hypothesis is no greater than  $\alpha$  as  $T \rightarrow \infty$ .

**Theorem 3.** *Under the assumptions of Theorem 1 and the null hypothesis  $\bar{\boldsymbol{\beta}}^* = \mathbf{0}$ , we have that  $\limsup_{T \rightarrow \infty} \mathbb{P}(p\text{-value} < \alpha) \leq \alpha$ .*

By inverting this test, we obtain an  $(1 - \alpha)100\%$  confidence set for  $\bar{\boldsymbol{\beta}}^*$  with limiting

coverage that is no less than  $1 - \alpha$  as  $T \rightarrow \infty$  as:

$$C_\alpha = \left\{ \bar{\beta}' : (T - M + 1)(\bar{\beta} - \bar{\beta}')^\top (\hat{\mathbf{J}} \mathbf{Q} \hat{\mathbf{V}}^H \mathbf{Q}^\top \hat{\mathbf{J}}^\top)^{-1} (\bar{\beta} - \bar{\beta}') < F_{\chi_L^2}^{-1}(1 - \alpha) \right\}, \quad (8)$$

where  $F_{\chi_L^2}^{-1}(q)$  is the  $q$ -quantile of the chi-square distribution with  $L$  degrees of freedom.

## 2.7 Adaptive stochastic interventions

The previous sections focus on static interventions, where the same treatment distribution is assigned across all time periods. We extend the framework to adaptive interventions, in which the treatment distribution may depend on prior outcomes and covariates. Such extensions are particularly challenging if interventions span multiple time periods and depend on recent history, including intermediate covariates. To handle this complexity, we build on literature on dynamic treatment regimes (e.g. [Moodie et al., 2012](#); [Barrett et al., 2014](#)) to define the new CATE estimand.

Formally, we consider an adaptive intervention that can be represented by a sequence of one-period intervention distributions  $F_{\mathbf{h}_t} = (F_{h_{t1}}, \dots, F_{h_{tM}})$ , where each  $F_{h_{tm}}$  is allowed to depend on the observed history  $\bar{H}_{t-m}$ , i.e.  $F_{h_{tm}}$  has density  $f_{h_{tm}}(w | \bar{H}_{t-m})$  for all  $w \in \mathcal{W}$  and  $m = 1, 2, \dots, M$ . We first define the expected number of outcome events in pixel  $i$  at time  $t$  under an adaptive intervention  $F_{h_{t1}}$  which may depend on  $\bar{H}_{t-1}$  as

$$N_{it}(F_{h_{t1}}; \bar{H}_{t-1}) = \int_{\mathcal{W}} N_{S_i}(Y_t(\bar{\mathbf{W}}_{t-1}, w_t)) f_{h_{t1}}(w_t | \bar{H}_{t-1}) dw_t.$$

Next, we define the expected value of  $N_{it}(F_{h_{t1}}; \bar{H}_{t-1})$  where the treatment in the previous period is drawn from  $F_{h_{t2}}$  based on  $\bar{H}_{t-2}$ ,

$$N_{it}(F_{h_{t1}}, F_{h_{t2}}; \bar{H}_{t-2}) = \int_{\mathcal{W}} N_{it}(F_{h_{t1}}; \bar{H}_{t-1}) f_{h_{t2}}(w_{t-1} | \bar{H}_{t-2}) dw_{t-1}. \quad (9)$$

Making the dependence on the observed history explicit in  $N_{it}(F_{h_{t1}}; \overline{H}_{t-1})$  highlights how the estimand is constructed sequentially and clarifies the integral in Equation (9). Repeating this construction sequentially, we define  $N_{it}(F_{h_t}; \overline{H}_{t-M})$ , which averages over the treatments at time periods  $t, t-1, \dots, t-M+1$  according to the adaptive stochastic intervention. For non-adaptive stochastic intervention,  $F_{h_t}, N_{it}(F_{h_t}; \overline{H}_{t-M})$  coincides with  $N_{it}(F_h)$  given in Equation (2). The corresponding CATE estimand can then be defined analogously to Section 2.2, replacing  $N_{it}$  with its adaptive version. For estimation, we adjust Assumption 2 as follows:

**Assumption 3.** *There exists  $\delta_W > 0$  such that  $e_{t-m+1}(w) > \delta_W f_{h_{tm}}(w \mid \overline{H}_{t-m})$  for all  $w \in \mathcal{W}$ ,  $1 \leq m \leq M$  and  $M \leq t \leq T$  for which  $f_{h_{tm}}(w) > 0$ , where  $e_t(w) = f(W_t = w \mid \overline{H}_{t-1})$ .*

Finally, define the pseudo-outcome  $\tilde{Y}_{it}^I(F_{h_t}; \hat{\gamma})$  as done in Section 2.4, using modified IPW weights:  $\tilde{Y}_{it}^I(F_{h_t}; \hat{\gamma}) = \rho_{h_t}(\hat{\gamma}) N_{S_i}(Y_t)$ , where  $\rho_{h_t}(\hat{\gamma}) = \prod_{m=1}^M \frac{f_{h_{tm}}(W_{t-m+1} \mid \overline{H}_{t-m})}{e_{t-m+1}(W_{t-m+1}; \hat{\gamma})}$ . The Hájek version of the pseudo-outcome is defined analogously. The theoretical results established in the previous sections continue to hold under the adaptive intervention framework. The details and the choice of  $\mathbf{Q}$  for our variance upper bound estimator are provided in Section G.

## 3 Simulation Studies

In this section, we conduct simulation studies. To create a realistic data generating process, we base our simulations on the Iraq data introduced in Section 4.1. We focus on a univariate moderator but consider both spatial and spatio-temporal variables.

### 3.1 Study design

For each simulation, we independently generate 500 datasets. We set the length of time series to be  $T = 500$ , closely following the corresponding length in our Iraq data (see

Section 4). We begin by generating a vector of confounders  $\mathbf{X}_t = (X_1, X_2, X_{3t}, X_{4t})^\top$ , as in Papadogeorgou et al. (2022). Specifically,  $X_1$  and  $X_2$  are spatial confounders;  $X_1$  is based on the distance to the main road network and the border of Iraq, while  $X_2$  is based on the distance to Baghdad (see Figure A.2a). Moreover,  $X_{3t}$  and  $X_{4t}$  are two spatio-temporal confounders based on the observed patterns of airstrikes and insurgent attacks in our Iraq data. We use the locations of all airstrikes in the entire study period to obtain a spatial density estimate of airstrike patterns,  $\hat{g}(\omega)$ . At each time period  $t$ , we first generate a point pattern  $Z$  from a Poisson point process with the intensity  $\exp(\rho_0 + \rho_1 \hat{g}(\omega))$  for  $\rho_0 \approx -2.7$  and  $\rho_1 = 8$ . Then, the confounder  $X_{3t}$  is computed as a function of the distance to the closest realized point in  $Z$ ,  $D(\omega; Z)$ , i.e.,  $X_{3t}(\omega) = \exp(-D(\omega; Z))$ . A realization of  $X_{3t}$  at a randomly chosen time period is shown in Figure A.2b. We generate  $X_{4t}$  similarly but estimate the spatial density  $\hat{g}$  based on the observed insurgent violence events with  $\rho_0 \approx -3.2$  and  $\rho_1 = 7$ . We conduct two sets of simulation studies: one with the spatial moderator  $X_2$  and the other with the spatio-temporal moderator  $X_{3t}$ . All variables are included as confounders in all simulations.

We generate the treatment and outcome point patterns conditional on the covariates. For each time period  $t$ , the treatment point pattern is generated from a Poisson point process with intensity function  $\lambda_t^W(\omega) = \exp\{\alpha_0 + \boldsymbol{\alpha}_X^\top \mathbf{X}_t(\omega) + \alpha_W W_{t-1}^*(\omega) + \alpha_Y Y_{t-1}^*(\omega)\}$ , where  $Y_{t-1}^*(\omega)$  and  $W_{t-1}^*(\omega)$  are the smoothed versions of the realized point patterns  $Y_{t-1}$  and  $W_{t-1}$ , respectively. Specifically,  $Y_{t-1}^*(\omega) = \exp(-2D(\omega; Y_{t-1}))$ , where  $D(\omega; Y_{t-1})$  denotes the minimum distance of location  $\omega \in \Omega$  from the observed outcome events at the previous time period,  $Y_{t-1}$ . We define  $W_{t-1}^*(\omega) = \exp(-2D(\omega; W_{t-1}))$  in a similar manner.

Additionally, we generate the outcome point pattern from a Poisson process with an intensity function  $\lambda_t^Y$ . For the simulations with the spatial moderator  $X_2$ , we use  $\lambda_t^Y(\omega) =$

$\exp\{\gamma_0 + \boldsymbol{\gamma}_X^\top \mathbf{X}_t(\omega) + \gamma_W W_{(t-3):t}^*(\omega) + \gamma_Y Y_{t-1}^*(\omega) + \gamma_1 X_2 W_{(t-3):t}^*(\omega)\}$ , where  $W_{(t-3):t}^* = \exp(-2D(\omega; \mathbf{W}_{(t-3):t}))$  and  $D(\omega; \mathbf{W}_{(t-3):t})$  denote the minimum distance of location  $\omega$  to treatment locations during any of the time periods  $t - 3$  to  $t$ . When the moderator is the spatio-temporal variable  $X_{3t}$ , we use the intensity function:  $\lambda_t^Y(\omega) = \exp\{\gamma_0 + \boldsymbol{\gamma}_X^\top \mathbf{X}_t(\omega) + \gamma_W W_{(t-3):t}^*(\omega) + \gamma_Y Y_{t-1}^*(\omega) + \sum_{j=1}^4 \gamma_j X_{3,t-j}(\omega) W_{t-j+1}^*(\omega)\}$ . These model specifications yield on average approximately 5 treatment events and 30 outcome events per time period, closely reflecting the observed data, which show an average of 4.9 airstrikes and 31.3 IED attacks per day. This data-generating process allows for spillover and carryover effects. In fact, the potential outcomes at time  $t$  depend on the realized treatments and outcomes in all previous time periods either directly or indirectly due to the inclusion of the lagged treatment and outcome variables.

We consider stochastic interventions of the form  $F_h^M = F_h \times \dots \times F_h$  where the intensity function is given by  $h(\omega) = c\phi(\omega)$ . We set  $\phi$  equal to a density estimate of the generated treatment events (shown in Figure A.2c). Here, the parameter  $c$  regulates the expected number of treatment events. For  $M = 1, 3, 7$ , we consider the stochastic interventions with  $c = 3, 5, 7$ , denoted as  $F_{h_1}^M, F_{h_2}^M$ , and  $F_{h_3}^M$  respectively. We estimate the CATE that contrasts between any two of these interventions.

## 3.2 Model specifications

In total, we evaluate four estimators: IPW/Hájek estimators based on the true propensity score and IPW/Hájek estimators based on the estimated propensity score. We use the consistent estimator of the variance upper bound discussed in Section 2.5 to construct confidence intervals. When computing pseudo-outcomes, we use either the IPW or stabilized Hájek weights. After obtaining the pseudo-outcomes, we choose functions  $z_1(r), \dots, z_L(r)$  for the working model in Equation (3). For all simulations, we include six basis functions

in the working model, i.e.,  $L = 6$ . Figure A.3 presents the histogram of the spatial and the spatio-temporal moderators across all pixels and all time periods. Since both moderators  $X_2$  and  $X_{3t}$  take values in  $[0, 1]$ , we set  $z_1(r), \dots, z_6(r)$  to be the basis functions of natural cubic splines on  $[0, 1]$  with equally spaced knots between 0 and 1. At each time period, we regress the pseudo-outcomes on the covariates formed by  $z_1(r), \dots, z_L(r)$ .

### 3.3 Results

We assess the empirical performance of the Hájek estimators under the most challenging scenario, which compares  $F_{h_1}^M$  and  $F_{h_3}^M$ . Figure 1 presents the true and estimated CATEs using the Hájek estimator, the bias and the coverage rates of 95% intervals, for the spatio-temporal moderator with  $M = 1, 3$ , and 7, averaged over 500 Monte Carlo simulations. The shaded region highlights the 0.025 and 0.975 quantile range of the spatio-temporal moderator values, on which we focus our discussion. Results outside this range are mostly based on extrapolation. The true value of the CATE is different across data sets. Since no closed-form expression is available, we use a Monte Carlo approximation for the true CATE values (see Section J.1 for details).

Overall, the Hájek estimators perform well within the shaded region: the estimated CATEs closely track the true CATEs, with minimal bias. Empirical coverage rates remain close to the nominal 95% level. Even in the most challenging scenario ( $M = 7$ ), the bias remains below 0.005, demonstrating that the Hájek estimators are essentially unbiased for commonly observed moderator values. As the number of intervention time periods increases, empirical coverage decreases slightly for certain moderator values but remains above 0.88. For regions with limited data, particularly near the upper end of the moderator range, the estimated CATEs show small biases, especially in the most challenging case of  $M = 7$ . However, the empirical coverage remains stable across all scenarios, indicating that

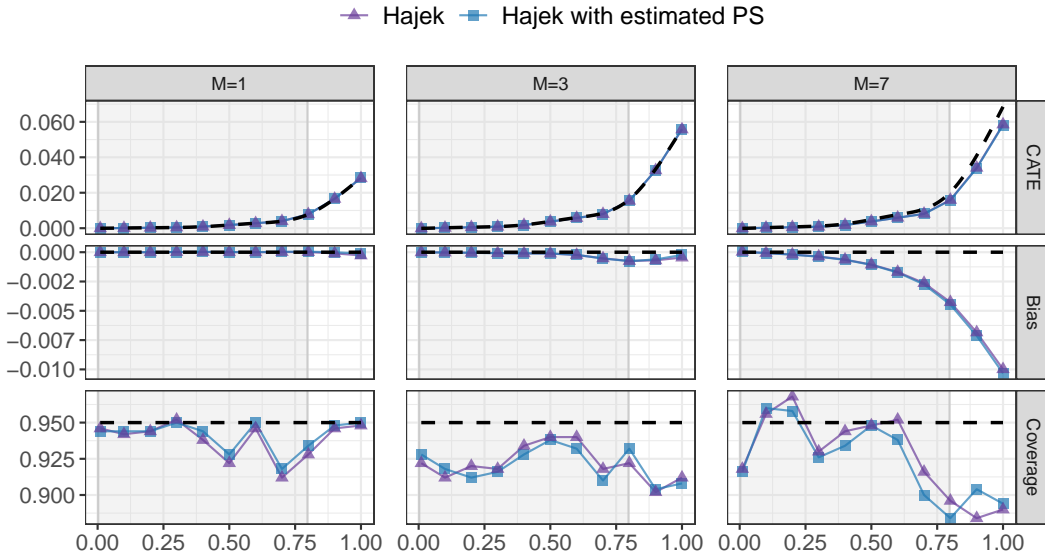


Figure 1: The average of estimated CATE (first row), bias (second row), and coverage (third row) based on Hájek estimators across 500 simulations. Dashed lines in the first, second, and third rows represent the true CATE, bias of zero, and the nominal coverage of 95%, respectively. The plot pertains to the stochastic intervention over  $M = 1, 3, 7$  time periods. The purple line with triangles denotes the estimator based on the true propensity score, while the blue line with squares represent the estimators based on the estimated propensity scores. The shaded region indicates the 0.025 and 0.975 quantile range of the moderator values.

the variance estimates account well for the limited information in that moderator range. The estimator performs equally well regardless of whether true or estimated propensity scores are used.

The results for the spatial moderator exhibit similar patterns, with the estimated CATEs closely following the true CATEs and empirical coverage rates remaining above 0.87. These findings are presented in Section J. Beyond the spatial moderator, Section J also examines the Hájek estimator for alternative CATE contrasts and shows results for IPW estimators. While both perform similarly in low-variance cases with  $M = 1$ , the Hájek estimators outperform IPW estimators for  $M = 3$  and  $M = 7$ , consistently exhibiting smaller variances. Lastly, estimated propensity scores generally improve efficiency over true propensity scores, consistent with our theoretical results.

## 4 Empirical Application

We examine how the effects of airstrikes on insurgent violence depend on the prior provision of aid during the Iraq War (2003–2011). We focus on the period of the so-called “Surge” (2007–2008) when US policymakers, alarmed by escalating violence, deployed additional forces, aid, and airstrikes. These efforts formed part of the broader *hearts and minds* counterinsurgency campaign, in which aid was meant to win over locals while airstrikes sought to deter insurgent groups.

Estimating heterogeneous effects allows us to test the widespread but largely untested claim that aid and airstrikes work in tandem to reduce insurgent attacks. Previous studies often aggregate data into coarse temporal windows (e.g., years) or administrative boundaries (e.g., provinces), limiting their ability to capture spillover and carryover dynamics (e.g. [Nunn and Qian, 2014](#); [Sexton, 2016](#); [Bianchi and Giorcelli, 2023](#)). By contrast, our analysis provides an explicit test of whether aid and airstrikes interact to shape insurgent attacks.

### 4.1 Data

We analyze newly declassified high-frequency data recording the date and precise location of US airstrikes and insurgent attacks against Coalition forces. Our data cover the time period from January 2007 to July 2008. The information about insurgent attacks is based on the Significant Act data collected by Coalition forces in Iraq. During this period, some 68,573 insurgent attacks against US forces were recorded across 57 different types of events, including Small Arms Fire (SAF) and Improvised Explosive Device (IED). Each incident report includes the time, date, and nature of an attack, along with precise coordinates that permit spatio-temporal analysis at a very fine-grained level. Figure [2a](#) plots the spatial

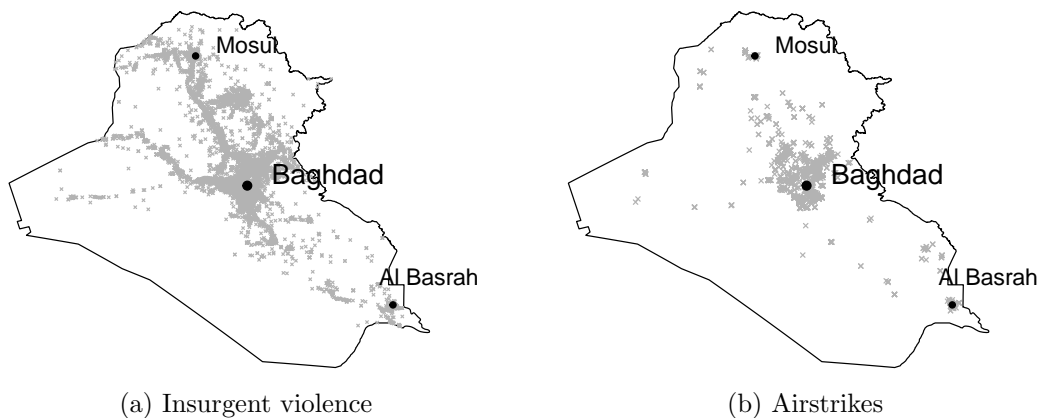


Figure 2: Distribution of US Airstrikes and Insurgent Attacks. Panels (a) and (b) illustrate the spatial distribution of all insurgent attacks (small arms fire and roadside improvised explosive devices) and all airstrikes from February 23, 2007 to July 5, 2008, respectively.

distribution of all insurgent attacks.

We use declassified data on airstrikes obtained from the US Air Force’s Combined Air Operations Center as our treatment variable. A total of 2,446 airstrikes were recorded during our study period. Each event records the date, coordinates, weapon type and number, and aircraft type(s) involved in the airstrike. Figure 2b plots the spatial distribution of these airstrikes.

We draw on a dataset of aid spending (in US dollars) as recorded by the US military and USAID. Some 23,204 aid projects totaling \$4.97 billion were delivered during this period. Two programs, the Commander’s Emergency Response Program (CERP) and its USAID equivalent, Economic Support Funds (ESF), dominate these aid expenditures, representing about 50% (n=11,714) and nearly 45% (n=10,370) of all completed projects, respectively.

As Figure 3 illustrates, aid spending during the previous month varied widely across districts and over time during the study period due to shifting priorities, budgetary cycles, and patterns of insurgent violence. The data are publicly available as part of the `geocausal` R package (Mukaigawara et al., 2025) and on the Harvard Dataverse (Mukaigawara et al., 2023).

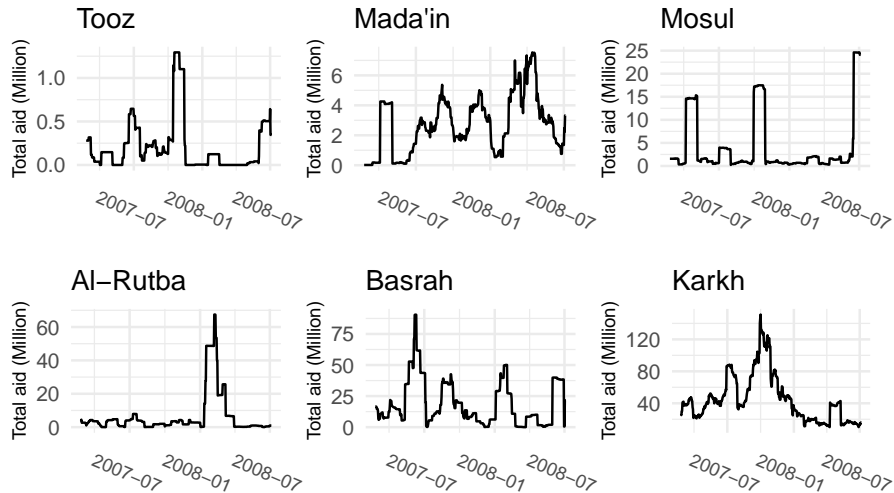


Figure 3: Total aid amount (in million US dollars) over the previous month for six selected districts across Iraq, spanning from February 23, 2007, to July 5, 2008. Aid spending shows significant variation across districts and over time throughout the study period.

## 4.2 Design and Implementation

We analyze how the effects of US airstrikes on insurgent violence change with the amount of recent aid spending. In particular, we first consider as a moderator a binary indicator for whether a district received any US aid spending in the previous month. Then, we consider the aid spending per capita in the previous month as a continuous moderator. Using both moderators allows us to report estimated effects for the presence of any recent aid and, separately, how those estimated effects vary with the amount of aid. Our analysis focuses on the two most frequent types of insurgent attacks, IED and SAF. Since IED and SAF have different operational dynamics, airstrikes may affect them in different ways.

We consider two types of interventions. We first construct static interventions following our simulation studies. The baseline density of U.S. airstrikes, denoted  $\phi_0(\omega)$ , is estimated using airstrikes prior to the surge period. We then estimate the causal contrast between the two stochastic interventions,  $F_{h_1} = F_{h_1}^M$  versus  $F_{h_2} = F_{h_2}^M$ , where  $h_1 = \phi_0(\omega)$  and  $h_2 = 6\phi_0(\omega)$  for  $M = 1, 2, \dots, 10$ . That is, we estimate the effects of increasing the

intensity of airstrikes sixfold for a period ranging from one to ten days. The scaling factors (1 and 6) are calibrated to the 25<sup>th</sup> and 75<sup>th</sup> percentiles of the observed airstrike counts. These counterfactual interventions allow us to estimate the effect of increasing the number of airstrikes while holding their spatial distribution fixed, and they ensure overlap between the counterfactual and observed distributions.

We also construct adaptive interventions, where the baseline intensity for each time period is estimated using data prior to the surge period. The analysis based on adaptive interventions compares two treatment assignment strategies that update sequentially according to the observed history. Particularly, the adaptive interventions allow the counterfactual treatment assignment to depend on prior observed outcomes, among other variables. The details of constructing adaptive interventions are provided in Section [K.5](#).

Our propensity score model is a non-homogeneous Poisson point process with intensity  $\lambda(\omega) = \exp(\boldsymbol{\beta}^\top \mathbf{X}_t(\omega))$ , where  $\mathbf{X}_t(\omega)$  includes temporal splines, an indicator for a surge period of airstrikes, and 32 spatial or spatio-temporal surfaces. The spatio-temporal surfaces are observed airstrikes, insurgent attacks, and shows of force (i.e., simulated bombing raids designed to deter insurgents) patterns from the last day, week, and month (9 surfaces), and the amount of aid spent (in US dollars) in each Iraqi district in the past month (1 surface). Time-invariant spatial covariates are distance from major cities, road networks and rivers (3 surfaces), population size (logged, measured in 2003; 1 surface), and distances from local settlements in each of the Iraqi districts (18 surfaces). In Section [K.1](#), we evaluate the propensity score model using out-of-sample prediction. We find that the fitted model captures the general trend of airstrikes in different governorates.

Using estimated propensity scores, we construct pseudo-outcomes by truncating IPW weights at the 95<sup>th</sup> percentile and using stabilized weights. Truncation is a common practice

in applied research to avoid extreme weights. We divide Iraq’s enclosing rectangle into a  $128 \times 128$  grid of equally-sized pixels (each covering approximately  $9 \text{ km} \times 8 \text{ km}$ ), yielding 8,451 pixels within Iraq. Pseudo-outcomes are computed for each pixel, with moderator values assigned by the Iraqi district containing the pixel’s centroid. The choice of a  $128 \times 128$  grid reflects a reasonable balance between computational cost and spatial resolution.

### 4.3 Findings

In this section, we present the results for static interventions. The corresponding results for adaptive interventions are shown in Section K.5. For the analysis with binary aid, we consider the model  $\tau_{t,h_1,h_2}(r; \beta_t) = \beta_{t,0} + \beta_{t,1}r$  for each time period, where  $r$  is the indicator variable for receiving aid in the previous month. Given that the moderator is a binary variable, we need not consider the projection estimand in this case. Under this model, the CATE,  $\frac{1}{T-M+1} \sum_{t=M}^T \beta_{t,1}$ , represents the average difference, between pixels that received aid in the previous month and those that did not, in the effect of changing the stochastic intervention from  $F_{h_1}^M$  to  $F_{h_2}^M$ . We multiply this value by the average number of pixels in a district, so that estimated quantities are interpreted as the estimated average moderation effect at the district level.

Figure 4a presents the estimated CATEs and 95% confidence intervals for  $r = 0$  and  $r = 1$ , for interventions that span from 1 to 10 days. The results of IED and SAF attacks show similar patterns. An increase in airstrikes over multiple consecutive days leads to an increase in subsequent insurgent violence. Districts with aid would experience a significant increase in SAF attacks for an increase in airstrikes spanning at least 7 days, while districts with or without aid would respond with a statistically significant increase in IED attacks for interventions spanning 10 days.

Importantly, the estimated CATE for  $r = 1$  is generally higher than that for  $r = 0$ ,

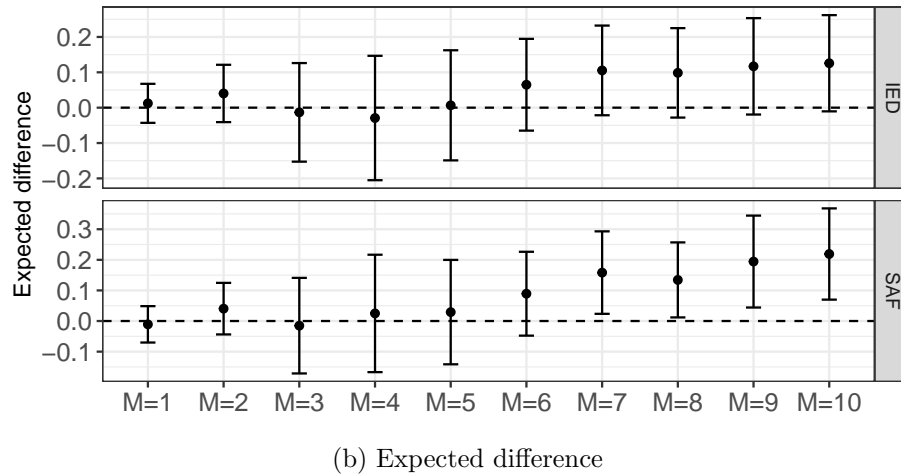
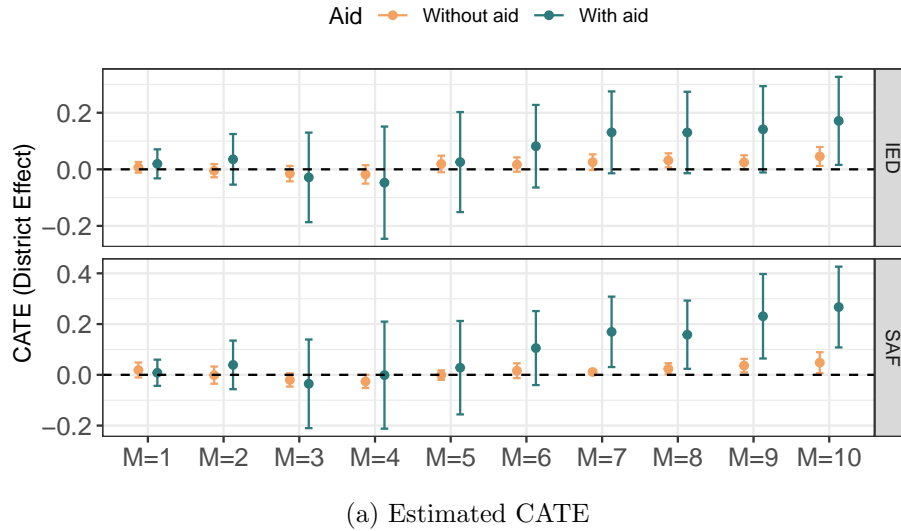


Figure 4: Results for the binary aid moderator. Plot (a) shows the estimated CATEs of increasing airstrike intensity on the number of insurgency attacks (Improvised Explosive Device or IED in the top panel, and Small Arms Fire or SAF in the bottom panel) a district with or without aid in the previous month. Plot (b) shows the estimated difference in the CATEs between a district that received aid in the previous month and those that did not. The corresponding 95% confidence intervals are also shown.

indicating locations that received prior aid respond more strongly to intensified airstrikes. Figure 4b shows the difference in the estimated CATE for  $r = 0$  and 1 with 95% confidence intervals. The confidence intervals are calculated based on Equation (8). For IED, the estimation uncertainty is too large to draw a definitive conclusion about whether regions with and without aid exhibit different reactions to the increase of airstrikes. For SAF, however, the estimated difference is positive and statistically significant for the intervention

period of at least seven days. This finding suggests that when the intervention period is sufficiently long, increasing the intensity of airstrikes sixfold leads to a greater number of insurgent attacks in districts with prior aid compared to those without.

Since the baseline distribution of airstrikes is not uniform across space, increasing airstrike intensity relative to the baseline leads to some regions experiencing a greater increase in airstrikes than others. Figure A.4a illustrates the estimated difference in the average number of airstrikes per district between the two interventions. One concern is that the significant differences observed in Figure 4b might be driven by this uneven increase in airstrike intensity. To address this, we incorporate the expected difference in airstrikes into the regression model and perform the analysis while controlling for this expected difference. Most results remain consistent. The confidence interval for the CATE for  $r = 0$  becomes wider, but the difference between the CATE for  $r = 0$  and  $r = 1$  becomes significant for IED when airstrike intensity is increased sixfold for 10 days after controlling for the expected difference in airstrikes. Detailed results are provided in Section K.4.

We next analyze the aid per capita. The histogram of continuous aid (Figure A.4b) reveals that many pixels have no aid during some time periods. To account for this, we include an indicator for zero aid in our working model. Consistent with simulation studies, we use four natural cubic spline basis functions,  $z_l(r)$ , based on strictly positive aid values, using equally spaced knots. Additionally, we set  $z_l(0) = 0$  for  $l = 1, 2, 3, 4$ . In sum, we consider the following working model:  $\tau_{t,h_1,h_2}^{\text{Proj.}}(r; \boldsymbol{\beta}_t) = \beta_{t,0} + \sum_{l=1}^4 \beta_{t,l} z_l(r) + \beta_{t,5} I\{r = 0\}$ , where  $r$  represent the aid per capita received during the previous month. We consider the projection CATE under this model and multiply all the estimates by the average number of pixels in a district to obtain a district-level effect.

Figure 5 displays the estimated CATEs for varying amounts of prior aid  $r$ , along with

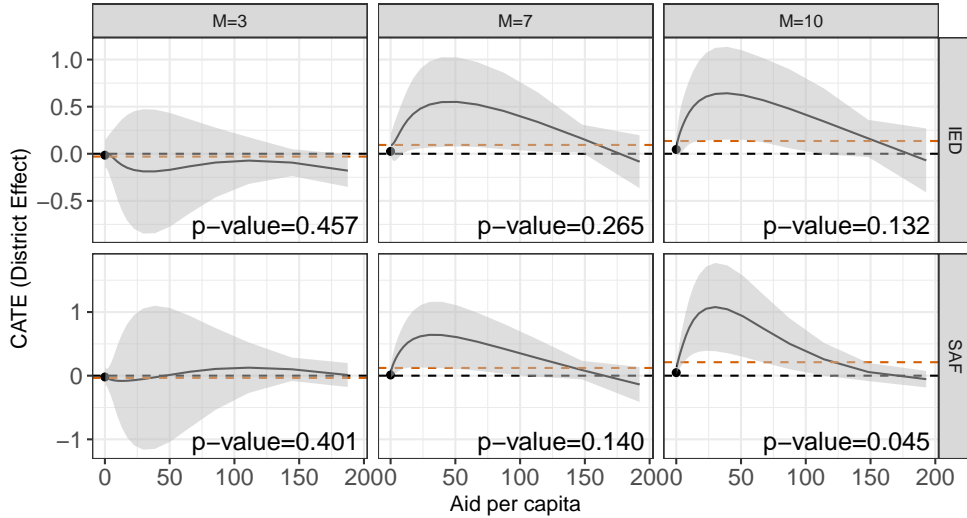


Figure 5: Estimated CATEs of increasing airstrike intensity on the number of insurgency attacks (Improvised Explosive Device or IED in the top panel, and Small Arms Fire or SAF in the bottom panel) for different values of aid per capita received in the previous month with the shaded region indicating the 95% confidence intervals. The red lines represent the estimated average treatment effects. The p-values correspond to tests for the overall heterogeneity effect.

the average treatment effect when the expected number of airstrikes over the previous  $M$  days increases from one to six per day. The p-values on the plot correspond to tests for the overall heterogeneous effect, with their calculation detailed in Section 2.6. The results show similar patterns for both IED and SAF attacks. The average treatment effects are positive for  $M = 7$  and  $M = 10$ , increasing as the intervention duration extends. For interventions lasting three days, the estimated CATE is relatively constant with the amount of economic aid per capita. However, for interventions lasting one week and 10 days, the estimated CATE increases as the amount of aid per capita rises from \$0 to \$25, followed by a gradual decline as the aid increases from \$25 to \$200. There is statistical evidence for the heterogeneous effect of increasing airstrikes on SAF attacks (p-value < 0.05), highlighting that areas with different levels of prior aid respond differently to increased airstrikes.

In sum, intensifying airstrikes for one week or more leads to a greater number of insurgent attacks. Among districts with relatively low levels of aid, those that have received

a greater amount of aid in the previous month tend to exhibit a stronger response to intensified airstrikes. However, when the amount of aid is sufficiently large, increasing the intensity of airstrikes appears to have a smaller effect on the number of insurgent attacks. We evaluate the robustness of our findings to alternative specifications in Sections [K.2](#) and [K.3](#).

## 5 Discussion

In this paper, we propose a method for analyzing treatment effect heterogeneity in spatio-temporal settings. The proposed method estimates the CATE without imposing structural assumptions about spillover and carryover effects. We establish asymptotic results for the proposed two-stage estimator based on stabilized weights, extending beyond existing work that considered only average treatment effects. We develop a new consistent estimator of the variance bound, which enables valid confidence intervals and shows improved finite-sample performance. In addition, we propose a statistical test of no heterogeneous treatment effects. The proposed estimator performs well in simulation studies and exhibits lower variance than the standard IPW estimator.

Our application shows that airstrikes increased insurgent attacks in the short term, even when aid had been disbursed in the prior month at substantial levels. Aid moderated these negative effects, but only after high and likely unsustainable levels of aid had been delivered. In addition, these large aid outlays were only sufficient to offset the increased attacks created by the airstrikes themselves. Taken together, our findings question whether aid and airstrikes, the two central planks in counterinsurgency, actually work to reduce short-term insurgent attacks.

There are several directions for future research. First, our asymptotic properties rely on the correct specification of the propensity score model. Future work could explore

estimators robust to model misspecification. Second, while we employed a parametric propensity score model, future research could consider semi-parametric or nonparametric models.

## References

- Abrevaya, J., Y.-C. Hsu, and R. P. Lieli (2015). Estimating conditional average treatment effects. *Journal of Business & Economic Statistics* 33(4), 485–505.
- Athey, S., J. Tibshirani, and S. Wager (2019). Generalized random forests.
- Bardaka, E., M. S. Delgado, and R. J. Florax (2018). Causal identification of transit-induced gentrification and spatial spillover effects: The case of the denver light rail. *Journal of Transport Geography* 71, 15–31.
- Bargagli-Stoffi, F. J., C. Tortù, and L. Forastiere (2020). Heterogeneous treatment and spillover effects under clustered network interference. *arXiv preprint arXiv:2008.00707*.
- Barkley, B. G., M. G. Hudgens, J. D. Clemens, M. Ali, and M. E. Emch (2020). Causal inference from observational studies with clustered interference, with application to a cholera vaccine study.
- Barrett, J. K., R. Henderson, and S. Rosthøj (2014). Doubly robust estimation of optimal dynamic treatment regimes. *Statistics in biosciences* 6(2), 244–260.
- Bianchi, N. and M. Giorcelli (2023). Reconstruction aid, public infrastructure, and economic development: the case of the marshall plan in italy. *The Journal of Economic History* 83(2), 501–537.
- Bind, M.-A. (2019). Causal modeling in environmental health. *Annual review of public health* 40, 23–43.

- Brunello, G., M. Fort, N. Schneeweis, and R. Winter-Ebmer (2016). The causal effect of education on health: What is the role of health behaviors? *Health economics* 25(3), 314–336.
- Christia, F., S. Zoumpoulis, M. Freedman, L. Yao, and A. Jadbabaie (2022). The effect of drone strikes on civilian communication: Evidence from yemen. *Political Science Research and Methods* 10(2), 419–427.
- Christiansen, R., M. Baumann, T. Kuemmerle, M. D. Mahecha, and J. Peters (2022). Toward causal inference for spatio-temporal data: conflict and forest loss in colombia. *Journal of the American Statistical Association* 117(538), 591–601.
- Credit, K. and M. Lehnert (2023). A structured comparison of causal machine learning methods to assess heterogeneous treatment effects in spatial data. *Journal of Geographical Systems*, 1–28.
- Crump, R. K., V. J. Hotz, G. W. Imbens, and O. A. Mitnik (2008). Nonparametric tests for treatment effect heterogeneity. *The Review of Economics and Statistics* 90(3), 389–405.
- Csörgő, M. (1968). On the strong law of large numbers and the central limit theorem for martingales. *Transactions of the American Mathematical Society* 131(1), 259–275.
- Ding, P., A. Feller, and L. Miratrix (2019). Decomposing treatment effect variation. *Journal of the American Statistical Association* 114(525), 304–317.
- Fan, Q., Y.-C. Hsu, R. P. Lieli, and Y. Zhang (2022). Estimation of conditional average treatment effects with high-dimensional data. *Journal of Business & Economic Statistics* 40(1), 313–327.

- Giffin, A., B. Reich, S. Yang, and A. Rappold (2023). Generalized propensity score approach to causal inference with spatial interference. *Biometrics* 79(3), 2220–2231.
- Hahn, P. R., J. S. Murray, and C. M. Carvalho (2020). Bayesian regression tree models for causal inference: Regularization, confounding, and heterogeneous effects (with discussion). *Bayesian Analysis* 15(3), 965–1056.
- Hirano, K., G. W. Imbens, and G. Ridder (2003). Efficient estimation of average treatment effects using the estimated propensity score. *Econometrica* 71(4), 1161–1189.
- Imai, K. and M. Ratkovic (2013, March). Estimating treatment effect heterogeneity in randomized program evaluation. *Annals of Applied Statistics* 7(1), 443–470.
- Jerzak, C. T., F. D. Johansson, and A. Daoud (2023, 11–14 Apr). Image-based treatment effect heterogeneity. In M. van der Schaar, C. Zhang, and D. Janzing (Eds.), *Proceedings of the Second Conference on Causal Learning and Reasoning*, Volume 213 of *Proceedings of Machine Learning Research*, pp. 531–552. PMLR.
- Kennedy, E. H. (2023). Towards optimal doubly robust estimation of heterogeneous causal effects. *Electronic Journal of Statistics* 17(2), 3008 – 3049.
- Kennedy, E. H., S. Lorch, and D. S. Small (2019). Robust causal inference with continuous instruments using the local instrumental variable curve. *Journal of the Royal Statistical Society Series b: Statistical Methodology* 81(1), 121–143.
- Kolak, M. and L. Anselin (2020). A spatial perspective on the econometrics of program evaluation. *International Regional Science Review* 43(1-2), 128–153.
- Meierrieks, D. and T. Gries (2013). Causality between terrorism and economic growth. *Journal of Peace Research* 50(1), 91–104.

- Moodie, E. E., B. Chakraborty, and M. S. Kramer (2012). Q-learning for estimating optimal dynamic treatment rules from observational data. *Canadian Journal of Statistics* 40(4), 629–645.
- Mukaigawara, M., G. Papadogeorgou, J. Lyall, and K. Imai (2023). Replication Data for: geocausal: R Package for Spatio-Temporal Causal Inference. Dataset.
- Mukaigawara, M., L. Zhou, G. Papadogeorgou, J. Lyall, and K. Imai (2025). *geocausal: Causal Inference with Spatio-Temporal Data*. R package version 0.3.4.
- Nunn, N. and N. Qian (2014). Us food aid and civil conflict. *American Economic Review* 104(6), 1630–66.
- Papadogeorgou, G., K. Imai, J. Lyall, and F. Li (2022). Causal inference with spatio-temporal data: estimating the effects of airstrikes on insurgent violence in iraq. *Journal of the Royal Statistical Society Series B: Statistical Methodology* 84(5), 1969–1999.
- Papadogeorgou, G., F. Mealli, and C. M. Zigler (2019). Causal inference with interfering units for cluster and population level treatment allocation programs. *Biometrics* 75(3), 778–787.
- Robins, J. M., M. A. Hernan, and B. Brumback (2000). Marginal structural models and causal inference in epidemiology. *Epidemiology*, 550–560.
- Sant’Anna, P. H. (2021). Nonparametric tests for treatment effect heterogeneity with duration outcomes. *Journal of Business & Economic Statistics* 39(3), 816–832.
- Sexton, R. (2016). Aid as a tool against insurgency: Evidence from contested and controlled territory in afghanistan. *American Political Science Review* 110(4), 731–749.

- Tchetgen Tchetgen, E. J., I. R. Fulcher, and I. Shpitser (2021). Auto-g-computation of causal effects on a network. *Journal of the American Statistical Association* 116(534), 833–844.
- van der Laan, M. J., S. Rose, et al. (2011). *Targeted learning: causal inference for observational and experimental data*, Volume 4. Springer.
- van der Vaart, A. W. (2010). Time series. *VU University Amsterdam, lecture notes*.
- Wager, S. and S. Athey (2018). Estimation and inference of heterogeneous treatment effects using random forests. *Journal of the American Statistical Association* 113(523), 1228–1242.
- Wang, L., A. Adiga, J. Chen, A. Sadilek, S. Venkatramanan, and M. Marathe (2022). Causalgnn: Causal-based graph neural networks for spatio-temporal epidemic forecasting. In *Proceedings of the AAAI conference on artificial intelligence*, Volume 36, pp. 12191–12199.
- Wang, Y. (2021). Causal inference under temporal and spatial interference. *arXiv preprint arXiv:2106.15074*.
- Wang, Y., C. Samii, H. Chang, and P. Aronow (2020). Design-based inference for spatial experiments with interference. *arXiv preprint arXiv:2010.13599*.
- Wodtke, G., K. Ard, C. Bulluck, K. White, and B. Priem (2022). Concentrated poverty, ambient air pollution, and child cognitive development. *Science Advances* 8(48), 1–19.
- Yang, Y., A. K. Kuchibhotla, and E. T. Tchetgen (2023). Forster-warmuth counterfactual regression: A unified learning approach. *arXiv preprint arXiv:2307.16798*.

Zhang, W. and K. Ning (2023). Spatiotemporal heterogeneities in the causal effects of mobility intervention policies during the covid-19 outbreak: A spatially interrupted time-series (SITS) analysis. *Annals of the American Association of Geographers* 113(5), 1112–1134.

Zigler, C. M., K. Watts, R. W. Yeh, Y. Wang, B. A. Coull, and F. Dominici (2013). Model feedback in bayesian propensity score estimation. *Biometrics* 69(1), 263–273.

# SUPPLEMENTARY APPENDIX FOR “ESTIMATING HETEROGENEOUS TREATMENT EFFECTS FOR SPATIO-TEMPORAL CAUSAL INFERENCE”

## Table of Contents

<b>A Table of notation</b>	<b>3</b>
<b>B Asymptotic properties of the IPW estimator</b>	
B.1 Regularity conditions . . . . .	4
B.2 Asymptotic normality . . . . .	6
B.3 Consistent estimation of variance bound for the IPW estimator . . . . .	7
B.4 Proof of Theorem A.1 . . . . .	7
B.5 Proof of Proposition A.1 . . . . .	9
B.6 Proof of Theorem A.2 . . . . .	10
B.7 Proof of Theorem A.3 . . . . .	17
B.8 Proof of Corollary A.1 . . . . .	17
<b>C Asymptotic properties of the Hájek estimator</b>	
C.1 Regularity conditions . . . . .	18
C.2 Asymptotic normality . . . . .	19
C.3 Consistent estimation of variance bound for the Hájek-estimator . . . . .	19
C.4 Proof of Theorem A.4 . . . . .	20
C.5 Proof of Proposition A.2 . . . . .	22
C.6 Proofs of Theorem 1, Theorem 2 and Proposition 1 . . . . .	22
<b>D Empirical performance of the proposed estimator</b>	
<b>E Statistical test of no heterogeneity</b>	
E.1 Proof of Lemma A.2 . . . . .	25

E.2	Proof of Theorem 3 . . . . .	25
<b>F</b>	<b>Extensions to dependent interventions</b>	<b>27</b>
<b>G</b>	<b>Extending proofs to adaptive interventions</b>	<b>28</b>
<b>H</b>	<b>Moderator variables and baseline density in simulations</b>	<b>29</b>
<b>I</b>	<b>Expected airstrike difference and aid distribution</b>	<b>29</b>
<b>J</b>	<b>Additional simulation results</b>	<b>30</b>
J.1	Monte Carlo approximation procedure . . . . .	31
J.2	The Hájek estimator . . . . .	31
J.3	The IPW estimator . . . . .	32
J.4	Efficiency due to the use of the estimated propensity score . . . . .	39
J.5	Efficiency comparison of IPW and Hájek estimators . . . . .	39
<b>K</b>	<b>Additional results for the empirical application</b>	<b>39</b>
K.1	Out-of-sample prediction for propensity scores . . . . .	39
K.2	Different moderator definitions . . . . .	43
K.3	Sensitivity to truncation levels of the estimated propensity scores . . . . .	44
K.4	Additional analysis for the binary moderator . . . . .	47
K.5	Additional analysis for adaptive interventions . . . . .	52

## A Table of notation

Definitions for notations used in the manuscript are given in Table A.1.

Table A.1: Table of Notation

	Symbol	Description
Paths	$\overline{\mathbf{W}}_t$	Treatment over the time periods $1, \dots, t$
	$\overline{\mathbf{w}}_t$	Realized treatment assignments for time periods $1 \dots, t$
	$\overline{\mathbf{Y}}_t$	Collection of all potential outcomes for time periods $1 \dots, t$
	$\overline{\mathbf{Y}}_t$	Observed outcomes for time periods $1 \dots, t$
Covariates	$\overline{\mathcal{X}}_t$	Collection of all potential values of confounders over the time periods $1, \dots, t$
	$\overline{\mathbf{X}}_t$	Observed confounders for time periods $1 \dots, t$
	$\mathbf{R}_t$	Observed values of moderators for time periods $1 \dots, t$
History	$\overline{H}_t$	Observed history preceding the treatment at time $t + 1$
	$\overline{H}_t^*$	Complete history including all counterfactual values
Intervention	$M$	The number of time periods over which we intervene
	$h$	Poisson point process intensity defining the stochastic intervention
Estimands	$N_{it}(F_{\mathbf{h}})$	The expected number of outcome events in pixel $S_i$ at time $t$ for an intervention with intensity $\mathbf{h}$
	$\tau_{it}(F_{\mathbf{h}'}, F_{\mathbf{h}''})$	Expected difference in the number of outcome events for interventions $F_{\mathbf{h}'}$ over interventions $F_{\mathbf{h}''}$ at time $t$ in pixel $S_i$
	$\tau_{t, \mathbf{h}', \mathbf{h}''}(\mathbf{r})$	The conditional average treatment effect of intervention with intensity $\mathbf{h}'$ v.s. intervention with intensity $\mathbf{h}''$ for time period $t$
	$\tau_{t, \mathbf{h}', \mathbf{h}''}^{\text{Proj.}}(\mathbf{r}; \boldsymbol{\beta}_t)$	The projected conditional average treatment effect for time period $t$
	$\tau_{\mathbf{h}', \mathbf{h}''}^{\text{Proj.}}(\mathbf{r}; \boldsymbol{\beta}_1, \dots, \boldsymbol{\beta}_T)$	Conditional average treatment effect of intervention $F_{\mathbf{h}'}$ over $F_{\mathbf{h}''}$
Estimators	$\hat{\boldsymbol{\beta}}^I$	The IPW estimator for $\boldsymbol{\beta}_t$
	$\hat{\boldsymbol{\beta}}^H$	The Hajek estimator for $\boldsymbol{\beta}_t$

## B Asymptotic properties of the IPW estimator

In this section, we present the asymptotic properties of the IPW estimator. We first formally present the regularity conditions (Section B.1) and then show the asymptotic normality, the variance bound, and its consistent estimation (Section B.2 and Section B.3).

Those results are similar to the results for the Hájek estimator shown in Section 2.5.

## B.1 Regularity conditions

We first state the regularity assumptions for establishing the asymptotic normality of the IPW estimator when the true propensity score is known. For distribution  $F_{\mathbf{h}''}$  and  $F_{\mathbf{h}'}$ , we define the IPW pseudo-outcome contrasts as  $\tilde{\tau}_{it}^I(F_{\mathbf{h}'}, F_{\mathbf{h}''}; \hat{\gamma}) = \tilde{Y}_{it}^I(F_{\mathbf{h}''}; \hat{\gamma}) - \tilde{Y}_{it}^I(F_{\mathbf{h}'}; \hat{\gamma})$ . For notational simplicity, we denote  $\tilde{\tau}_{it}^I(F_{\mathbf{h}'}, F_{\mathbf{h}''}; \hat{\gamma})$  as  $\tilde{\tau}_{it, \mathbf{h}', \mathbf{h}''}^I(\hat{\gamma})$ , and let

$$\tilde{\boldsymbol{\tau}}_t^I(\hat{\gamma}) = (\tilde{\tau}_{1t, \mathbf{h}', \mathbf{h}''}^I(\hat{\gamma}), \dots, \tilde{\tau}_{pt, \mathbf{h}', \mathbf{h}''}^I(\hat{\gamma}))^\top$$

represent the vector of pseudo-outcome contrasts for the  $p$  pixels at time period  $t$ . These contrasts are the IPW analogue of the Hájek pseudo-outcomes defined in Section 2.4.

**Assumption A.1** (Regularity conditions for the IPW estimator with the true propensity score). *The following two conditions hold.*

- (a) *(Bounded outcome and covariates)* There exist positive constants  $\delta_Y, \delta_z < \infty$  such that  $N_\Omega(Y_t) < \delta_Y$  and  $|z_j(\mathbf{R}_t)| < \delta_z$  for all  $j \in \{1, \dots, L\}$ ,  $Y_t \in \bar{\mathcal{Y}}_T$  and  $\mathbf{R}_t \in \bar{\mathcal{X}}_T$ .
- (b) *(Non-singularity and asymptotic variance)* For all  $t$ ,  $\mathbf{Z}_t^\top \mathbf{Z}_t$  is non-singular and there exists a positive definite matrix  $\tilde{\mathbf{V}}^I$  such that

$$\frac{1}{T - M + 1} \sum_{t=M}^T \mathbb{V}[\mathbf{A}_t \mid \bar{H}_{t-M}^*] \xrightarrow{p} \tilde{\mathbf{V}}^I$$

as  $T \rightarrow \infty$ , where  $\mathbf{A}_t = (\mathbf{Z}_t^\top \mathbf{Z}_t)^{-1} \mathbf{Z}_t^\top \tilde{\boldsymbol{\tau}}_t^I(\gamma^*)$

Assumption A.1.(a) states that there exist uniform upper bounds on the number of outcome events and the absolute value of the moderator over all time period. In our empirical application, it is reasonable to assume that the number of insurgent attacks occurring in Iraq and the amount of aid does not diverge to infinity as  $t$  increases. Assumption A.1.(b) requires that the moderators for each time period are linearly independent and that the sequence of covariance matrices converges to a positive definite matrix. The assumption about the convergence of the covariance matrix is relatively mild, given that the random vector  $\mathbf{A}_t$  is bounded above and bounded away from  $\mathbf{0}$ .

The following two sets of assumptions are needed for the asymptotic normality of the IPW estimator with the estimated propensity score. Those assumptions are also made in Papadogeorgou et al. (2022). The first set of assumptions is about the behavior of the propensity score model.

**Assumption A.2** (Regularity conditions for the propensity score model). *Assume that the parametric form of the propensity score indexed by  $\gamma$ ,  $f(W_t = w_t \mid \bar{H}_{t-1}; \gamma)$ , is correctly specified and differentiable with respect to  $\gamma \in \mathbb{R}^K$ , and let*

$$\psi(W_t, \bar{H}_{t-1}; \gamma) = \frac{\partial}{\partial \gamma} \log f(W_t = w_t \mid \bar{H}_{t-1} = \bar{h}_{t-1}; \gamma)$$

*be twice continuously differentiable score functions. Let  $\gamma^*$  denote the true values of the parameters, where  $\gamma^*$  is in an open subset of the Euclidean space. Denote  $\mathcal{F}_t = \bar{H}_{t-M+1}^*$ . We assume that the following conditions hold:*

1. (a)  $\mathbb{E}_{\gamma^*} \left[ \|\psi(W_t, \bar{H}_{t-1}; \gamma^*)\|^2 \right] < \infty,$

(b) *There exists a positive definite matrix  $\mathbf{V}_{ps}$  such that*

$$\frac{1}{T} \sum_{t=1}^T \mathbb{E}_{\gamma^*} \left( \psi(W_t, \bar{H}_{t-1}; \gamma^*) \psi(W_t, \bar{H}_{t-1}; \gamma^*)^\top \mid \mathcal{F}_{t-1} \right) \xrightarrow{p} \mathbf{V}_{ps}$$

(c)  $\frac{1}{T} \sum_{t=1}^T \mathbb{E}_{\gamma^*} \left[ \|\psi(W_t, \bar{H}_{t-1}; \gamma^*)\|^2 I \left( \|\psi(W_t, \bar{H}_{t-1}; \gamma^*)\| > \epsilon \sqrt{T} \right) \mid \mathcal{F}_{t-1} \right] \xrightarrow{p} 0,$  for all  $\epsilon > 0$ , as  $T \rightarrow \infty$ .

2. *For all  $k, j$ , if we denote the  $k^{\text{th}}$  element of the  $\psi(w_t, \bar{H}_{t-1}; \gamma)$  vector by  $\psi_k(w_t, \bar{H}_{t-1}; \gamma)$  and  $P_{kjt} = \frac{\partial}{\partial \gamma_j} \psi_k(W_t, \bar{H}_{t-1}; \gamma) \mid_{\gamma^*}$ , then  $\mathbb{E}_{\gamma^*} [|P_{kjt}|] < \infty$  and there exists  $0 < r_{kj} \leq 2$  such that  $\sum_{t=1}^T \frac{1}{t^{r_{kj}}} \mathbb{E}_{\gamma^*} (|P_{kjt} - \mathbb{E}_{\gamma^*}(P_{kjt} \mid \mathcal{F}_{t-1})|^{r_{kj}} \mid \mathcal{F}_{t-1}) \xrightarrow{p} 0$*

3. *There exists an integrable function  $\ddot{\psi}(w_t, \bar{h}_{t-1})$  such that  $\ddot{\psi}(w_t, \bar{h}_{t-1})$  dominates the second partial derivatives of  $\psi(w_t, \bar{h}_{t-1}; \gamma)$  in a neighborhood of  $\gamma^*$  for all  $(w_t, \bar{h}_{t-1})$*

Assumption A.2 states that the model is correctly specified and the score function is bounded in the  $L^2$ -norm. That is, the model has finite variance, which is a mild requirement under standard positivity and common parametric models. Moreover, the expectation of the product of the score function averaged over all time periods stabilizes to a specific positive definite matrix. This condition guarantees that the asymptotic variance is well-defined and nonsingular. The Lindeberg-type tail condition in part 1(c) rules out rare, extremely large score contributions. This is a usual device for martingale central limit theorems in time-series settings. The assumption also limits the extent to which the derivative of the score function varies around its conditional expectation. Lastly, the assumption ensures that the second partial derivatives of the score function are bounded in magnitude by an integrable function, which controls their growth and guarantees stability in a neighborhood of  $\gamma^*$ . Overall, these assumptions represent standard regularity conditions of large-sample M-estimation with dependent data (smooth model, bounded moments, and stable information), and they are typically satisfied by common propensity score specifications.

**Assumption A.3** (Regularity conditions on the score function of propensity score model for IPW estimators). Let  $\tilde{\boldsymbol{\tau}}_t^I(\boldsymbol{\gamma})$  denote the pseudo-effect depend on the parameter  $\boldsymbol{\gamma}$ . For

$$s(\bar{H}_{t-1}, W_t, Y_t; \boldsymbol{\gamma}) = (\mathbf{Z}_t^\top \mathbf{Z}_t)^{-1} \mathbf{Z}_t^\top \tilde{\boldsymbol{\tau}}_t^I(\boldsymbol{\gamma}) - \boldsymbol{\beta}_t^*,$$

and a propensity score function  $\psi(W_t, \bar{H}_{t-1}; \boldsymbol{\gamma})$  satisfying Assumption A.2, the following conditions hold.

(a) There exists  $\mathbf{U} \in \mathbb{R}^{K \times L}$  such that

$$\frac{1}{T - M + 1} \sum_{t=M}^T \mathbb{E}_{\boldsymbol{\gamma}^*} [\psi(W_t, \bar{H}_{t-1}; \boldsymbol{\gamma}^*) s(\bar{H}_{t-1}, W_t, Y_t; \boldsymbol{\gamma}^*)^\top \mid \bar{H}_{t-M}^*] \xrightarrow{p} \mathbf{U}, \text{ and}$$

$$\mathbf{V}^* = \begin{bmatrix} \tilde{\mathbf{V}}^I & \mathbf{U}^\top \\ \mathbf{U} & \mathbf{V}_{ps} \end{bmatrix} \text{ is positive definite.}$$

(b) If  $P_{jt} = \frac{\partial}{\partial \gamma_j} s(\bar{H}_{t-1}, W_t, Y_t; \boldsymbol{\gamma}) \Big|_{\boldsymbol{\gamma}^*}$ , where  $\gamma_j$  is the  $j^{\text{th}}$  entry of  $\boldsymbol{\gamma}$ , then there exists  $r_j \in (0, 2]$  such that

$$\frac{1}{T - M + 1} \sum_{t=M}^T \frac{1}{t^{r_j}} (|P_{jt} - \mathbb{E}_{\boldsymbol{\gamma}^*} [P_{jt} \mid \bar{H}_{t-M}^*]|) \xrightarrow{p} 0.$$

Assumption A.3 regulates the behavior of the propensity score  $\psi(W_t, \bar{H}_{t-1}; \boldsymbol{\gamma})$  and the function  $s(\bar{H}_{t-1}, W_t, Y_t; \boldsymbol{\gamma})$ . Specifically, it states that the average expectation of the outer product of  $s(\bar{H}_{t-1}, W_t, Y_t; \boldsymbol{\gamma})$  and  $s(\bar{H}_{t-1}, W_t, Y_t; \boldsymbol{\gamma})$  converges to a matrix as  $T$  grows and  $\mathbf{V}^*$  is positive definite. This is the common requirement from large-sample M-estimation, which ensures that the limiting covariance matrix is nonsingular. Furthermore, part (b) imposes a mild condition that the derivative of  $s(\bar{H}_{t-1}, W_t, Y_t; \boldsymbol{\gamma})$  does not fluctuate wildly on average.

## B.2 Asymptotic normality

We now establish the asymptotic normality of the IPW estimator using the true and estimated propensity score.

**Theorem A.1** (Asymptotic normality of the IPW estimator using the true propensity score). Suppose that Assumptions 1, 2, and A.1. Then

$$\frac{1}{\sqrt{T - M + 1}} \sum_{t=M}^T (\hat{\boldsymbol{\beta}}_t^I - \boldsymbol{\beta}_t^*) \xrightarrow{d} N(\mathbf{0}, \tilde{\mathbf{V}}^I),$$

where  $\tilde{\mathbf{V}}^I$  represents the probability limit of  $\frac{1}{T - M + 1} \sum_{t=M}^T \mathbf{V}_t^I$  as  $T \rightarrow \infty$  with  $\mathbf{V}_t^I = \mathbb{V}[\hat{\boldsymbol{\beta}}_t^I \mid \bar{H}_{t-M}^*]$  for  $t \geq M$ .

**Theorem A.2** (Asymptotic normality of the IPW estimator using the estimated propensity score). *Suppose that Assumptions 1, 2, A.1, A.2, and A.3 hold. Let  $\hat{\gamma}$  be the estimate obtained by solving the estimating equation  $\sum_{t=M}^T \psi(W_t, \bar{H}_{t-1}; \gamma) = 0$ , where  $\psi(W_t, \bar{H}_{t-1}; \gamma)$  is defined in Assumption A.2. Then, as  $T \rightarrow \infty$ , we have*

$$\frac{1}{\sqrt{T-M+1}} \sum_{t=M}^T (\hat{\beta}_t^I - \beta_t^*) \xrightarrow{d} N(\mathbf{0}, \mathbf{V}^I).$$

**Theorem A.3** (Asymptotic efficiency of the IPW estimator using the estimated propensity score). *If the propensity score model is correctly specified, the estimator  $\frac{1}{T-M+1} \sum_{t=M}^T \hat{\beta}_t^H$  based on the estimated propensity score has an asymptotic variance that is no greater than the asymptotic variance of the same estimator using the known propensity score. That is, for  $\tilde{\mathbf{V}}^I$  defined in Theorem A.1 and  $\mathbf{V}^I$  defined in Theorem A.2,  $(\tilde{\mathbf{V}}^I - \mathbf{V}^I)$  is a positive semidefinite matrix.*

### B.3 Consistent estimation of variance bound for the IPW estimator

Similarly to the case of the Hájek estimator, it is not possible to consistently estimate the asymptotic variance of the IPW estimator. Thus, we consider a variance bound and propose a consistent estimator.

**Proposition A.1** (Consistent estimator of the variance upper bound). *Suppose that Assumptions 1, 2, and A.1 hold. Let*

$$\hat{\mathbf{V}}^{I*} = \frac{1}{T-M+1} \sum_{t=M}^T \hat{\beta}_t^I \hat{\beta}_t^{I\top}.$$

*Then  $\hat{\mathbf{V}}^{I*}$  is a consistent estimator of  $\mathbf{V}^{I*}$ .*

**Corollary A.1** (Consistent estimator of the variance upper bound using the estimated propensity score). *Suppose that Assumptions 1, 2, A.1, A.2, and A.3 hold. Moreover, let*

$$\hat{\mathbf{V}}^I = \frac{1}{T-M+1} \sum_{t=M}^T \hat{\beta}_t^I \hat{\beta}_t^{I\top}$$

*Then,  $\hat{\mathbf{V}}^I$  is a consistent estimator of  $\mathbf{V}^{I*}$ .*

### B.4 Proof of Theorem A.1

We will apply Theorem A.2 of Papadogeorgou et al. (2022), which is a multivariate version of Theorem 4.16 of van der Vaart (2010). Define  $\mathbf{A}_t^* = \mathbf{A}_t - \beta_t^*$ . We need to verify the

existence of a filtration  $\mathcal{F}_t$  such that the following conditions hold:

1.  $\mathbb{E}_{\beta_t^*}[\mathbf{A}_t^* | \mathcal{F}_{t-1}] = 0$  and  $\mathbb{E}_{\beta_t^*}[\|\mathbf{A}_t^*\|] < \infty$ .
2. There exists a positive definite  $\tilde{\mathbf{V}}^I$  such that

$$\frac{1}{T - M + 1} \sum_{t=M}^T \mathbb{E}_{\beta_t^*}[\mathbf{A}_t^* \mathbf{A}_t^{*\top} | \mathcal{F}_{t-1}] \xrightarrow{p} \tilde{\mathbf{V}}^I$$

- 3.

$$\frac{1}{T - M + 1} \sum_{t=M}^T \mathbb{E}_{\beta_t^*} \left[ \|\mathbf{A}_t^*\|^2 I \left( \|\mathbf{A}_t^*\| > \epsilon \sqrt{T} \right) \mid \mathcal{F}_{t-1} \right] \xrightarrow{p} 0$$

as  $T \rightarrow \infty$  for all  $\epsilon > 0$ .

To check the first condition, take  $\mathcal{F}_t = \overline{H}_{t-M+1}^*$ . Then for a stochastic intervention  $F_h$  over  $M$  time periods,

$$\begin{aligned} & \mathbb{E}_{\beta_t^*} \left[ \tilde{Y}_{it}^I(F_h; \hat{\gamma}) \mid \mathcal{F}_{t-1} \right] \\ &= \mathbb{E}_{\beta_t^*} \left[ \prod_{j=t-M+1}^t \frac{f_h(W_j)}{e_j(W_j)} N_{S_i}(Y_t) \mid \mathcal{F}_{t-1} \right] \\ &= \int_{\mathcal{W}^M} \prod_{j=t-M+1}^t \frac{f_h(w_j)}{e_j(w_j)} N_{S_i}(Y_t(\overline{\mathbf{W}}_{t-M}, w_{t-M+1}, \dots, w_t)) \times \\ & \quad f(w_{t-M+1} \mid \overline{H}_{t-M}^*) f(w_{t-M+2} \mid \overline{H}_{t-M+1}^*) \dots f(w_t \mid \overline{H}_{t-1}^*) d\mathbf{w}_{(t-M+1):t} \\ &= \int_{\mathcal{W}^M} \prod_{j=t-M+1}^t \frac{f_h(w_j)}{e_j(w_j)} N_{S_i}(Y_t(\overline{\mathbf{W}}_{t-M}, w_{t-M+1}, \dots, w_t)) \prod_{j=t-M+1}^t e_j(w_j) d\mathbf{w}_{(t-M+1):t} \\ &= \int_{\mathcal{W}^M} N_{S_i}(Y_t) \prod_{j=t-M+1}^t f_h(w_j) d\mathbf{w}_{(t-M+1):t} \\ &= N_{it}(F_h), \end{aligned}$$

where the third equality follows from Assumption 1. Let  $\mathbf{N}_t(F_h) = (N_{1t}(F_h), \dots, N_{pt}(F_h))$ , and  $\tilde{\mathbf{Y}}_t^I(F_h; \gamma) = \left( \tilde{Y}_{1t}^I(F_h; \gamma), \dots, \tilde{Y}_{pt}^I(F_h; \gamma) \right)^\top$ . Then

$$\begin{aligned} (\mathbf{Z}_t^\top \mathbf{Z}_t)^{-1} \mathbf{Z}_t^\top \mathbb{E}_{\beta_t^*}[\tilde{\boldsymbol{\tau}}_t^I(\gamma^*) \mid \mathcal{F}_{t-1}] &= (\mathbf{Z}_t^\top \mathbf{Z}_t)^{-1} \mathbf{Z}_t^\top \mathbb{E}_{\beta_t^*} \left[ \tilde{\mathbf{Y}}_t^I(F_{h''}; \gamma) - \tilde{\mathbf{Y}}_t^I(F_{h'}; \gamma) \mid \mathcal{F}_{t-1} \right] \\ &= (\mathbf{Z}_t^\top \mathbf{Z}_t)^{-1} \mathbf{Z}_t^\top (\mathbf{N}_t(F_{h''}) - \mathbf{N}_t(F_{h'})) \\ &= \beta_t^*. \end{aligned}$$

Thus,

$$\begin{aligned}
\mathbb{E}_{\beta_t^*}[\mathbf{A}_t^* \mid \mathcal{F}_{t-1}] &= (\mathbf{Z}_t^\top \mathbf{Z}_t)^{-1} \mathbf{Z}_t^\top \mathbb{E}_{\beta_t^*}[\tilde{\boldsymbol{\tau}}_t^I(\boldsymbol{\gamma}^*) - \boldsymbol{\beta}_t^* \mid \mathcal{F}_{t-1}] \\
&= \boldsymbol{\beta}_t^* - \boldsymbol{\beta}_t^* \\
&= \mathbf{0}
\end{aligned}$$

Moreover, by Assumptions 2 and A.1(a), each term in  $\mathbf{A}_t^*$  is bounded, and so is  $\mathbb{E}_{\beta_t^*}[\|\mathbf{A}_t^*\|]$ .

Next, Condition 2 is satisfied by Assumption A.1(b), while Condition 3 follows from the fact that  $\mathbb{E}_{\beta_t^*}[\|\mathbf{A}_t^*\|^2 \mid \mathcal{F}_{t-1}]$  is bounded. Hence, as  $T \rightarrow \infty$ , we have,

$$\frac{1}{\sqrt{T-M+1}} \sum_{t=M}^T \mathbf{A}_t^* \xrightarrow{d} N(\mathbf{0}, \mathbf{V})$$

and

$$\frac{1}{T-M+1} \sum_{t=M}^T \mathbb{E}_{\beta_t^*}[\mathbf{A}_t^* \mathbf{A}_t^{*\top} \mid \mathcal{F}_{t-1}] = \frac{1}{T-M+1} \sum_{t=M}^T \mathbb{V}[\mathbf{A}_t \mid \mathcal{F}_{t-1}] \xrightarrow{p} \tilde{\mathbf{V}}^I.$$

Note that

$$\frac{1}{\sqrt{T-M+1}} \sum_{t=M}^T \mathbf{A}_t^* = \frac{1}{\sqrt{T-M+1}} \sum_{t=M}^T (\hat{\boldsymbol{\beta}}_t^I - \boldsymbol{\beta}_t^*)$$

Thus, as  $T \rightarrow \infty$ , we have:

$$\frac{1}{\sqrt{T-M+1}} \sum_{t=M}^T (\hat{\boldsymbol{\beta}}_t^I - \boldsymbol{\beta}_t^*) \xrightarrow{d} N(\mathbf{0}, \tilde{\mathbf{V}}^I).$$

□

## B.5 Proof of Proposition A.1

Let  $\hat{\mathbf{V}}_t^I = \hat{\boldsymbol{\beta}}_t^I \hat{\boldsymbol{\beta}}_t^{I\top}$  and  $\mathbf{V}_t^I = \mathbb{E}_{\beta_t^*}[\hat{\boldsymbol{\beta}}_t^I \hat{\boldsymbol{\beta}}_t^{I\top} \mid \bar{H}_{t-M}^*]$ . Consider the sequence  $\hat{\mathbf{V}}_t^I - \mathbf{V}_t^I$ . Note that  $\mathbb{E}[\hat{\mathbf{V}}_t^I - \mathbf{V}_t^I \mid \bar{H}_{t-M}^*] = \mathbf{0}$ . Since  $\hat{\mathbf{V}}_t^I - \mathbf{V}_t^{I*}$  is bounded,  $\mathbb{E}|\hat{\mathbf{V}}_t^I - \mathbf{V}_t^{I*}| < \infty$ . Also,  $\sum_{t=1}^\infty t^{-2} \mathbb{E}[(\hat{\mathbf{V}}_t^I - \mathbf{V}_t^{I*})^2] < \infty$ . Then, Theorem 1 of Csörgő (1968) implies:

$$\frac{1}{T-M+1} \sum_{t=M}^T (\hat{\mathbf{V}}_t^I - \mathbf{V}_t^{I*}) = \frac{1}{T-M+1} \sum_{t=M}^T \hat{\mathbf{V}}_t^I - \frac{1}{T-M+1} \sum_{t=M}^T \mathbf{V}_t^{I*} \xrightarrow{p} \mathbf{0}.$$

Since  $\mathbf{V}^{I*}$  is the probability limit of  $\frac{1}{T-M+1} \sum_{t=M}^T \mathbf{V}_t^{I*}$  as  $T \rightarrow \infty$ , we have  $\frac{1}{T-M+1} \sum_{t=M}^T \hat{\mathbf{V}}_t^I \xrightarrow{p} \mathbf{V}^{I*}$ .  $\square$

## B.6 Proof of Theorem A.2

We begin by introducing the following lemma. The proof of this lemma is omitted because it is similar to that of Lemma A.2 given in Papadogeorgou et al. (2022).

**Lemma A.1.** *Suppose that Assumption 1 holds. Let  $\psi(w_t, \bar{h}_{t-1}; \gamma)$  be the score functions of a propensity score model that satisfy Assumption A.2. Recall the definition of  $s(\bar{H}_{t-1}, W_t, Y_t; \gamma)$  given in Assumption A.3. Let  $\mathcal{F}_t = \bar{H}_{t-M+1}^*$ . Then, we have*

1.  $\mathbb{E}_{\gamma^*} [s(\bar{H}_{t-1}, W_t, Y_t; \gamma^*) \psi(W_t, \bar{H}_{t-1}; \gamma^*)^\top \mid \mathcal{F}_{t-1}] = -\mathbb{E}_{\gamma^*} \left[ \frac{\partial}{\partial \gamma^\top} s(\bar{H}_{t-1}, W_t, Y_t; \gamma^*) \Big|_{\gamma^*} \Big| \mathcal{F}_{t-1} \right]$ .
2.  $\frac{\partial}{\partial \gamma_l} s(\bar{h}_{t-1}, w_t, y_t; \gamma) = -(\mathbf{Z}_t^\top \mathbf{Z}_t)^{-1} \mathbf{Z}_t^\top \tilde{\boldsymbol{\tau}}_t^I \sum_{j=t-M+1}^t \psi_l(w_t, \bar{h}_{t-1}; \gamma)$ , where  $\psi_l(w_t, \bar{h}_{t-1}; \gamma)$  is the  $l^{\text{th}}$  element of  $\psi(w_t, \bar{h}_{t-1}; \gamma)$ .
- 3.

$$\begin{aligned} & \frac{\partial}{\partial \gamma_m} \frac{\partial}{\partial \gamma_l} s(\bar{h}_{t-1}, w_t, y_t; \gamma) \\ &= -(\mathbf{Z}_t^\top \mathbf{Z}_t)^{-1} \mathbf{Z}_t^\top \tilde{\boldsymbol{\tau}}_t^I \left\{ \left[ \sum_{j=t-M+1}^t \frac{\partial}{\partial \gamma_m} \psi_l(W_t, \bar{H}_{t-1}; \gamma) \right] \right. \\ & \quad \left. - \left[ \sum_{j=t-M+1}^t \psi_m(W_t, \bar{H}_{t-1}; \gamma) \right] \left[ \sum_{j=t-M+1}^t \psi_l(W_t, \bar{H}_{t-1}; \gamma) \right] \right\}. \end{aligned}$$

**Proof of Theorem A.2.** Let  $\boldsymbol{\gamma} \in \mathbb{R}^K$  be the parameters in the propensity score model whose score function is denoted by  $\psi(w_t, \bar{h}_{t-1}; \boldsymbol{\gamma})$ . Consider the following estimating equations:

$$s(\bar{H}_{t-1}, W_t, Y_t; \boldsymbol{\theta}) = \begin{pmatrix} \mathbf{A}_t^* - \boldsymbol{\mu} \\ \psi(W_t, \bar{H}_{t-1}; \boldsymbol{\gamma}) \end{pmatrix}$$

where  $\mathbf{A}_t^* = (\mathbf{Z}_t^\top \mathbf{Z}_t)^{-1} \mathbf{Z}_t^\top \tilde{\boldsymbol{\tau}}_t^I(\boldsymbol{\gamma}) - \boldsymbol{\beta}_t^*$  and  $\boldsymbol{\theta}^\top = (\boldsymbol{\mu}^\top, \boldsymbol{\gamma}^\top)$ . We apply Theorem A.3 of Papadogeorgou et al. (2022) to establish the asymptotic normality of the estimating equations. This requires verifying the following conditions.

1. (a)  $\mathbb{E}_{\boldsymbol{\theta}^*} [s(\bar{H}_{t-1}, W_t, Y_t; \boldsymbol{\theta}^*) \mid \mathcal{F}_{t-1}] = 0$  and  $\mathbb{E}_{\boldsymbol{\theta}^*} [||s(\bar{H}_{t-1}, W_t, Y_t; \boldsymbol{\theta}^*)||] < \infty$ .
- (b) There exists a positive definite  $\mathbf{V}_a$  such that, as  $T \rightarrow \infty$ ,

$$\frac{1}{T-M+1} \sum_{t=M}^T \mathbb{E}_{\boldsymbol{\theta}^*} [s(\bar{H}_{t-1}, W_t, Y_t; \boldsymbol{\theta}^*) s(\bar{H}_{t-1}, W_t, Y_t; \boldsymbol{\theta}^*)^\top \mid \mathcal{F}_{t-1}] \xrightarrow{p} \mathbf{V}_a$$

(c) As  $T \rightarrow \infty$  for all  $\epsilon > 0$ , we have:

$$\frac{1}{T - M + 1} \sum_{t=M}^T \mathbb{E}_{\boldsymbol{\theta}^*} \left[ \|s(\bar{H}_{t-1}, W_t, Y_t; \boldsymbol{\theta}^*)\|^2 I(\|s(\bar{H}_{t-1}, W_t, Y_t; \boldsymbol{\theta}^*)\| > \epsilon\sqrt{T}) \mid \mathcal{F}_{t-1} \right] \xrightarrow{p} 0$$

2. As  $T \rightarrow \infty$ , we have:

$$\frac{1}{T} \mathbb{E}_{\boldsymbol{\theta}^*} \left[ \frac{\partial}{\partial \boldsymbol{\theta}^\top} s(\bar{H}_{t-1}, W_t, Y_t; \boldsymbol{\theta}) \Big|_{\boldsymbol{\theta}^*} \mid \mathcal{F}_{t-1} \right] \xrightarrow{p} \mathbf{V}_d$$

where  $\mathbf{V}_d$  is invertible.

3. For all  $k, j$ , if we denote  $P_{kjt} = \frac{\partial}{\partial \theta_j} s_k(\bar{H}_{t-1}, W_t, Y_t; \boldsymbol{\theta}) \Big|_{\boldsymbol{\theta}^*}$ , we have  $\mathbb{E}_{\boldsymbol{\theta}^*} [|P_{kjt}|] < \infty$ , and there exists  $0 < r_{kj} \leq 2$  such that  $\sum_{t=1}^T \frac{1}{t^{r_{kj}}} \mathbb{E}_{\boldsymbol{\theta}^*} [|P_{kjt} - \mathbb{E}_{\boldsymbol{\theta}^*} [P_{kjt} \mid \mathcal{F}_{t-1}]|^{r_{kj}} \mid \mathcal{F}_{t-1}] \xrightarrow{p} 0$  as  $T \rightarrow \infty$ .

4. There exists an integrable function  $\ddot{\psi}(x)$  such that  $\ddot{\psi}(x)$  dominates second partial derivatives of  $s(\bar{H}_{t-1}, W_t, Y_t; \boldsymbol{\theta})$  in a neighborhood of  $\boldsymbol{\theta}^*$  for all  $\{\bar{h}_{t-1}, w_t, y_t\}$

We check each of these four conditions in turn.

**Condition 1.** Recall the definition of  $\mathbf{A}_t$  given in the proof of Theorem A.1 under the true value of  $\boldsymbol{\gamma}$ . As shown in Appendix B.4, we have  $\mathbb{E}_{\boldsymbol{\theta}^*} [\mathbf{A}_t^* \mid \mathcal{F}_{t-1}] = 0$ . Therefore, under  $\boldsymbol{\theta}^{*\top} = (\boldsymbol{\mu}^{*\top}, \boldsymbol{\gamma}^{*\top}) = (\mathbf{0}^\top, \boldsymbol{\gamma}^{*\top})$ , we have

$$\mathbb{E}_{\boldsymbol{\theta}^*} [s(\bar{H}_{t-1}, W_t, Y_t; \boldsymbol{\theta}^*) \mid \mathcal{F}_{t-1}] = 0.$$

According to Lemma A.1 of Papadogeorgou et al. (2022), we have  $\mathbb{E}_{\boldsymbol{\gamma}^*} [\psi(W_t, \bar{H}_{t-1}; \boldsymbol{\gamma}^*) \mid \mathcal{F}_{t-1}] = 0$ . Therefore,  $\mathbb{E}_{\boldsymbol{\theta}^*} [s(\bar{H}_{t-1}, W_t, Y_t; \boldsymbol{\theta}^*) \mid \mathcal{F}_{t-1}] = 0$ . Moreover, by Jensen's inequality, we have

$$\begin{aligned} \mathbb{E}_{\boldsymbol{\theta}^*} [\|s(\bar{H}_{t-1}, W_t, Y_t; \boldsymbol{\theta}^*)\|^2] &\leq \mathbb{E}_{\boldsymbol{\theta}^*} [\|s(\bar{H}_{t-1}, W_t, Y_t; \boldsymbol{\theta}^*)\|^2] \\ &\leq \mathbb{E}_{\boldsymbol{\theta}^*} [\|\mathbf{A}_t^*\|^2] + \mathbb{E}_{\boldsymbol{\theta}^*} [\|\psi(W_t, \bar{H}_{t-1}; \boldsymbol{\gamma}^*)\|^2]. \end{aligned}$$

The first term is bounded due to Assumption A.1.(a) and the second term is bounded due to Assumption A.2.1. Thus,  $\mathbb{E}_{\boldsymbol{\theta}^*} [\|s(\bar{H}_{t-1}, W_t, Y_t; \boldsymbol{\theta}^*)\|] < \infty$ . Note that

$$\begin{aligned} &\mathbb{E}_{\boldsymbol{\theta}^*} [s(\bar{H}_{t-1}, W_t, Y_t; \boldsymbol{\theta}^*) s(\bar{H}_{t-1}, W_t, Y_t; \boldsymbol{\theta}^*)^\top \mid \mathcal{F}_{t-1}] \\ &= \begin{bmatrix} \mathbb{E}_{\boldsymbol{\theta}^*} [\mathbf{A}_t^* \mathbf{A}_t^{*\top} \mid \mathcal{F}_{t-1}] & \mathbb{E}_{\boldsymbol{\theta}^*} [\mathbf{A}_t^* \psi(W_t, \bar{H}_{t-1}; \boldsymbol{\gamma}^*)^\top \mid \mathcal{F}_{t-1}] \\ \mathbb{E}_{\boldsymbol{\theta}^*} [\psi(W_t, \bar{H}_{t-1}; \boldsymbol{\gamma}^*) \mathbf{A}_t^{*\top} \mid \mathcal{F}_{t-1}] & \mathbb{E}_{\boldsymbol{\theta}^*} [\psi(W_t, \bar{H}_{t-1}; \boldsymbol{\gamma}^*) \psi(W_t, \bar{H}_{t-1}; \boldsymbol{\gamma}^*)^\top \mid \mathcal{F}_{t-1}] \end{bmatrix}. \end{aligned}$$

By Assumptions A.1.(b), A.2.1 and A.3, we have

$$\frac{1}{T-M+1} \sum_{t=M}^T \mathbb{E}_{\theta^*} [s(\bar{H}_{t-1}, W_t, Y_t; \theta^*) s(\bar{H}_{t-1}, W_t, Y_t; \theta^*)^\top | \mathcal{F}_{t-1}] \xrightarrow{p} \begin{bmatrix} \mathbf{V} & \mathbf{U}^\top \\ \mathbf{U} & \mathbf{V}_{ps} \end{bmatrix},$$

which is positive definite. For Condition (c), we observe that for  $\epsilon > 0$ ,

$$\begin{aligned} & \frac{1}{T-M+1} \sum_{t=M}^T \mathbb{E}_{\theta^*} [\|s(\bar{H}_{t-1}, W_t, Y_t; \theta^*)\|^2 I(\|s(\bar{H}_{t-1}, W_t, Y_t; \theta^*)\| > \epsilon\sqrt{T}) | \mathcal{F}_{t-1}] \\ &= \frac{1}{T-M+1} \sum_{t=M}^T \mathbb{E}_{\theta^*} [\|\mathbf{A}_t^*\|^2 I(\|\mathbf{A}_t^*\|^2 + \|\psi(W_t, \bar{H}_{t-1}; \gamma^*)\|^2 > \epsilon^2 T) | \mathcal{F}_{t-1}] \end{aligned} \quad (\text{A.1})$$

$$+ \frac{1}{T-M+1} \sum_{t=M}^T \mathbb{E}_{\theta^*} [\|\psi(W_t, \bar{H}_{t-1}; \gamma^*)\|^2 I(\|\psi(W_t, \bar{H}_{t-1}; \gamma^*)\|^2 > \epsilon^2 T - \|\mathbf{A}_t^*\|^2) | \mathcal{F}_{t-1}]. \quad (\text{A.2})$$

By Assumption A.2.1 and the fact that  $\|\mathbf{A}_t^*\|^2$  is bounded, the term in Equation (A.1) converges in probability to 0. Since

$$I(\|\mathbf{A}_t^*\|^2 + \|\psi(W_t, \bar{H}_{t-1}; \gamma^*)\|^2 > \epsilon^2 T) \leq I(\|\mathbf{A}_t^*\|^2 > \epsilon^2 T/2) + I(\|\psi(W_t, \bar{H}_{t-1}; \gamma^*)\|^2 > \epsilon^2 T/2),$$

we have

$$\begin{aligned} & \mathbb{E}_{\theta^*} [\|\mathbf{A}_t^*\|^2 I(\|\mathbf{A}_t^*\|^2 + \|\psi(W_t, \bar{H}_{t-1}; \gamma^*)\|^2 > \epsilon^2 T) | \mathcal{F}_{t-1}] \\ & \leq \mathbb{E}_{\theta^*} [\|\mathbf{A}_t^*\|^2 I(\|\mathbf{A}_t^*\|^2 > \epsilon^2 T/2) | \mathcal{F}_{t-1}] \\ & \quad + \mathbb{E}_{\theta^*} [\|\mathbf{A}_t^*\|^2 I(\|\psi(W_t, \bar{H}_{t-1}; \gamma^*)\|^2 > \epsilon^2 T/2) | \mathcal{F}_{t-1}]. \end{aligned}$$

By the arguments in the Proof of Theorem A.1, we have  $\frac{1}{T-M+1} \sum_{t=M}^T \mathbb{E}_{\theta^*} [\|\mathbf{A}_t^*\|^2 I(\|\mathbf{A}_t^*\|^2 > \epsilon^2 T/2) | \mathcal{F}_{t-1}] \xrightarrow{p} 0$ . Let  $B$  be the event that  $\|\mathbf{A}_t^*\|^2 \leq \|\psi(W_t, \bar{H}_{t-1}; \gamma^*)\|^2$ . Then

$$\begin{aligned} & \mathbb{E}_{\theta^*} [\|\mathbf{A}_t^*\|^2 I(\|\psi(W_t, \bar{H}_{t-1}; \gamma^*)\|^2 > \epsilon^2 T/2) | \mathcal{F}_{t-1}] \\ &= \mathbb{E}_{\theta^*} [\|\mathbf{A}_t^*\|^2 I(\|\psi(W_t, \bar{H}_{t-1}; \gamma^*)\|^2 > \epsilon^2 T/2) | B, \mathcal{F}_{t-1}] \mathbb{P}(B | \mathcal{F}_{t-1}) \\ & \quad + \mathbb{E}_{\theta^*} [\|\mathbf{A}_t^*\|^2 I(\|\psi(W_t, \bar{H}_{t-1}; \gamma^*)\|^2 > \epsilon^2 T/2) | B^c, \mathcal{F}_{t-1}] \mathbb{P}(B^c | \mathcal{F}_{t-1}) \\ & \leq \mathbb{E}_{\theta^*} [\|\psi(W_t, \bar{H}_{t-1}; \gamma^*)\|^2 I(\|\psi(W_t, \bar{H}_{t-1}; \gamma^*)\|^2 > \epsilon^2 T/2) | B, \mathcal{F}_{t-1}] \mathbb{P}(B | \mathcal{F}_{t-1}) \\ & \quad + \mathbb{E}_{\theta^*} [\|\mathbf{A}_t^*\|^2 I(\|\mathbf{A}_t^*\|^2 > \epsilon^2 T/2) | B^c, \mathcal{F}_{t-1}] \mathbb{P}(B^c | \mathcal{F}_{t-1}) \\ & \leq \mathbb{E}_{\theta^*} [\|\psi(W_t, \bar{H}_{t-1}; \gamma^*)\|^2 I(\|\psi(W_t, \bar{H}_{t-1}; \gamma^*)\|^2 > \epsilon^2 T/2) | \mathcal{F}_{t-1}] \end{aligned}$$

$$+ \mathbb{E}_{\boldsymbol{\theta}^*} [\|\mathbf{A}_t^*\|^2 I(\|\mathbf{A}_t^*\|^2 > \epsilon^2 T/2) \mid \mathcal{F}_{t-1}]$$

where the last inequality follows from the law of total expectation. Since the mean of the last two terms converge in probability to 0 under Assumption A.2.1, Condition 1.(c) holds.

**Condition 2.** Observe that

$$\begin{aligned} \frac{\partial}{\partial \boldsymbol{\theta}^\top} s(\bar{H}_{t-1}, W_t, Y_t; \boldsymbol{\theta}) &= \begin{bmatrix} -\mathbf{I}_L & \frac{\partial}{\partial \boldsymbol{\gamma}^\top} s_{1:L}(\bar{H}_{t-1}, W_t, Y_t; \boldsymbol{\theta}) \\ \frac{\partial}{\partial \boldsymbol{\mu}} \psi(W_t, \bar{H}_{t-1}; \boldsymbol{\gamma}) & \frac{\partial}{\partial \boldsymbol{\gamma}^\top} \psi(W_t, \bar{H}_{t-1}; \boldsymbol{\gamma}) \end{bmatrix} \\ &= \begin{bmatrix} -\mathbf{I}_L & \frac{\partial}{\partial \boldsymbol{\gamma}^\top} s_{1:L}(\bar{H}_{t-1}, W_t, Y_t; \boldsymbol{\theta}) \\ \mathbf{0} & \frac{\partial}{\partial \boldsymbol{\gamma}^\top} \psi(W_t, \bar{H}_{t-1}; \boldsymbol{\gamma}) \end{bmatrix} \end{aligned} \quad (\text{A.3})$$

By Lemma A.1, we have

$$\begin{aligned} & -\frac{1}{T-M+1} \sum_{t=M}^T \mathbb{E}_{\boldsymbol{\theta}^*} \left[ \frac{\partial}{\partial \boldsymbol{\gamma}^\top} s_{1:L}(\bar{H}_{t-1}, W_t, Y_t; \boldsymbol{\theta}^*) \mid \mathcal{F}_{t-1} \right] \\ &= \frac{1}{T-M+1} \sum_{t=M}^T \mathbb{E}_{\boldsymbol{\theta}^*} \left[ s_{1:L}(\bar{H}_{t-1}, W_t, Y_t; \boldsymbol{\theta}^*) \psi(W_t, \bar{H}_{t-1}; \boldsymbol{\gamma}^*)^\top \mid \mathcal{F}_{t-1} \right] \xrightarrow{p} \mathbf{U}^\top. \end{aligned}$$

Moreover, by Lemma A.1 of Papadogeorgou et al. (2022), we have

$$-\frac{1}{T-M+1} \sum_{t=M}^T \mathbb{E}_{\boldsymbol{\gamma}^*} \left[ \frac{\partial}{\partial \boldsymbol{\gamma}^\top} \psi(W_t, \bar{H}_{t-1}; \boldsymbol{\gamma}) \Big|_{\boldsymbol{\gamma}^*} \mid \mathcal{F}_{t-1} \right] \xrightarrow{p} \mathbf{V}_{ps}.$$

Since  $\mathbf{V}_{ps}$  is positive definite, it is also invertible. Hence

$$-\frac{1}{T-M+1} \sum_{t=M}^T \mathbb{E}_{\boldsymbol{\theta}^*} \left[ \frac{\partial}{\partial \boldsymbol{\theta}^\top} s(\bar{H}_{t-1}, W_t, Y_t; \boldsymbol{\theta}) \Big|_{\boldsymbol{\theta}^*} \right] \xrightarrow{p} \begin{bmatrix} \mathbf{I}_L & \mathbf{U}^\top \\ \mathbf{0} & \mathbf{V}_{ps} \end{bmatrix},$$

and this limit matrix is invertible.

**Condition 3.** Let  $s_k(\bar{H}_{t-1}, W_t, Y_t; \boldsymbol{\theta})$  be the  $k^{\text{th}}$  element of  $s(\bar{H}_{t-1}, W_t, Y_t; \boldsymbol{\theta})$ . We need to show that for  $j, k = 1, \dots, L+K$ , if we denote

$$P_{kjt} = \frac{\partial}{\partial \theta_j} s_k(\bar{H}_{t-1}, W_t, Y_t; \boldsymbol{\theta}) \Big|_{\boldsymbol{\theta}^*},$$

then  $\mathbb{E}_{\boldsymbol{\theta}^*}[|P_{kjt}|] < \infty$ , and there exists  $0 < r_{kj} \leq 2$  such that

$$\sum_{t=1}^T \frac{1}{t^{r_{kj}}} \mathbb{E}_{\boldsymbol{\theta}^*} [ |P_{kjt} - \mathbb{E}_{\boldsymbol{\theta}^*}[P_{kjt} | \mathcal{F}_{t-1}]|^{r_{kj}} | \mathcal{F}_{t-1} ] \xrightarrow{p} 0$$

as  $T \rightarrow \infty$ . We will consider four cases.

**Case1:** For  $L < k, j \leq K + L$ , the desired condition holds by Assumption A.2.1.

**Case2:** Let  $1 \leq k, j \leq L$ . By Equation (A.3), we have  $P_{jkt} = -1$  or  $0$ . Thus,  $P_{kjt} = \mathbb{E}_{\boldsymbol{\theta}^*}[P_{kjt} | \mathcal{F}_{t-1}]$  and  $\mathbb{E}_{\boldsymbol{\theta}^*}[|P_{kjt}|] < \infty$ .

**Case3:** Let  $1 \leq j \leq L$  and  $L < k \leq K + L$ . Then

$$\frac{\partial}{\partial \theta_j} s_k(\bar{H}_{t-1}, W_t, Y_t; \boldsymbol{\theta}) = 0.$$

Therefore, the condition is satisfied.

**Case4:** For  $1 \leq k \leq L$  and  $L < j \leq K + L$ , there exists  $0 < r_{kj} \leq 2$  such that

$$\sum_{t=1}^T \frac{1}{t^{r_{kj}}} \mathbb{E}_{\boldsymbol{\theta}^*} [ |P_{kjt} - \mathbb{E}_{\boldsymbol{\theta}^*}[P_{kjt} | \mathcal{F}_{t-1}]|^{r_{kj}} | \mathcal{F}_{t-1} ] \xrightarrow{p} 0$$

by Assumption A.3.(b). Moreover, Lemma A.1 implies that

$$\begin{aligned} \mathbb{E}_{\boldsymbol{\theta}^*}[|P_{kjt}|] &= \mathbb{E}_{\boldsymbol{\theta}^*} \left[ \left| \frac{\partial}{\partial \gamma_{j-L}} s_k(\bar{H}_{t-1}, W_t, Y_t; \boldsymbol{\theta}) \Big|_{\boldsymbol{\theta}^*} \right| \right] \\ &= \mathbb{E}_{\boldsymbol{\theta}^*} \left[ \left| -(\mathbf{Z}_t^\top \mathbf{Z}_t)^{-1} \mathbf{Z}_t^\top \tilde{\boldsymbol{\tau}}_t^I(\boldsymbol{\gamma}^*) \sum_{\ell'=t-M+1}^t \psi_{j-L}(W_{\ell'}, \bar{H}_{\ell'-1}; \boldsymbol{\gamma}^*) \right| \right] \end{aligned}$$

By Assumption A.1,  $\mathbf{Z}_t$  and  $\tilde{\boldsymbol{\tau}}_t^I(\boldsymbol{\gamma}^*)$  are bounded. Since

$$\begin{aligned} \mathbb{E}_{\boldsymbol{\gamma}^*} [ |\psi_{j-L}(W_{\ell'}, \bar{H}_{\ell'-1}; \boldsymbol{\gamma}^*)|^2 ] &\leq \mathbb{E}_{\boldsymbol{\gamma}^*} [ \psi_{j-L}(W_{\ell'}, \bar{H}_{\ell'-1}; \boldsymbol{\gamma}^*)^2 ] \\ &\leq \mathbb{E}_{\boldsymbol{\gamma}^*} [ |\psi(W_{\ell'}, \bar{H}_{\ell'-1}; \boldsymbol{\gamma}^*)|^2 ] < \infty, \end{aligned}$$

where the first inequality follows from Jensen's inequality and the second inequality follows from Assumption A.2. Therefore, it follows that  $\mathbb{E}_{\boldsymbol{\theta}^*}[|P_{kjt}|] < \infty$ .

**Condition 4.** We need to show that there exists an integrable function  $\ddot{\psi}(x)$  such that  $\ddot{\psi}(x)$  dominates the second partial derivatives of  $s(\bar{H}_{t-1}, W_t, Y_t; \boldsymbol{\theta})$  in a neighborhood of  $\boldsymbol{\theta}^*$  for all  $\{\bar{h}_{t-1}, w_t, y_t\}$ . Let  $k, l, m = 1, \dots, K + L$ . We consider the following three cases.

**Case1:** If  $l \leq L$  or  $m \leq L$ , then  $\frac{\partial}{\partial \theta_m} \frac{\partial}{\partial \theta_j} \psi(W_t, \bar{H}_{t-1}; \gamma_k) = 0$ , implying that the condition is satisfied.

**Case2:** If  $k, l, m > L$ , the condition holds by Assumption A.2.3.

**Case3:** Suppose  $k \leq L$  and  $m, l > L$ . Lemma A.1 implies:

$$\begin{aligned} \frac{\partial}{\partial \gamma_m} \frac{\partial}{\partial \gamma_l} s_k(\bar{h}_{t-1}, w_t, y_t; \boldsymbol{\theta}) &= - (\mathbf{Z}_t^\top \mathbf{Z}_t)^{-1} \mathbf{Z}_{t,k}^\top \tilde{\boldsymbol{\tau}}_t^I(\boldsymbol{\gamma}) \left\{ \sum_{j=t-M+1}^t \frac{\partial}{\partial \gamma_{m-L}} \psi_{l-L}(w_j, \bar{h}_{j-1}; \boldsymbol{\gamma}) \right. \\ &\quad \left. - \sum_{j=t-M+1}^t \psi_{m-L}(w_j, \bar{h}_{j-1}; \boldsymbol{\gamma}) \sum_{j'=t-M+1}^t \psi_{l-L}(w_{j'}, \bar{h}_{j'-1}; \boldsymbol{\gamma}) \right\}. \end{aligned}$$

Note that  $|(\mathbf{Z}_t^\top \mathbf{Z}_t)^{-1} \mathbf{Z}_{t,k}^\top \tilde{\boldsymbol{\tau}}_t^I(\boldsymbol{\gamma})| \leq \delta$  for some  $\delta \in \mathbb{R}$ , so

$$\begin{aligned} &\left| \frac{\partial}{\partial \gamma_m} \frac{\partial}{\partial \gamma_l} s_k(\bar{h}_{t-1}, w_t, y_t; \boldsymbol{\theta}) \right| \\ &\leq \delta \left| \sum_{j=t-M+1}^t \frac{\partial}{\partial \gamma_{m-L}} \psi_{l-L}(w_j, \bar{h}_{j-1}; \boldsymbol{\gamma}) \right| \\ &\quad + \delta \left| \sum_{j=t-M+1}^t \sum_{j'=t-M+1}^t \psi_{m-L}(w_j, \bar{h}_{j-1}; \boldsymbol{\gamma}) \psi_{l-L}(w_{j'}, \bar{h}_{j'-1}; \boldsymbol{\gamma}) \right| \\ &\leq \sum_{j=t-M+1}^t \delta \left| \frac{\partial}{\partial \gamma_{m-L}} \psi_{l-L}(w_j, \bar{h}_{j-1}; \boldsymbol{\gamma}) \right| \\ &\quad + \sum_{j=t-M+1}^t \sum_{j'=t-M+1}^t \delta |\psi_{m-L}(w_j, \bar{h}_{j-1}; \boldsymbol{\gamma}) \psi_{l-L}(w_{j'}, \bar{h}_{j'-1}; \boldsymbol{\gamma})| \end{aligned}$$

Consider the first term. Assumption A.2 implies that the second derivatives of  $\psi(w_t, \bar{h}_{t-1}; \boldsymbol{\gamma})$  is dominated by  $\ddot{\psi}(w_t, \bar{h}_{t-1})$  in a neighborhood of  $\boldsymbol{\gamma}^*$ . Let  $B_\epsilon(\boldsymbol{\gamma}^*)$  be an open ball contained in the neighborhood. By Taylor's expansion, we have

$$\left| \frac{\partial}{\partial \gamma_{m-L}} \psi_{l-L}(w_t, \bar{h}_{t-1}; \boldsymbol{\gamma}) \right| \leq \left| \frac{\partial}{\partial \gamma_{m-L}} \psi_{l-L}(w_t, \bar{h}_{t-1}; \boldsymbol{\gamma}^*) \right| + \epsilon K \ddot{\psi}(w_t, \bar{h}_{t-1}),$$

on the ball  $B_\epsilon(\boldsymbol{\gamma}^*)$ . By Assumption A.2.2, the quantity on the right hand side is an integrable function fixed in  $\boldsymbol{\gamma}$ , where we denote the maximum of these functions over  $m, l$  by  $\ddot{\psi}_1(w_t, \bar{h}_{t-1})$ .

Next, consider the second term. On the open ball  $B_\epsilon(\boldsymbol{\gamma}^*)$ , we have

$$|\psi_{m-1}(w_t, \bar{h}_{t-1}; \boldsymbol{\gamma})| \leq |\psi_{m-1}(w_t, \bar{h}_{t-1}; \boldsymbol{\gamma}^*)| + \epsilon K \ddot{\psi}_1(w_t, \bar{h}_{t-1}),$$

and  $\mathbb{E}_{\gamma^*}[|\psi_{m-1}(w_t, \bar{h}_{t-1}; \gamma^*)|] < \infty$  by Assumption A.2. Then, the right hand side is an integrable function fixed in  $\gamma$  where we denote the maximum of these functions over  $m$  by  $\ddot{\psi}_2(w_t, \bar{h}_{t-1})$ . Putting these together, we have

$$\left| \frac{\partial}{\partial \gamma_m} \frac{\partial}{\partial \gamma_l} s_k(\bar{h}_{t-1}, w_t, y_t; \boldsymbol{\theta}) \right| \leq M \delta \ddot{\psi}_1(w_t, \bar{h}_{t-1}) + M^2 \delta [\ddot{\psi}_2(w_t, \bar{h}_{t-1})]^2,$$

where the right hand side is an integrable function that satisfy the condition.

Finally, we need to show that the solution of the following equation is consistent for  $\boldsymbol{\theta}^*$ ,

$$\frac{1}{T - M + 1} \sum_{t=M}^T s(\bar{H}_{t-1}, W_t, Y_t; \boldsymbol{\theta}) = 0.$$

Let  $s_{1:L}(\bar{H}_{t-1}, W_t, Y_t; \boldsymbol{\theta})$  denote the first  $L$  entries of  $s(\bar{H}_{t-1}, W_t, Y_t; \boldsymbol{\theta})$ . Theorem A.1 shows that the IPW estimator based on the true propensity score is consistent, while the parameter estimates of the propensity score model  $\hat{\gamma}$  are also consistent for  $\gamma$ . Furthermore,  $s_{1:L}(\bar{H}_{t-1}, W_t, Y_t; \boldsymbol{\theta})$  is a continuous function of the propensity score, which is itself continuous in  $\gamma$ . Thus, Slutsky's theorem implies that solving the following equation with the estimated propensity score parameters is also consistent,

$$\frac{1}{T - M + 1} \sum_{t=M}^T s_{1:L}(\bar{H}_{t-1}, W_t, Y_t; \boldsymbol{\theta}) = 0.$$

Hence, all the conditions of Theorem A.3 in Papadogeorgou et al. (2022) are satisfied, and as  $T \rightarrow \infty$ , we have

$$\sqrt{T}(\hat{\boldsymbol{\theta}}_T - \boldsymbol{\theta}^*) \xrightarrow{d} N(0, \mathbf{V}_\theta),$$

where  $\hat{\boldsymbol{\theta}}_T$  is the solution to

$$\frac{1}{T - M + 1} \sum_{t=M}^T s(\bar{H}_{t-1}, W_t, Y_t; \boldsymbol{\theta}) = 0$$

and  $\mathbf{V}_\theta = \mathbf{A}^{-1} \mathbf{B} (\mathbf{A}^{-\top})$  for

$$\mathbf{A} = \begin{bmatrix} \mathbf{I}_L & \mathbf{U}^\top \\ \mathbf{0} & \mathbf{V}_{ps} \end{bmatrix} \quad \text{and} \quad \mathbf{B} = \begin{bmatrix} \tilde{\mathbf{V}}^I & \mathbf{U}^\top \\ \mathbf{U} & \mathbf{V}_{ps} \end{bmatrix}. \quad (\text{A.4})$$

Note that  $\frac{1}{T-M+1} \sum_{t=M}^T \hat{\beta}_t^I - \beta_t^*$  is the first  $L$  entries of  $\hat{\theta}_T$ . As a result, we have

$$\frac{1}{\sqrt{T-M+1}} \sum_{t=M}^T (\hat{\beta}_t^I - \beta_t^*) \xrightarrow{d} N(\mathbf{0}, \mathbf{V}^I).$$

□

## B.7 Proof of Theorem A.3

The asymptotic variance  $\mathbf{V}^I$  corresponds to the  $L \times L$  submatrix located in the upper-left corner of matrix  $\mathbf{A}^{-1} \mathbf{B} \mathbf{A}^{-\top}$  where  $\mathbf{A}, \mathbf{B}$  are defined in Equation (A.4). We have

$$\begin{aligned} \mathbf{A}^{-1} \mathbf{B} \mathbf{A}^{-\top} &= \begin{bmatrix} \mathbf{I}_L & \mathbf{U}^\top \\ \mathbf{0} & \mathbf{V}_{ps} \end{bmatrix}^{-1} \begin{bmatrix} \tilde{\mathbf{V}}^I & \mathbf{U}^\top \\ \mathbf{U} & \mathbf{V}_{ps} \end{bmatrix} \begin{bmatrix} \mathbf{I}_L & \mathbf{U}^\top \\ \mathbf{0} & \mathbf{V}_{ps} \end{bmatrix}^{-\top} \\ &= \begin{bmatrix} \mathbf{I}_L^{-1} & -\mathbf{I}_L^{-1} \mathbf{U}^\top \mathbf{V}_{ps}^{-1} \\ \mathbf{0} & \mathbf{V}_{ps}^{-1} \end{bmatrix} \begin{bmatrix} \tilde{\mathbf{V}}^I & \mathbf{U}^\top \\ \mathbf{U} & \mathbf{V}_{ps} \end{bmatrix} \begin{bmatrix} \mathbf{I}_L^{-\top} & \mathbf{0} \\ -\mathbf{V}_{ps}^{-1\top} \mathbf{U}^\top \mathbf{I}_L^{-1\top} & \mathbf{V}_{ps}^{-\top} \end{bmatrix} \\ &= \begin{bmatrix} \tilde{\mathbf{V}}^I - \mathbf{U}^\top \mathbf{V}_{ps}^{-1} \mathbf{U}^\top & \dots \\ \dots & \dots \end{bmatrix}. \end{aligned}$$

Note that  $\mathbf{V}^I$  is the asymptotic variance of the estimator based on the true propensity score. Let  $\mathbf{x}$  be a nonzero vector in  $\mathbb{R}^L$ . Then  $\mathbf{x}^* = \mathbf{U}^\top \mathbf{x} \in \mathbb{R}^K$ . Since  $\mathbf{V}_{ps}$  is positive definite, so is  $\mathbf{V}_{ps}^{-1}$ , implying  $\mathbf{x}^\top \mathbf{U}^\top \mathbf{V}_{ps}^{-1} \mathbf{U}^\top \mathbf{x} = \mathbf{x}^{*\top} \mathbf{V}_{ps}^{-1} \mathbf{x}^* \geq 0$ . Thus,  $\mathbf{U}^\top \mathbf{V}_{ps}^{-1} \mathbf{U}^\top$  is a positive semidefinite matrix, completing the proof. □

## B.8 Proof of Corollary A.1

The proof follows directly from the proof of Proposition A.1 and the fact that  $\hat{\gamma}$  is consistent for  $\gamma$ . □

## C Asymptotic properties of the Hájek estimator

In this section, we present the asymptotic properties of Hájek estimator based on either the true or estimated propensity score. We begin by stating the required regularity conditions and then establish that the Hájek estimator is asymptotically normal. Although the asymptotic variance is not identifiable, we derive its upper bound and propose a consistent estimator of the bound.

## C.1 Regularity conditions

We represent an additional assumption that is required to achieve the asymptotic normality of the Hájek estimator. For  $M \leq t \leq T$ , define

$$\beta'_t = (\mathbf{Z}_t^\top \mathbf{Z}_t)^{-1} \mathbf{Z}_t^\top \mathbf{N}_t(F_{\mathbf{h}'}) \text{ and } \beta''_t = (\mathbf{Z}_t^\top \mathbf{Z}_t)^{-1} \mathbf{Z}_t^\top \mathbf{N}_t(F_{\mathbf{h}''}).$$

**Assumption A.4.** *Define*

$$\mathbf{A}_t = \begin{pmatrix} (\mathbf{Z}_t^\top \mathbf{Z}_t)^{-1} \mathbf{Z}_t^\top \tilde{\mathbf{Y}}_t^I(F_{\mathbf{h}'}; \gamma^*) \\ (\mathbf{Z}_t^\top \mathbf{Z}_t)^{-1} \mathbf{Z}_t^\top \tilde{\mathbf{Y}}_t^I(F_{\mathbf{h}''}; \gamma^*) \\ \rho_{t\mathbf{h}'}(\gamma^*) \\ \rho_{t\mathbf{h}''}(\gamma^*) \end{pmatrix}.$$

Then, there exists a positive definite matrix  $\mathbf{V}^H$  such that as  $T \rightarrow \infty$ ,

$$\frac{1}{T - M + 1} \sum_{t=M}^T \mathbb{V}[\mathbf{A}_t \mid \bar{H}_{t-M}^*] \xrightarrow{p} \tilde{\mathbf{V}}^H.$$

Assumption A.4 is slightly stronger than Assumption A.1.(b), since  $\tilde{\boldsymbol{\tau}}_t^H(\gamma) = \tilde{\mathbf{Y}}_t^H(F_{\mathbf{h}''}; \gamma) - \tilde{\mathbf{Y}}_t^H(F_{\mathbf{h}'}; \gamma)$ .

The next assumption is similar to Assumption A.3 with a different form of  $s(\bar{H}_{t-1}, W_t, Y_t; \gamma)$ .

**Assumption A.5** (Regularity conditions on score function of propensity score model for Hájek estimators). *For a stochastic intervention  $F_{\mathbf{h}}$ , let  $\rho_{t\mathbf{h}}(\gamma) = \prod_{j=t-M+1}^t \frac{f_{\mathbf{h}}(W_j)}{e_t(W_j; \gamma)}$  and  $\tilde{\mathbf{Y}}_t^H(F_{\mathbf{h}}; \gamma) = \rho_{t\mathbf{h}}(\gamma) (N_{S_1}(Y_t), \dots, N_{S_p}(Y_t))^\top$ , and  $\tilde{\boldsymbol{\tau}}_t^H(\gamma) = \tilde{\mathbf{Y}}_t^H(F_{\mathbf{h}''}; \gamma) - \tilde{\mathbf{Y}}_t^H(F_{\mathbf{h}'}; \gamma)$ . Define*

$$s(\bar{H}_{t-1}, W_t, Y_t; \gamma) = \begin{pmatrix} (\mathbf{Z}_t^\top \mathbf{Z}_t)^{-1} \mathbf{Z}_t^\top \tilde{\mathbf{Y}}_t^I(F_{\mathbf{h}'}; \gamma) - \beta'_t \\ (\mathbf{Z}_t^\top \mathbf{Z}_t)^{-1} \mathbf{Z}_t^\top \tilde{\mathbf{Y}}_t^I(F_{\mathbf{h}''}; \gamma) - \beta''_t \\ \rho_{t\mathbf{h}'}(\gamma) - 1 \\ \rho_{t\mathbf{h}''}(\gamma) - 1 \end{pmatrix},$$

and a propensity score function  $\psi(W_t, \bar{H}_{t-1}; \gamma)$  satisfying Assumption A.2, the following conditions hold.

(a) There exists  $\mathbf{U} \in \mathbb{R}^{K \times 2L}$  such that

$$\frac{1}{T - M + 1} \sum_{t=M}^T \mathbb{E}_{\gamma^*}[\psi(W_t, \bar{H}_{t-1}; \gamma^*) s(\bar{H}_{t-1}, W_t, Y_t; \gamma^*)^\top \mid \bar{H}_{t-M}^*] \xrightarrow{p} \mathbf{U}, \text{ and}$$

$$\mathbf{V}^* = \begin{bmatrix} \tilde{\mathbf{V}}^H & \mathbf{U}^\top \\ \mathbf{U} & \mathbf{V}_{ps} \end{bmatrix} \text{ is positive definite.}$$

(b) If  $P_{jt} = \frac{\partial}{\partial \gamma_j} s(\bar{H}_{t-1}, W_t, Y_t; \gamma) \Big|_{\gamma^*}$ , where  $\gamma_j$  is the  $j^{\text{th}}$  entry of  $\gamma$ , then there exists  $r_j \in (0, 2]$  such that

$$\frac{1}{T-M+1} \sum_{t=M}^T \frac{1}{t^{r_j}} \left( |P_{jt} - \mathbb{E}_{\theta^*}[P_{jt} | \bar{H}_{t-M}^*]| \right) \xrightarrow{p} 0.$$

## C.2 Asymptotic normality

The asymptotic normality of the Hájek estimator based on the estimated propensity score is presented as Theorem 1. Here, we state the analogous result for the Hájek estimator with the true propensity score.

**Theorem A.4** (Asymptotic normality of the Hájek estimator using the true propensity score). *Suppose that Assumptions 1, 2, A.1, and A.4 hold. Then,*

$$\frac{1}{\sqrt{T-M+1}} \sum_{t=M}^T (\hat{\beta}_t^H - \beta_t^*) \xrightarrow{d} N(\mathbf{0}, \mathbf{J} \tilde{\mathbf{V}}^H \mathbf{J}^\top),$$

where  $\tilde{\mathbf{V}}^H$  represents the probability limit of  $\frac{1}{T-M+1} \sum_{t=M}^T \tilde{\mathbf{V}}_t^H$  as  $T \rightarrow \infty$  with  $\tilde{\mathbf{V}}_t^H = \mathbb{V}[\mathbf{A}_t(\gamma^*) | \bar{H}_{t-M}^*]$  for  $t \geq M$ , where  $\mathbf{A}_t$  and  $\mathbf{J}$  are defined as,

$$\mathbf{A}_t(\gamma) = \begin{pmatrix} (\mathbf{Z}_t^\top \mathbf{Z}_t)^{-1} \mathbf{Z}_t^\top \tilde{\mathbf{Y}}_t^I(F_{\mathbf{h}'}; \gamma^*) \\ (\mathbf{Z}_t^\top \mathbf{Z}_t)^{-1} \mathbf{Z}_t^\top \tilde{\mathbf{Y}}_t^I(F_{\mathbf{h}''}; \gamma^*) \\ \rho_{t\mathbf{h}'}(\gamma) \\ \rho_{t\mathbf{h}''}(\gamma) \end{pmatrix},$$

$$\text{and } \mathbf{J} = \begin{bmatrix} \mathbf{I} & -\mathbf{I} & -\frac{1}{T-M+1} \sum_{t=M}^T \beta_t' & \frac{1}{T-M+1} \sum_{t=M}^T \beta_t'' \end{bmatrix}.$$

## C.3 Consistent estimation of variance bound for the Hájek-estimator

For the case of the estimated propensity score, the result is stated as Proposition 1. We state the result for the Hájek estimator with the true propensity score.

**Proposition A.2** (Consistent estimation of variance bound for the Hájek estimator with the true propensity score). *Suppose that Assumptions 1, 2, A.1, and A.4 hold. Let*

$$\hat{\mathbf{V}}^H = \frac{1}{T-M+1} \sum_{t=M}^T \hat{\mathbf{V}}_t^H \text{ with } \hat{\mathbf{V}}_t^H = \mathbf{A}_t(\gamma^*) \mathbf{A}_t(\gamma^*)^\top \text{ and}$$

$$\hat{\mathbf{J}} = \begin{bmatrix} \mathbf{I} & -\mathbf{I} & -\frac{1}{T-M+1} \sum_{t=M}^T (\mathbf{Z}_t^\top \mathbf{Z}_t)^{-1} \mathbf{Z}_t^\top \tilde{\mathbf{Y}}_t^H(F_{\mathbf{h}'}; \gamma^*) & \frac{1}{T-M+1} \sum_{t=M}^T (\mathbf{Z}_t^\top \mathbf{Z}_t)^{-1} \mathbf{Z}_t^\top \tilde{\mathbf{Y}}_t^H(F_{\mathbf{h}''}; \gamma^*) \end{bmatrix}$$

Then  $\hat{\mathbf{J}} \hat{\mathbf{V}}^H \hat{\mathbf{J}}^\top$  is a consistent estimator for  $\mathbf{J} \mathbf{V}^H \mathbf{J}^\top$ .

## C.4 Proof of Theorem A.4

The proof is similar to that of Theorem A.1. The key difference is the definition of  $\mathbf{A}_t^*$ . We apply Theorem A.2 of Papadogeorgou et al. (2022). Set  $\mathcal{F}_t = \overline{H}_{t-M+1}^*$ , and define  $\mathbf{A}_t^* = \mathbf{A}_t(\gamma^*) - (\boldsymbol{\beta}_t^{\prime\top}, \boldsymbol{\beta}_t^{\prime\prime\top}, \rho_{\mathbf{h}'}, \rho_{\mathbf{h}''})^\top$  where  $\rho_{\mathbf{h}'} = \rho_{\mathbf{h}''} = 1$ .

We first show that  $\mathbf{A}_t^*$  is a martingale difference sequence, i.e.,  $\mathbb{E}[\mathbf{A}_t^*] = 0$  and  $\mathbb{E}[||\mathbf{A}_t^*||] < \infty$ . By similar arguments used in the proof of Theorem A.1 (see Section B.4), for any  $F_{\mathbf{h}}$ , we have  $\mathbb{E}[\tilde{\mathbf{Y}}_t^I(F_{\mathbf{h}}) | \mathcal{F}_{t-1}] = N_t(F_{\mathbf{h}})$ , and thus,

$$\mathbb{E}[(\mathbf{Z}_t^\top \mathbf{Z}_t)^{-1} \mathbf{Z}_t^\top \tilde{\mathbf{Y}}_t^I(F_{\mathbf{h}'}) | \mathcal{F}_{t-1}] = (\mathbf{Z}_t^\top \mathbf{Z}_t)^{-1} \mathbf{Z}_t^\top N_t(F_{\mathbf{h}'}) = \boldsymbol{\beta}_t'.$$

We have

$$\begin{aligned} \mathbb{E}[\rho_{t\mathbf{h}'} | \mathcal{F}_{t-1}] &= \int_{\mathcal{W}^M} \prod_{j=t-M+1}^t \frac{f_{\mathbf{h}'}(w_j)}{e_j(w_j)} f(w_j | \overline{H}_{j-1}^*) d\mathbf{w}_{(t-M+1):t} \\ &= \int_{\mathcal{W}^M} \prod_{j=t-M+1}^t \frac{f_{\mathbf{h}'}(w_j)}{e_j(w_j)} e_j(w_j) d\mathbf{w}_{(t-M+1):t} \\ &= \int_{\mathcal{W}^M} \prod_{j=t-M+1}^t f_{\mathbf{h}'}(w_j) d\mathbf{w}_{(t-M+1):t} \\ &= 1. \end{aligned}$$

where the second equality follows from Assumption 1.

Similarly,  $\mathbb{E}[(\mathbf{Z}_t^\top \mathbf{Z}_t)^{-1} \mathbf{Z}_t^\top \tilde{\mathbf{Y}}_t^I(F_{\mathbf{h}''}) | \mathcal{F}_{t-1}] = \boldsymbol{\beta}_t''$  and  $\mathbb{E}[\rho_{t\mathbf{h}''} | \mathcal{F}_{t-1}] = 1$ . Thus,  $\mathbb{E}[\mathbf{A}_t^* | \mathcal{F}_{t-1}] = 0$ . Furthermore, since every element in  $\mathbf{A}_t^*$  is bounded by Assumptions 2 and A.1.(a),  $||\mathbf{A}_t^*||$  is bounded and hence  $\mathbb{E}[||\mathbf{A}_t^*||] < \infty$ . For an arbitrary  $\epsilon > 0$ ,  $I(||\mathbf{A}_t^*|| > \epsilon\sqrt{T}) = 0$  for large  $t$ , since  $||\mathbf{A}_t^*||$  is bounded. Therefore, as  $T \rightarrow \infty$  for all  $\epsilon > 0$ , we have

$$\frac{1}{T-M+1} \sum_{t=M}^T E \left[ ||\mathbf{A}_t^*||^2 I(||\mathbf{A}_t^*|| > \epsilon\sqrt{T}) \mid \mathcal{F}_{t-1} \right] \xrightarrow{p} 0.$$

The remaining condition of the multivariate Martingale central limit theorem is satisfied

by Assumption A.4. Hence,

$$\frac{1}{\sqrt{T-M+1}} \sum_{t=M}^T \mathbf{A}_t^* \xrightarrow{d} N(\mathbf{0}, \tilde{\mathbf{V}}^H)$$

where, as  $T \rightarrow \infty$ ,

$$\frac{1}{T-M+1} \sum_{t=M}^T \mathbb{E}[\mathbf{A}_t^* \mathbf{A}_t^{*\top} \mid \mathcal{F}_{t-1}] \xrightarrow{p} \tilde{\mathbf{V}}^H.$$

Then, as  $T \rightarrow \infty$ , we have

$$\sqrt{T-M+1}(\hat{\boldsymbol{\theta}} - \boldsymbol{\theta}^*) \xrightarrow{d} N(\mathbf{0}, \tilde{\mathbf{V}}^H),$$

where

$$\begin{aligned} \boldsymbol{\theta} &= \frac{1}{T-M+1} \left( \sum_{t=M}^T \boldsymbol{\beta}'_t, \sum_{t=M}^T \boldsymbol{\beta}''_t, \rho_{h'}, \rho_{h''} \right)^\top, \\ \hat{\boldsymbol{\theta}} &= \frac{1}{T-M+1} \sum_{t=M}^T \left( (\mathbf{Z}_t^\top \mathbf{Z}_t)^{-1} \mathbf{Z}_t^\top \tilde{\mathbf{Y}}_t^I(F_{h'}), (\mathbf{Z}_t^\top \mathbf{Z}_t)^{-1} \mathbf{Z}_t^\top \tilde{\mathbf{Y}}_t^I(F_{h''}), \rho_{th'}, \rho_{th''} \right)^\top. \end{aligned}$$

Finally, we apply the Delta method. Define

$$h(\boldsymbol{\theta}) = \frac{\frac{1}{T-M+1} \sum_{t=M}^T \boldsymbol{\beta}'_t}{\rho_{h'}} - \frac{\frac{1}{T-M+1} \sum_{t=M}^T \boldsymbol{\beta}''_t}{\rho_{h''}}.$$

The Jacobian matrix is

$$\mathbf{J}(\boldsymbol{\theta}) = \begin{bmatrix} \frac{1}{\rho_{h'}} \mathbf{I} & -\frac{1}{\rho_{h''}} \mathbf{I} & -\frac{\frac{1}{T-M+1} \sum_{t=M}^T \boldsymbol{\beta}'_t}{\rho_{h'}^2} & \frac{\frac{1}{T-M+1} \sum_{t=M}^T \boldsymbol{\beta}''_t}{\rho_{h''}^2} \end{bmatrix}$$

where  $\mathbf{I}$  is the identity matrix. Denote

$$\mathbf{J} = \mathbf{J}(\boldsymbol{\theta}^*) = \begin{bmatrix} \mathbf{I} & -\mathbf{I} & -\frac{1}{T-M+1} \sum_{t=M}^T \boldsymbol{\beta}'_t & \frac{1}{T-M+1} \sum_{t=M}^T \boldsymbol{\beta}''_t \end{bmatrix}$$

Then, we obtain,

$$\sqrt{T-M+1}(h(\hat{\boldsymbol{\theta}}) - h(\boldsymbol{\theta}^*)) \xrightarrow{d} N(\mathbf{0}, \mathbf{J} \tilde{\mathbf{V}}^H \mathbf{J}^\top)$$

as  $T \rightarrow \infty$ . Thus, as  $T \rightarrow \infty$ , we have

$$\frac{1}{\sqrt{T-M+1}} \sum_{t=M}^T (\hat{\boldsymbol{\beta}}_t^H - \boldsymbol{\beta}_t^*) \xrightarrow{d} N(\mathbf{0}, \mathbf{J} \tilde{\mathbf{V}}^H \mathbf{J}^\top).$$

□

## C.5 Proof of Proposition A.2

Assuming the same notations in the previous proof. Note that

$$\hat{\boldsymbol{\theta}} = \left[ \frac{1}{T-M+1} \sum_{t=M}^T ((\mathbf{Z}_t^\top \mathbf{Z}_t)^{-1} \mathbf{Z}_t^\top \tilde{\mathbf{Y}}_t^H(F_{\mathbf{h}'}; \boldsymbol{\gamma}^*))^\top, \right. \\ \left. \frac{1}{T-M+1} \sum_{t=M}^T ((\mathbf{Z}_t^\top \mathbf{Z}_t)^{-1} \mathbf{Z}_t^\top \tilde{\mathbf{Y}}_t^H(F_{\mathbf{h}''}; \boldsymbol{\gamma}^*))^\top, 1, 1 \right]^\top$$

is a consistent estimator of  $\boldsymbol{\theta}$ . So  $\hat{\mathbf{J}} = \mathbf{J}(\hat{\boldsymbol{\theta}})$  is a consistent estimator of  $\mathbf{J}(\boldsymbol{\theta})$ . By similar arguments used in Section B.5, we have  $\hat{\mathbf{V}}^H \xrightarrow{p} \mathbf{V}^{H*}$ . Hence,  $\hat{\mathbf{J}} \hat{\mathbf{V}}^H \hat{\mathbf{J}}^\top \xrightarrow{p} \mathbf{J} \mathbf{V}^{H*} \mathbf{J}^\top$ . □

**Remark A.1.** By Slutsky's theorem, if  $\mathbf{Q}$  is a matrix such that  $\mathbf{Q} \xrightarrow{p} \mathbf{I}$  as  $T \rightarrow \infty$ , then  $\hat{\mathbf{J}} \mathbf{Q} \hat{\mathbf{V}}^H \hat{\mathbf{Q}}^\top \hat{\mathbf{J}}^\top$  is also a consistent estimator for  $\mathbf{J} \mathbf{V}^{H*} \mathbf{J}^\top$ .

**Remark A.2.** There are several possible choices for  $\mathbf{Q}$ . In addition to the one presented in Section 2.5, another natural choice is

$$\mathbf{Q} = \text{diag}(\rho_{\mathbf{h}'}^{-1} \mathbf{1}_L, \rho_{\mathbf{h}''}^{-1} \mathbf{1}_L, \rho_{\mathbf{h}'}^{-1}, \rho_{\mathbf{h}''}^{-1}).$$

It is straightforward to show that  $\mathbf{Q}$  converges to  $\mathbf{I}$  in probability as  $T \rightarrow \infty$ . Although this choice also helps stabilize the elements of  $\hat{\mathbf{V}}^H$ , we find that the estimated variance bound based on this  $\mathbf{Q}$  generally performs worse than the proposed variance bound using the choice of  $\mathbf{Q}$  in Section 2.5. The bias introduced by this stabilization (bias which occurs when using stabilized weights in general) can be non-negligible when  $M$  is relatively large in finite samples, resulting in under-coverage of the confidence intervals.

## C.6 Proofs of Theorem 1, Theorem 2 and Proposition 1

The proofs of Theorem 1 and Theorem 2 follow directly from those of Theorem A.2 and Theorem A.3 with the following alternative definition,

$$s(\bar{H}_{t-1}, W_t, Y_t; \boldsymbol{\theta}) = \begin{pmatrix} (\mathbf{Z}_t^\top \mathbf{Z}_t)^{-1} \mathbf{Z}_t^\top \tilde{\mathbf{Y}}_t^I(F_{\mathbf{h}'}; \boldsymbol{\gamma}) - \boldsymbol{\beta}'_t - \boldsymbol{\mu}_1 \\ (\mathbf{Z}_t^\top \mathbf{Z}_t)^{-1} \mathbf{Z}_t^\top \tilde{\mathbf{Y}}_t^I(F_{\mathbf{h}''}; \boldsymbol{\gamma}) - \boldsymbol{\beta}''_t - \boldsymbol{\mu}_2 \\ \rho_{t\mathbf{h}'}(\boldsymbol{\gamma}) - 1 - \mu_3 \\ \rho_{t\mathbf{h}''}(\boldsymbol{\gamma}) - 1 - \mu_4 \\ \psi(W_t, \bar{H}_{t-1}; \boldsymbol{\gamma}) \end{pmatrix}.$$

Thus, we omit the details. In addition, the proof of Proposition 1 follows directly from Proposition A.2 and the fact that  $\hat{\gamma}$  is a consistent estimator of  $\gamma^*$ .

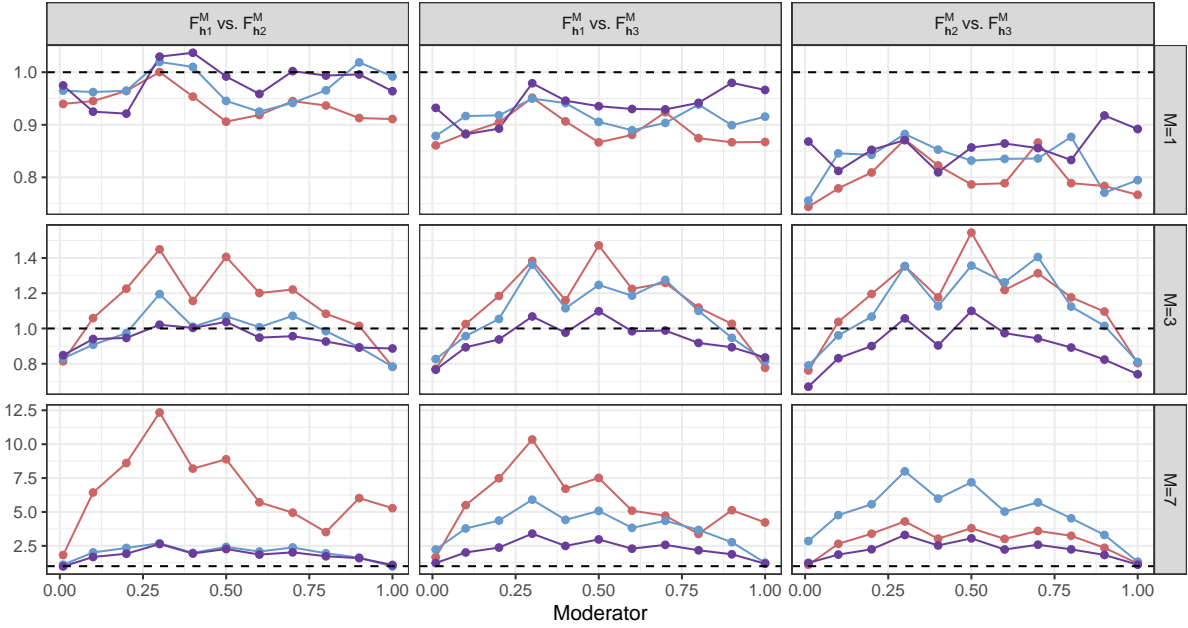
## D Empirical performance of the proposed estimator

In this section, we examine the empirical performance of the proposed variance bound estimator through a simulation study. We generate data of different lengths  $T$  (200, 500, 1000), consider interventions over different time periods  $M$  (1, 3, 7), and analyze two types of moderators: spatial and spatio-temporal. For each scenario, we conducted 500 simulations, where the data-generating process follows the same design as described in Section 3.1.

For each simulation, we compute the square root of the estimated variance bound for the Hájek estimator, averaged over all simulations. We also calculate the Monte Carlo standard deviation of the Hájek estimator. We report the ratio of these two values in Figure A.1. Theoretically, this ratio should be greater than 1.

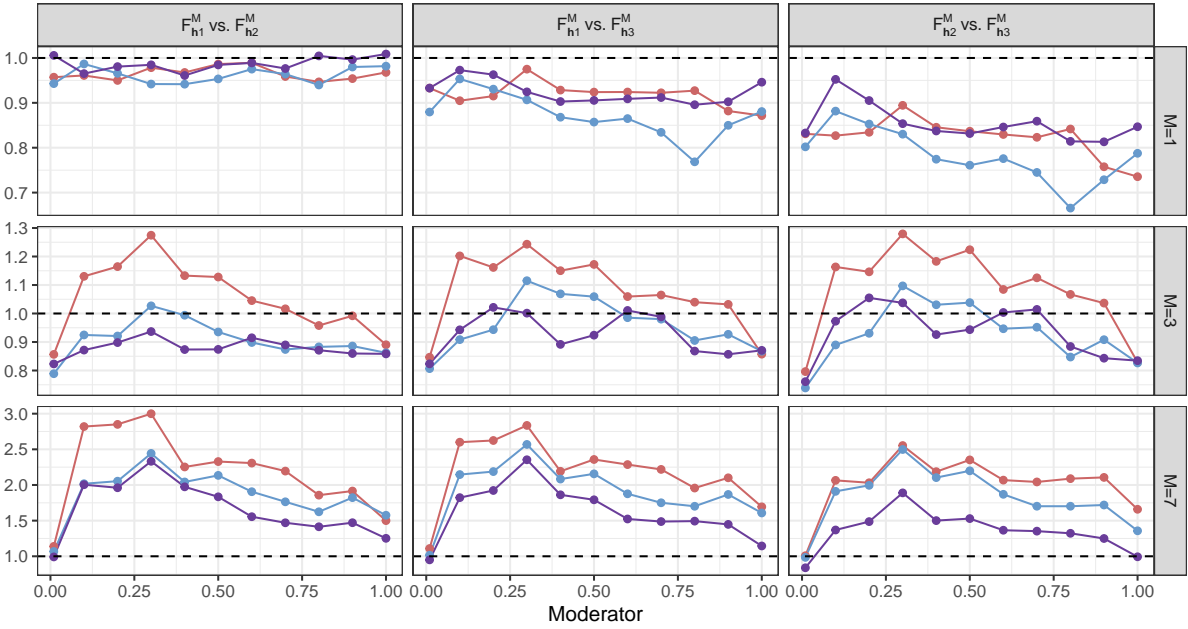
Figure A.1a examines the empirical performance of the variance bound estimator when the moderator is spatial. Each row corresponds to a different intervention time period  $M$  (1, 3, 7), and each column compares the results under different interventions. The results show that the ratio of the square root of the variance bound to the Monte Carlo standard deviation generally exceeds 1, aligning with theoretical expectations. However, for  $M = 1$ , the ratio occasionally falls below 1, particularly when  $T$  is small. As  $T$  increases from 200 to 1000, the ratio becomes more stable and approaches 1 across all moderator values, reflecting the improved accuracy of the estimator with longer time periods. Furthermore, for larger  $M$  (3 and 7), the trends are smoother, suggesting that longer intervention periods reduce variability in the performance of the variance bound estimator.

Figure A.1b presents the results for the spatio-temporal moderator. Similarly to the results for the spatial moderator, the rows correspond to different intervention time periods  $M$ , while the columns compare the results under different interventions. The ratio of square root of the variance bound to the Monte Carlo standard deviation remains close to or above 1, particularly for larger values of  $M$  and  $T$ . As  $T$  increases, the ratio stabilizes and approaches 1, especially when  $M = 3$  or  $M = 7$ . Compared to the spatial moderator case, the spatio-temporal results exhibit less fluctuation, even for small  $T$ , indicating that the variance bound estimator performs more reliably under the spatio-temporal setting.



(a) Spatial moderator

— T=200 — T=500 — T=1000



(b) Spatio-temporal moderator

Figure A.1: Ratio of the square root of the estimated variance bound, averaged across 500 simulations, to the mean standard deviation of the Hájek estimator based on the estimated propensity score with a spatio-temporal moderator. The standard deviation is computed by the Monte Carlo approximation. Interventions are considered over different time periods ( $M = 1, 3, 7$ ) and for time series of varying lengths ( $T = 200, 500, 1000$ ).

## E Statistical test of no heterogeneity

In this section, we prove Theorem 3. To do this, we first prove the following lemma, which shows the limiting reference distribution of the test statistic under the null hypothesis.

**Lemma A.2.** *Suppose that the assumptions of Theorem 1 hold and  $\bar{\boldsymbol{\beta}}^* = \mathbf{0}$ . Then, as  $T \rightarrow \infty$ , we have:*

$$(T - M + 1)(\bar{\boldsymbol{\beta}} - \bar{\boldsymbol{\beta}}^*)^\top (\mathbf{J}\mathbf{V}^H \mathbf{J}^\top)^{-1} (\bar{\boldsymbol{\beta}} - \bar{\boldsymbol{\beta}}^*) \xrightarrow{d} \chi_L^2.$$

### E.1 Proof of Lemma A.2

According to Theorem 1, we have, as  $T \rightarrow \infty$ ,

$$\sqrt{T - M + 1}(\bar{\boldsymbol{\beta}} - \bar{\boldsymbol{\beta}}^*) \xrightarrow{d} N(\mathbf{0}, \mathbf{J}\mathbf{V}^H \mathbf{J}^\top),$$

Since  $\mathbf{J}\mathbf{V}^H \mathbf{J}^\top$  is positive definite, by Cholesky decomposition, we have  $(\mathbf{J}\mathbf{V}^H \mathbf{J}^\top)^{-1} = \mathbf{L}\mathbf{L}^\top$  for some lower triangular matrix  $\mathbf{L}$ . Then, as  $T \rightarrow \infty$ ,

$$\mathbf{L}^\top \sqrt{T - M + 1}(\bar{\boldsymbol{\beta}} - \bar{\boldsymbol{\beta}}^*) \xrightarrow{d} N(\mathbf{0}, \mathbf{I}),$$

By continuous mapping theorem, we have, as  $T \rightarrow \infty$ ,

$$\begin{aligned} (T - M + 1)(\bar{\boldsymbol{\beta}} - \bar{\boldsymbol{\beta}}^*)^\top (\mathbf{L}\mathbf{L}^\top)^{-1} (\bar{\boldsymbol{\beta}} - \bar{\boldsymbol{\beta}}^*) &= (T - M + 1)(\bar{\boldsymbol{\beta}} - \bar{\boldsymbol{\beta}}^*)^\top (\mathbf{J}\mathbf{V}^H \mathbf{J}^\top)^{-1} (\bar{\boldsymbol{\beta}} - \bar{\boldsymbol{\beta}}^*) \\ &\xrightarrow{d} \chi_L^2. \end{aligned}$$

□

### E.2 Proof of Theorem 3

By Lemma A.2, we have

$$\lim_{T \rightarrow \infty} \mathbb{P} \left( (T - M + 1)(\bar{\boldsymbol{\beta}} - \mathbf{0})^\top (\mathbf{J}\mathbf{V}^H \mathbf{J}^\top)^{-1} (\bar{\boldsymbol{\beta}} - \mathbf{0}) > \chi_{1-\alpha, L}^2 \right) = \alpha$$

Since  $\mathbf{V}^{H*} - \mathbf{V}^H$  is positive semidefinite matrix,

$$(T - M + 1)\bar{\boldsymbol{\beta}}^\top (\mathbf{J}\mathbf{V}^{H*} \mathbf{J}^\top)^{-1} \bar{\boldsymbol{\beta}} \leq (T - M + 1)\bar{\boldsymbol{\beta}}^\top (\mathbf{J}\mathbf{V}^H \mathbf{J}^\top)^{-1} \bar{\boldsymbol{\beta}}.$$

Therefore,

$$\mathbb{P}\left((T - M + 1)\bar{\boldsymbol{\beta}}^\top (\mathbf{J}\mathbf{V}^{H*} \mathbf{J}^\top)^{-1} \bar{\boldsymbol{\beta}} > \chi_{1-\alpha, L}^2\right) \leq \mathbb{P}\left((T - M + 1)\bar{\boldsymbol{\beta}}^\top (\mathbf{J}\mathbf{V}^H \mathbf{J}^\top)^{-1} \bar{\boldsymbol{\beta}} > \chi_{1-\alpha, L}^2\right).$$

This implies,

$$\limsup_{T \rightarrow \infty} \mathbb{P}\left((T - M + 1)\bar{\boldsymbol{\beta}}^\top (\mathbf{J}\mathbf{V}^{H*} \mathbf{J}^\top)^{-1} \bar{\boldsymbol{\beta}} > \chi_{1-\alpha, L}^2\right) \leq \alpha.$$

Let  $n \in \mathbb{N}$  be given. Define  $\mathbf{D} = (\hat{\mathbf{J}}\mathbf{Q}\hat{\mathbf{V}}^H\mathbf{Q}^\top\hat{\mathbf{J}}^\top)^{-1} - (\mathbf{J}\mathbf{V}^{H*} \mathbf{J}^\top)^{-1}$ . Since  $\hat{\mathbf{J}}\mathbf{Q}\hat{\mathbf{V}}^H\mathbf{Q}^\top\hat{\mathbf{J}}^\top$  is a consistent estimator of  $\mathbf{J}\mathbf{V}^{H*} \mathbf{J}^\top$ ,  $(\hat{\mathbf{J}}\mathbf{Q}\hat{\mathbf{V}}^H\mathbf{Q}^\top\hat{\mathbf{J}}^\top)^{-1}$  is a consistent estimator of  $(\mathbf{J}\mathbf{V}^{H*} \mathbf{J}^\top)^{-1}$ . Therefore, we have  $\lim_{T \rightarrow \infty} \mathbb{P}(\|\mathbf{D}\| > \frac{1}{n}) = 0$ . Since  $\bar{\boldsymbol{\beta}}$  is bounded, we have

$$\lim_{T \rightarrow \infty} \mathbb{P}\left(\left|\bar{\boldsymbol{\beta}}^\top \mathbf{D} \bar{\boldsymbol{\beta}}\right| > \frac{1}{n}\right) \leq \lim_{T \rightarrow \infty} \mathbb{P}\left(\|\bar{\boldsymbol{\beta}}\|^2 \|\mathbf{D}\| > \frac{1}{n}\right) = 0.$$

Note that

$$\begin{aligned} & \mathbb{P}\left((T - M + 1)\bar{\boldsymbol{\beta}}^\top (\hat{\mathbf{J}}\hat{\mathbf{V}}^H\hat{\mathbf{J}}^\top)^{-1} \bar{\boldsymbol{\beta}} > \chi_{1-\alpha, L}^2 + \frac{1}{n}\right) \\ &= \mathbb{P}\left((T - M + 1)\bar{\boldsymbol{\beta}}^\top (\mathbf{J}\mathbf{V}^{H*} \mathbf{J}^\top)^{-1} \bar{\boldsymbol{\beta}} + \bar{\boldsymbol{\beta}}^\top \mathbf{D} \bar{\boldsymbol{\beta}} > \chi_{1-\alpha, L}^2 + \frac{1}{n}\right) \\ &\leq \mathbb{P}\left((T - M + 1)\bar{\boldsymbol{\beta}}^\top (\mathbf{J}\mathbf{V}^{H*} \mathbf{J}^\top)^{-1} \bar{\boldsymbol{\beta}} > \chi_{1-\alpha, L}^2\right) + \mathbb{P}\left(\left|\bar{\boldsymbol{\beta}}^\top \mathbf{D} \bar{\boldsymbol{\beta}}\right| > \frac{1}{n}\right) \\ &\leq \alpha + \mathbb{P}\left(\left|\bar{\boldsymbol{\beta}}^\top \mathbf{D} \bar{\boldsymbol{\beta}}\right| > \frac{1}{n}\right). \end{aligned}$$

Taking the lim sup of both sides, we obtain

$$\limsup_{T \rightarrow \infty} \mathbb{P}\left((T - M + 1)\bar{\boldsymbol{\beta}}^\top (\hat{\mathbf{J}}\hat{\mathbf{V}}^H\hat{\mathbf{J}}^\top)^{-1} \bar{\boldsymbol{\beta}} > \chi_{1-\alpha, L}^2 + \frac{1}{n}\right) \leq \alpha + 0 = \alpha.$$

Let  $E_n$  denote the event that

$$(T - M + 1)\bar{\boldsymbol{\beta}}^\top (\hat{\mathbf{J}}\hat{\mathbf{V}}^H\hat{\mathbf{J}}^\top)^{-1} \bar{\boldsymbol{\beta}} > \chi_{1-\alpha, L}^2 + \frac{1}{n}.$$

Since  $\{E_n\}_{n \geq 1}$  is an increasing sequence of events, taking the limit of  $n \rightarrow \infty$ , we have

$$\limsup_{T \rightarrow \infty} \mathbb{P}\left((T - M + 1)\bar{\boldsymbol{\beta}}^\top (\hat{\mathbf{J}}\hat{\mathbf{V}}^H\hat{\mathbf{J}}^\top)^{-1} \bar{\boldsymbol{\beta}} > \chi_{1-\alpha, L}^2\right) \leq \alpha.$$

Note that

$$\mathbb{P}(\text{p-value} < \alpha) = \mathbb{P}(T_c > \chi_{1-\alpha, L}^2) = \mathbb{P}\left((T - M + 1)\bar{\boldsymbol{\beta}}^\top (\hat{\mathbf{J}}\hat{\mathbf{V}}^H\hat{\mathbf{J}}^\top)^{-1}\bar{\boldsymbol{\beta}} > \chi_{1-\alpha, L}^2\right).$$

We obtain the desired result,

$$\limsup_{T \rightarrow \infty} \mathbb{P}(\text{p-value} < \alpha) \leq \alpha.$$

□

## F Extensions to dependent interventions

In this section, we present detailed extensions of the framework to allow intervention distributions that are dependent across time periods.

Consider a dependent (joint) intervention distribution over  $M$  time periods, denoted by  $F_{\mathbf{h}}$ , with density  $f_{\mathbf{h}}(w_1, w_2, \dots, w_M)$  for  $(w_1, w_2, \dots, w_M) \in \mathcal{W}^M$ . Under this more general intervention scheme, the estimand of the expected number of outcome events in pixel  $S_i$  at time  $t$  remains identical to the one introduced in Section 2.2:

$$N_{it}(F_{\mathbf{h}}) = \int_{\mathcal{W}^M} N_{S_i}(Y_t(\bar{\mathbf{W}}_{t-M}, w_{t-M+1}, \dots, w_t)) dF_{\mathbf{h}}(w_{t-M+1}, \dots, w_t).$$

The CATE estimand is defined in the same manner, replacing the independent intervention distribution by  $F_{\mathbf{h}}$ . For estimation, we modify Assumption 2 as follows.

**Assumption A.6.** *There exists  $\delta_W > 0$  such that*

$$e_{t-M+1}(w_1) e_{t-M+2}(w_2) \cdots e_t(w_M) > \delta_W f_{\mathbf{h}}(w_1, \dots, w_M)$$

for all  $(w_1, \dots, w_M) \in \mathcal{W}^M$  for which  $f_{\mathbf{h}}(w_1, \dots, w_M) > 0$ , where  $e_t(w) = f(W_t = w | \bar{H}_{t-1})$ .

As expected, when  $F_{\mathbf{h}} = F_h \times \cdots \times F_h$  (identical and independent distribution across periods), Assumption A.6 reduces to Assumption 2. The pseudo-outcomes  $\tilde{Y}_{it}^I(F_{\mathbf{h}}; \hat{\boldsymbol{\gamma}})$  and  $\tilde{Y}_{it}^H(F_{\mathbf{h}}; \hat{\boldsymbol{\gamma}})$  can be defined in the same way as done in Section 2.4, using modified inverse-probability weights:

$$\rho_{t\mathbf{h}}(\hat{\boldsymbol{\gamma}}) = \frac{f_{\mathbf{h}}(W_{t-M+1}, \dots, W_t)}{\prod_{j=t-M+1}^t e_j(W_j; \hat{\boldsymbol{\gamma}})}.$$

None of the proofs in the main sections depend on the intervention distribution being independent over time. Therefore, all theoretical results remain valid under the dependent

intervention distribution, provided the modified overlap assumption holds.

The dependent intervention presented here extends the framework in the main text by allowing treatments to be correlated across time periods. This setup can be regarded as a special case of the adaptive intervention, where the current treatment depends only on past treatments. Accordingly, the choice of matrix  $\mathbf{Q}$  for constructing the estimated variance bound is the same as that described for adaptive interventions in Section G.

## G Extending proofs to adaptive interventions

In this section, we discuss how to extending proofs the previous sections in the adaptive case. Consider an adaptive intervention over  $M$  time periods,  $F_{\mathbf{h}_t} = (F_{h_{t1}}, \dots, F_{h_{tM}})$ , where each  $F_{h_{tm}}$  is allowed to depend on the observed history, i.e.  $F_{h_{tm}}$  has density  $f_{h_{tm}}(w \mid \overline{H}_{t-m})$  for all  $w \in \mathcal{W}$  and  $1 \leq m \leq M$ . We first show that  $\tilde{Y}_{it}^I(F_{\mathbf{h}_t}; \gamma)$  defined in Section 2.7 is unbiased to  $N_{it}(F_{\mathbf{h}_t}; \overline{H}_{t-M})$  conditional on  $\overline{H}_{t-M}^*$ , under the true propensity score.

**Lemma A.3.** *Under Assumption 1,*

$$\mathbb{E} \left[ \tilde{Y}_{it}^I(F_{\mathbf{h}_t}; \gamma^*) \mid \overline{H}_{t-M}^* \right] = N_{it}(F_{\mathbf{h}_t}; \overline{H}_{t-M})$$

**Proof.** We will prove the statement for  $M = 2$ . The proofs for  $M = 1$  and  $M > 2$  are similar. When  $M = 2$ , we have

$$\begin{aligned} & \mathbb{E} \left[ \tilde{Y}_{it}^I(F_{h_{t1}}, F_{h_{t2}}; \gamma^*) \mid \overline{H}_{t-2}^* \right] \\ & \mathbb{E} \left[ \frac{f_{h_{t1}}(W_t \mid \overline{H}_{t-1}) f_{h_{t2}}(W_{t-1} \mid \overline{H}_{t-2})}{e_t(W_t; \gamma^*) e_{t-1}(W_{t-1}; \gamma^*)} N_{S_i}(Y_t) \mid \overline{H}_{t-2}^* \right] \\ &= \int_{\mathcal{W}} \int_{\mathcal{W}} \frac{f_{h_{t1}}(W_t \mid \overline{H}_{t-1}) f_{h_{t2}}(W_{t-1} \mid \overline{H}_{t-2})}{e_t(W_t; \gamma^*) e_{t-1}(W_{t-1}; \gamma^*)} N_{S_i}(Y_t(\overline{\mathbf{W}}_{t-2}, w_{t-1}, w_t)) \\ & \quad \times f(w_{t-1} \mid \overline{H}_{t-2}^*) f(w_t \mid \overline{H}_{t-1}^*) dw_{t-1} dw_t \\ &= \int_{\mathcal{W}} \left[ \int_{\mathcal{W}} f_{h_{t1}}(W_t \mid \overline{H}_{t-1}) N_{S_i}(Y_t(\overline{\mathbf{W}}_{t-2}, w_{t-1}, w_t)) dw_t \right] f_{h_{t2}}(W_{t-1} \mid \overline{H}_{t-2}) dw_{t-1} \text{ (Assumption 1)} \\ &= \int_{\mathcal{W}} N_{it}(F_{h_{t1}}; \overline{H}_{t-1}) f_{h_{t2}}(W_{t-1} \mid \overline{H}_{t-2}) dw_{t-1} \\ &= N_{it}(F_{h_{t1}}, F_{h_{t2}}; \overline{H}_{t-2}), \end{aligned}$$

as desired.  $\square$

According to Lemma A.3, we can construct martingale difference sequence based on  $\tilde{Y}_{it}^I(F_{\mathbf{h}_t}; \gamma^*) - N_{it}(F_{\mathbf{h}_t}; \overline{H}_{t-M})$ . Then the proofs from the previous sections carry through in this adaptive case.

For the estimated variance bound, we can use a similar choice of  $\mathbf{Q}$  as the one introduced in Section 2.5. Specifically, when comparing two adaptive interventions  $F_{\mathbf{h}'_t} = (F_{h'_{t1}}, \dots, F_{h'_{tM}})$  and  $F_{\mathbf{h}''_t} = (F_{h''_{t1}}, \dots, F_{h''_{tM}})$ , we define

$$\xi_{h'_{tm}} = \frac{1}{T} \sum_{t=1}^T \frac{f_{h'_{tm}}(W_t | \bar{H}_{t-1})}{e_t(W_t; \hat{\gamma})} \quad \text{and} \quad \xi_{h''_{tm}} = \frac{1}{T} \sum_{t=1}^T \frac{f_{h''_{tm}}(W_t | \bar{H}_{t-1})}{e_t(W_t; \hat{\gamma})}, \quad m = 1, \dots, M.$$

We then choose

$$\mathbf{Q} = \text{diag}(\rho_{\mathbf{h}'_t}^{-1} \mathbf{1}_L, \rho_{\mathbf{h}''_t}^{-1} \mathbf{1}_L, \prod_{m=1}^M \xi_{h'_{tm}}^{-1}, \prod_{m=1}^M \xi_{h''_{tm}}^{-1}).$$

Since non-adaptive and dependent interventions are special cases of the adaptive framework, this choice of  $\mathbf{Q}$  also applies to these settings. When the interventions are independent and identical across time periods,  $\mathbf{Q}$  reduces to the one introduced in Section 2.5.

## H Moderator variables and baseline density in simulations

In this section, we present additional visualizations of the spatial and spatio-temporal moderator variables used in the simulation study, as well as the baseline density for the intervention distribution.

Figure A.2 provides an illustration of the moderators used in the simulation study. Panel (a) depicts the spatial moderator  $X_2$ , which is derived based on the distance to Baghdad. Panel (b) shows a realization of the spatio-temporal moderator  $X_{3t}$ , which is generated using a Poisson point process based on estimated airstrike density. Panel (c) presents the logarithm of the baseline density for the intervention distribution, which is used to model the spatial allocation of treatment. In addition, Figure A.3 presents the distribution of the spatial moderator  $X_2$  and the spatio-temporal moderator  $X_{3t}$  in the simulation.

## I Expected airstrike difference and aid distribution

In this section, we visualize the expected airstrike difference and the moderator variable used in the empirical study. Figure A.4 presents two relevant distributions. Panel (a) illustrates the expected change in airstrike intensity under intervention  $F_{h_2}^M$  relative to intervention  $F_{h_1}^M$  considered in the empirical analysis. Panel (b) presents the histogram of continuous aid (in log scale), which serves as a moderator in the empirical analysis.

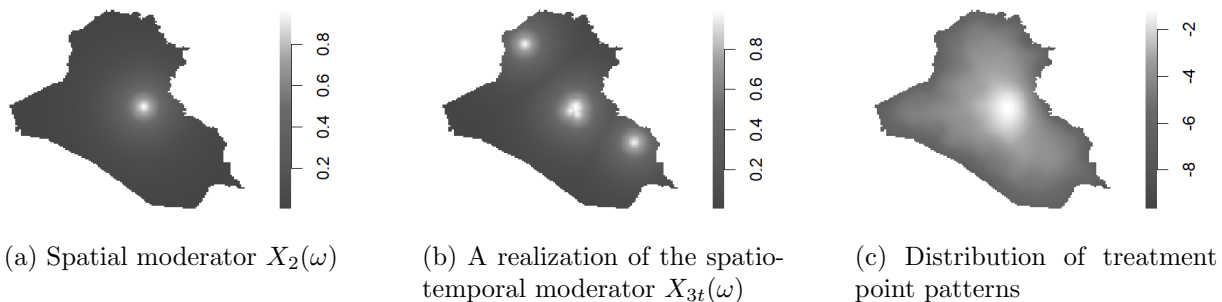


Figure A.2: Panels (a) and (b) present the spatial and spatio-temporal moderator variables. Panel (c) shows the logarithm of the baseline density for the intervention distribution.

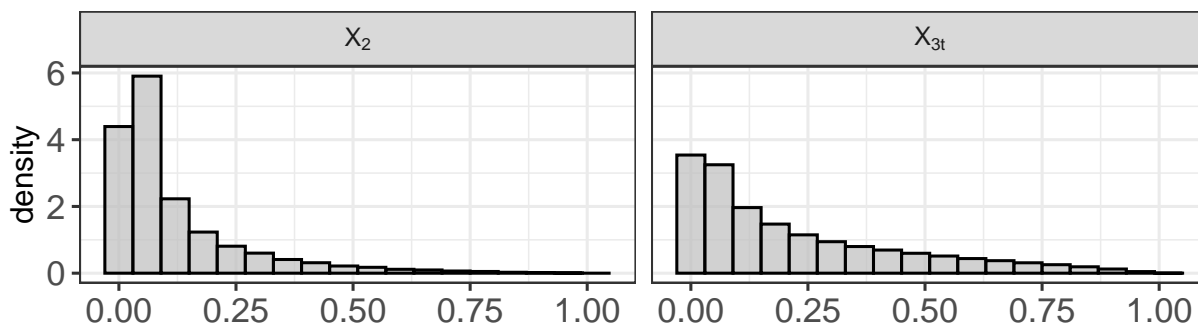


Figure A.3: Histograms of spatial moderator  $X_2$  and spatio-temporal temporal moderator  $X_{3t}$  across all pixels and all time periods.

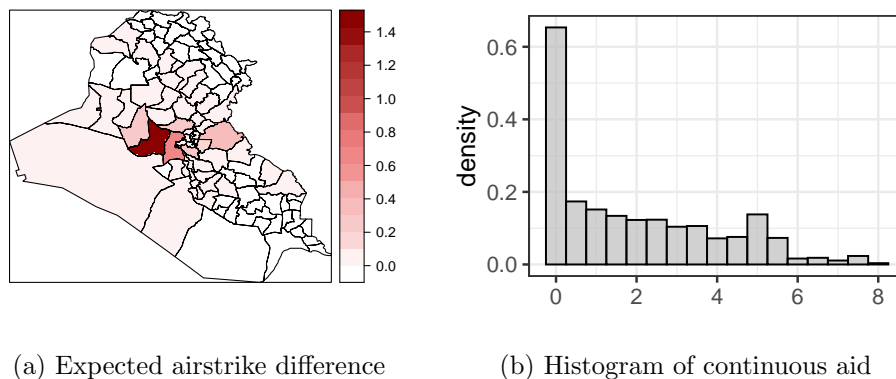


Figure A.4: Panel (a) shows the expected changes in number of airstrikes under intervention  $F_{h_2}^M$  over intervention  $F_{h_1}^M$  for each district. Plot (b) shows the histogram of the continuous aid in the log scale

## J Additional simulation results

In this section, we first discuss how we use Monte Carlo approximation to the true CATE values. We then present additional simulation results for the Hájek and IPW estimators. We also compare those two estimators and examine the efficiency gain resulting from the

use of the estimated propensity score rather than the true propensity score.

## J.1 Monte Carlo approximation procedure

As a concrete example, we outline the procedure for approximating the true CATE value  $\tau_{\mathbf{h}_1, \mathbf{h}_2}(r)$  that compares two intervention distributions  $F_{\mathbf{h}_1}$  and  $F_{\mathbf{h}_2}$ . At each time period  $t$  and a given Monte Carlo draw  $k = 1, \dots, K$ , we sample treatment point patterns  $w_{t-M+1}^{(jk)}, \dots, w_t^{(jk)}$  from the intervention distribution  $F_{\mathbf{h}_j}$  separately for  $j = 1, 2$ . Then, we generate outcome point patterns  $y_{t-M+1}^{(jk)}, \dots, y_t^{(jk)}$  based on the treatment path  $(\overline{\mathbf{W}}_{t-M}, w_{t-M+1}^{(jk)}, \dots, w_t^{(jk)})$ , and compute the difference of outcomes in each pixel  $S_i$  at time  $t$ ,  $D_{it}^{(k)} = N_{S_i}(y_t^{2k}) - N_{S_i}(y_t^{1k})$ . Let  $r_{it}$  be the value of the moderator in pixel  $S_i$  at time  $t$ . We compute  $\tau_{t, \mathbf{h}_1, \mathbf{h}_2}^{(k)}(r)$  by regressing  $D_{it}^{(k)}$  on  $z_1(r_{it}), \dots, z_L(r_{it})$  as shown in Equation (3). Averaging  $\tau_{t, \mathbf{h}_1, \mathbf{h}_2}^{(k)}(r)$  over all the iterations and time periods gives an approximation of  $\tau_{t, \mathbf{h}_1, \mathbf{h}_2}^{\text{Proj.}}(r; \boldsymbol{\beta}_t^*)$ .

## J.2 The Hájek estimator

We present additional simulation results for the Hájek estimator. Figure A.5 shows the results for spatial effect moderator in the scenario assessed in Section 3.3. Figure A.6 shows the results for the comparison between the two interventions,  $F_{\mathbf{h}_1}^M$  and  $F_{\mathbf{h}_2}^M$ , while Figure A.7 compares  $F_{\mathbf{h}_2}^M$  with  $F_{\mathbf{h}_3}^M$ .

Figure A.5 presents the results for the spatial moderator in the comparison of  $F_{\mathbf{h}_1}^M$  and  $F_{\mathbf{h}_3}^M$ . The Hájek estimators perform well for the spatial moderator, closely tracking the true CATEs with minimal bias and maintaining empirical coverage near the nominal 95% level. The estimator performs similarly regardless of whether true or estimated propensity scores are used. Even for  $M = 7$ , the average bias remains below 0.001. As the number of intervention time periods increases, empirical coverage decreases slightly but remains above 0.87 across all scenarios. In regions with limited data, particularly near the upper end of the moderator range, small biases emerge, but coverage remains stable, indicating that the variance estimates effectively account for data sparsity.

In Figure A.6, we present results for the comparison between  $F_{\mathbf{h}_1}^M$  and  $F_{\mathbf{h}_2}^M$ . For the spatial moderator (Figure A.6a), we observe that the Hájek estimator performs well for  $M = 1$ , with estimated CATEs closely tracking the true CATEs and minimal bias. The empirical coverage of the 95% confidence intervals remains close to the nominal level within the shaded region, highlighting the 0.025 and 0.975 quantiles of the moderator values. However, as  $M$  increases to 3 and 7, the bias begins to increase slightly near the upper end of the moderator range (values close to 1). This indicates that longer time series may be required in these regions to achieve better performance. For the spatio-temporal moderator

(Figure A.6b), similar trends emerge. The Hájek estimator performs well for small  $M$ , with coverage rates remaining stable and close to 0.95. However, for  $M = 7$ , the bias increases for larger moderator values, although it remains small overall.

In Figure A.7, we present results for the comparison between  $F_{h_2}^M$  and  $F_{h_3}^M$ . For the spatial moderator (Figure A.7a), the Hájek estimator again performs well when  $M = 1$ , with minimal bias and empirical coverage rates close to the nominal 0.95 level. As  $M$  increases, deviations from the true CATE become more apparent near the upper range of the moderator values. In the spatio-temporal moderator case (Figure A.7b), the performance of the Hájek estimator remains robust for  $M = 1$ , with small bias and stable coverage rates. For larger  $M$ , the estimated CATEs continue to closely follow the true CATEs within the shaded region, although small biases appear near the large values of the moderator.

Overall, these additional results demonstrate that the Hájek estimator performs consistently well in the different scenarios. For both spatial and spatio-temporal moderators, the empirical coverage rates remain close to the nominal 95% level, especially for small  $M$ . However, as  $M$  increases, deviations from the true CATEs become noticeable at higher moderator values, suggesting that longer time series are needed to maintain performance in sparse regions.

### J.3 The IPW estimator

We present the performance of IPW estimators in the simulation studies described in Section 3. Figures A.8, A.9, and A.10 show the results of the comparison of  $F_{h_1}^M$  v.s  $F_{h_2}^M$ ,  $F_{h_1}^M$  v.s  $F_{h_3}^M$  and  $F_{h_2}^M$  v.s  $F_{h_3}^M$  respectively.

In Figure A.8, which compares  $F_{h_1}^M$  and  $F_{h_2}^M$ , the IPW estimators perform well in the spatial moderator case when  $M = 1$ , where the estimated CATEs align closely with the true CATEs and exhibit minimal bias. The empirical coverage remains near the nominal 95% level. As  $M$  increases to 3 and 7, unstabilized weights result in larger biases, particularly near the upper range of the moderator values, and the empirical coverage deteriorate as  $M$  increases. In contrast, stabilized weights produce smaller biases and maintain more reliable coverage. For the spatio-temporal moderator, a similar pattern holds: stabilized weights consistently outperform their unstabilized counterparts, delivering more accurate estimates and better coverage properties. Additionally, estimators using the estimated propensity scores generally achieve comparable or even superior performance relative to those based on the true propensity scores.

Figure A.9 displays the results for  $F_{h_1}^M$  versus  $F_{h_3}^M$ . In the spatial moderator case, the IPW estimators perform well when  $M = 1$ , but as  $M$  increases, bias becomes more pronounced for unstabilized weights, particularly near higher moderator values. Empirical

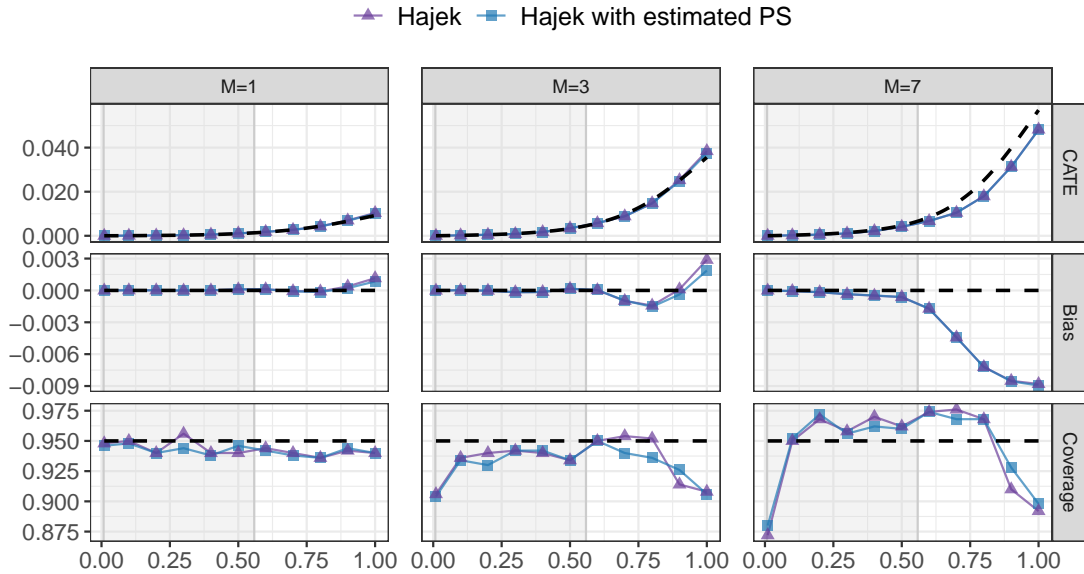
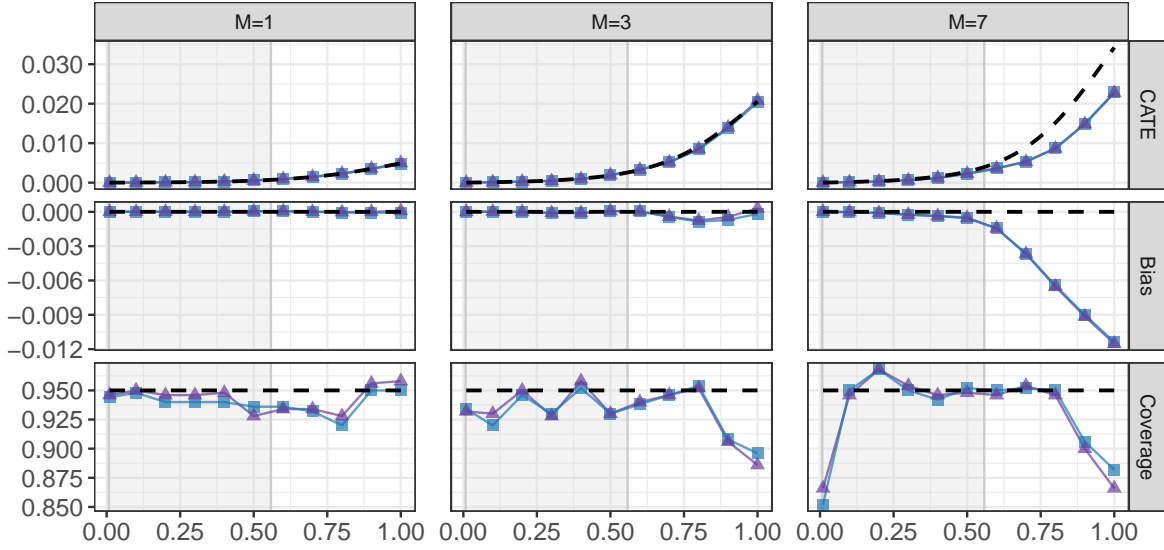


Figure A.5: The average of estimated CATE (first row), bias (second row), and coverage (third row) based on Hájek estimators for  $F_{h_1}^M$  versus  $F_{h_3}^M$  across 500 simulations for the spatial moderator. Dashed lines in the first, second, and third rows represent the true CATE, bias of zero, and the nominal coverage of 95%, respectively. The purple line with triangles denotes the estimator based on the true propensity score, while the blue line with squares represent the estimators based on the estimated propensity scores. The shaded region indicates the 0.025 and 0.975 quantile range of the moderator values.

coverage remains mostly stable across the range but drops for larger  $M$ . Similar trends are observed for the spatio-temporal moderator.

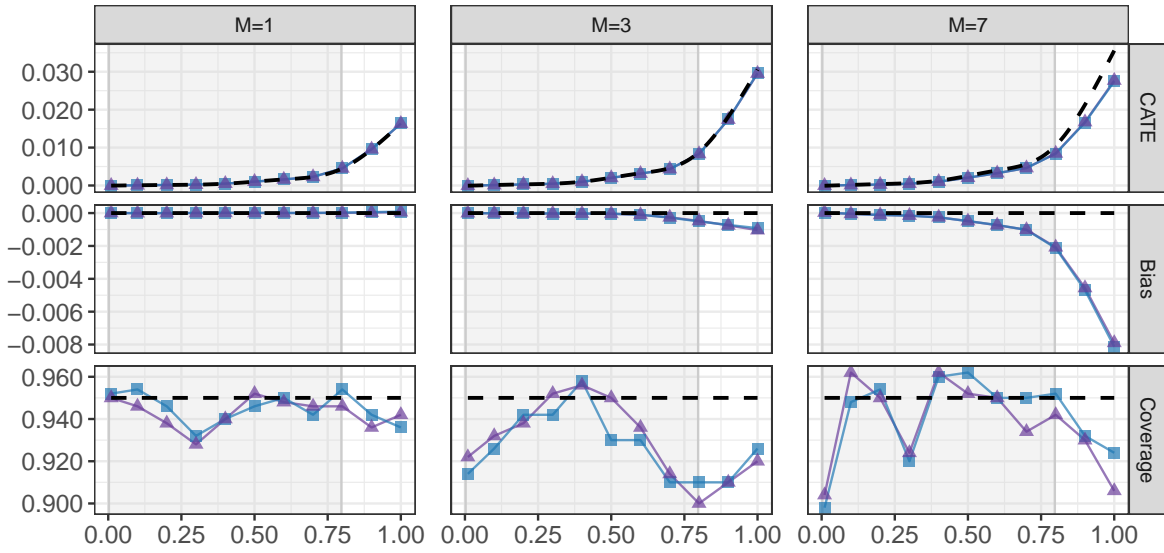
For  $F_{h_2}^M$  versus  $F_{h_3}^M$ , the results are shown in Figure A.10. In the spatial moderator case, the IPW estimators again perform well for  $M = 1$ , with estimated CATEs exhibiting minimal bias and empirical coverage close to 0.95. As  $M$  increases, unstabilized weights result in noticeable bias at higher moderator values and the coverage drops. In particular, for  $M = 7$ , the empirical coverage falls below 50% for all IPW-type estimators. The spatio-temporal results are consistent with earlier findings.

Overall, the IPW estimators perform well in low-variance settings, such as  $M = 1$ . However, for larger values of  $M$ , stabilized weights substantially enhance performance, reducing bias and improving empirical coverage. Across all comparisons and moderator types, Hájek estimators often outperform IPW estimators. These findings align with broader results in causal inference, where stabilized weights are known to improve finite-sample properties, especially in higher-variance settings.



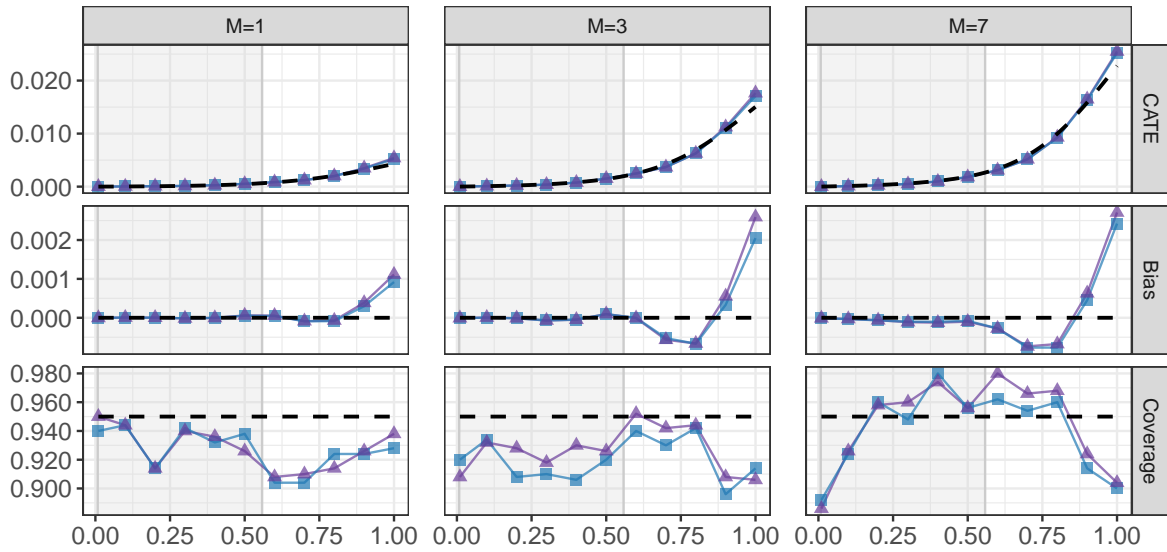
(a) Spatial moderator

▲ Hajek    ■ Hajek with estimated PS



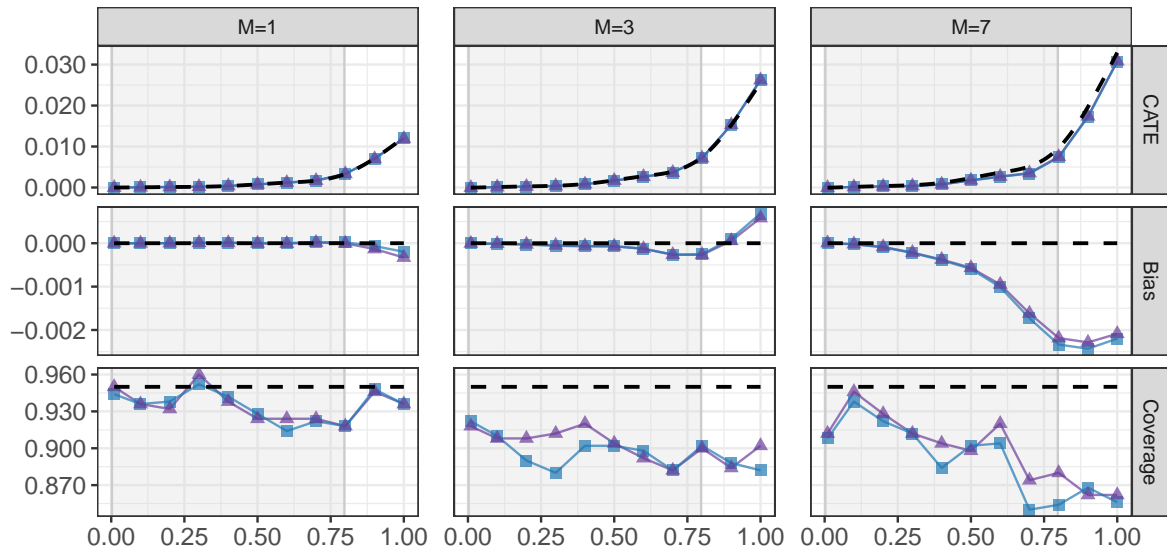
(b) Spatio-temporal moderator

Figure A.6: The average of estimated CATE (first row), bias (second row) and coverage (third row) based on the Hájek estimator for  $F_{h_1}^M$  versus  $F_{h_2}^M$  across 500 simulations. Dashed lines in the first, second, and third rows represent the true CATE, zero bias, and the theoretical minimum coverage, respectively. Plot (a) corresponds to the spatial moderator, while plot (b) pertains to the spatio-temporal moderator, both for various values of  $M = 1, 3, 7$ . The purple line with triangles denotes the estimator based on the true propensity score, while the blue line with squares represent the estimators based on the estimated propensity scores. The shaded region indicates the 0.025 and 0.975 quantile range of the moderator values.



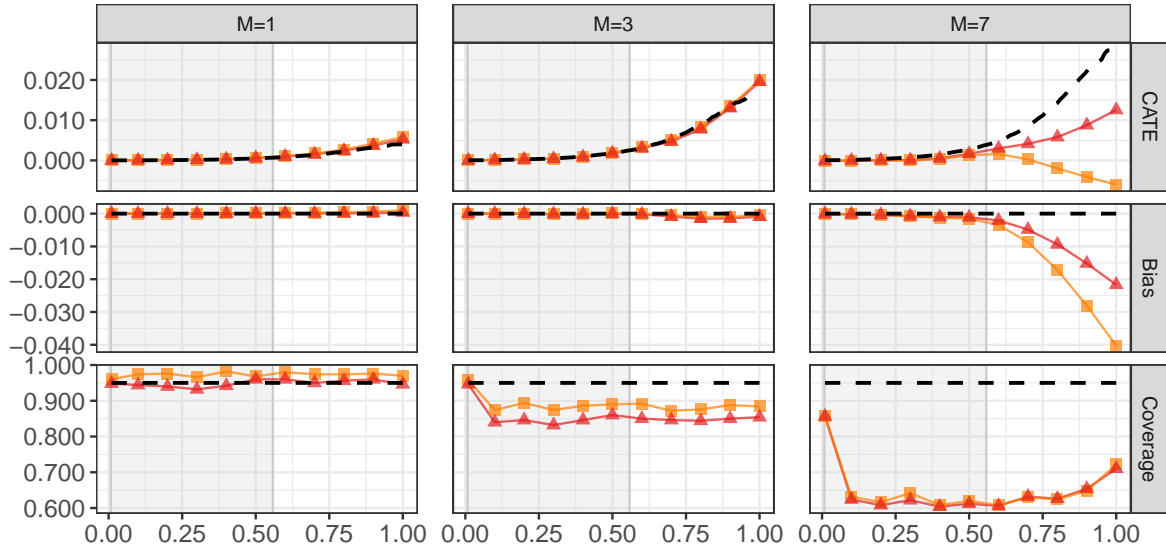
(a) Spatial moderator

▲ Hajek ■ Hajek with estimated PS



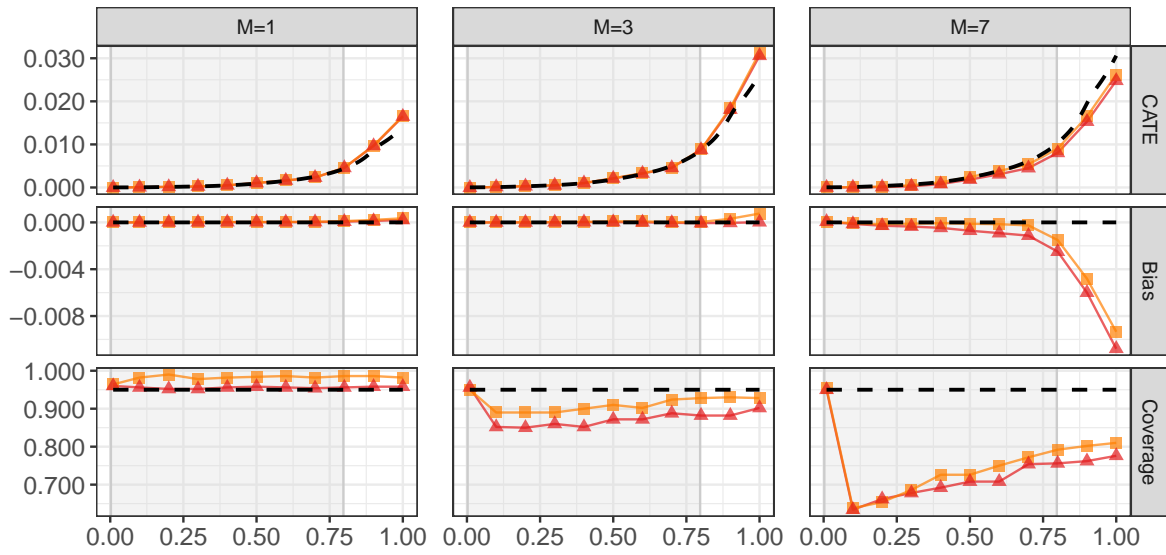
(b) Spatio-temporal moderator

Figure A.7: The average of estimated CATE (first row), bias (second row) and coverage (third row) based on the Hájek estimator for  $F_{h_2}^M$  versus  $F_{h_3}^M$  across 500 simulations. Dashed lines in the first, second, and third rows represent the true CATE, zero bias, and the theoretical minimum coverage, respectively. Plot (a) corresponds to the spatial moderator, while plot (b) pertains to the spatio-temporal moderator, both for various values of  $M = 1, 3, 7$ . The purple line with triangles denotes the estimator based on the true propensity score, while the blue line with squares represent the estimators based on the estimated propensity scores. The shaded region indicates the 0.025 and 0.975 quantile range of the moderator values.



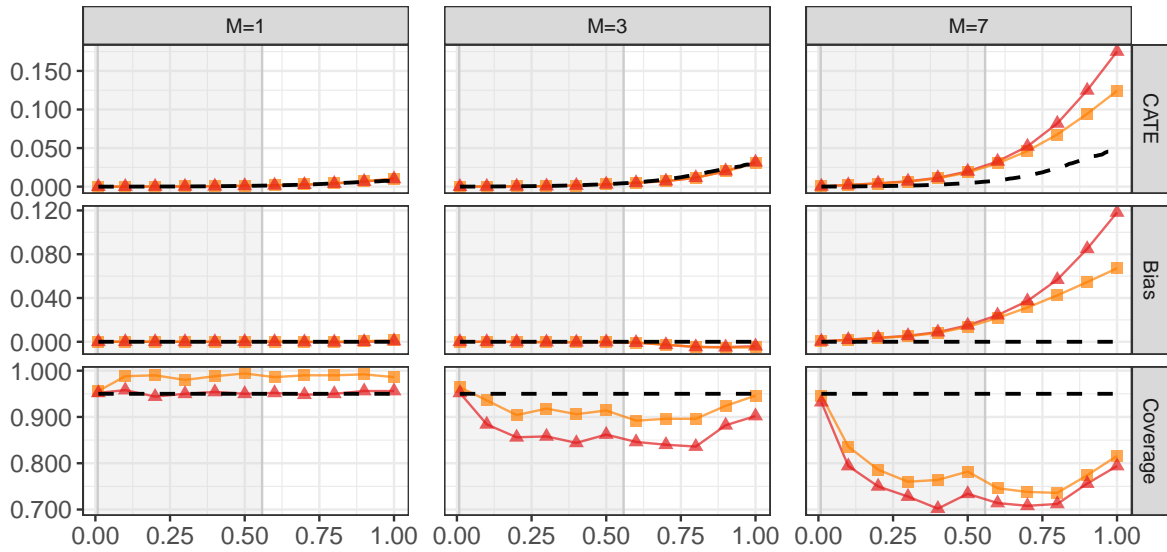
(a) Spatial moderator

—▲ IPW —■ IPW with estimated PS



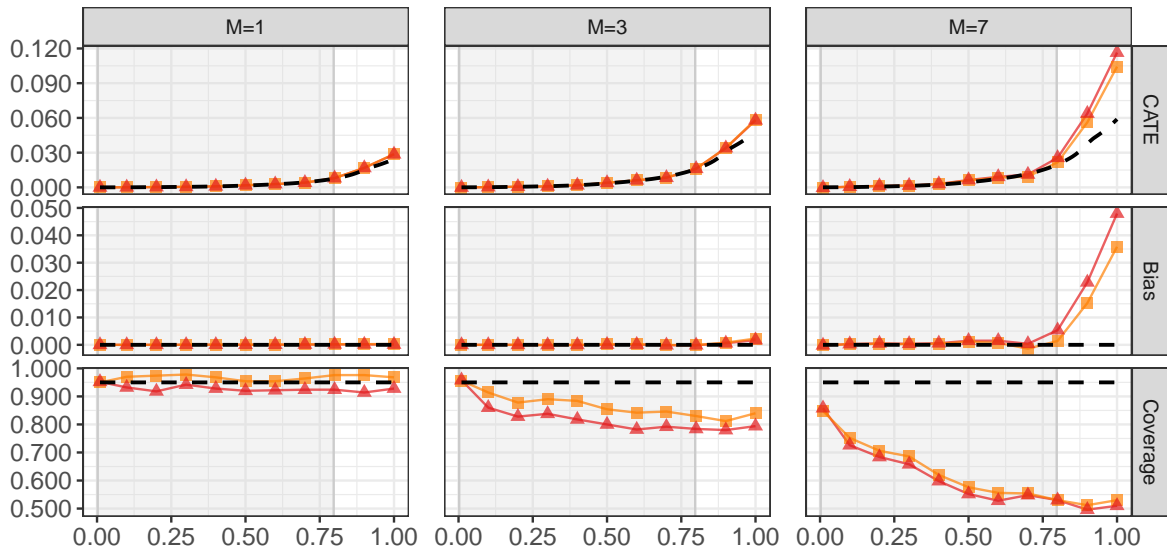
(b) Spatio-temporal moderator

Figure A.8: The average of estimated CATE (first row), bias (second row) and coverage (third row) based on IPW estimators for  $F_{h_1}^M$  versus  $F_{h_2}^M$  across 500 simulations. Dashed lines in the first, second, and third rows represent the true CATE, zero bias, and the theoretical minimum coverage, respectively. Plot (a) corresponds to the spatial moderator, while plot (b) pertains to the spatio-temporal moderator, both for various values of  $M = 1, 3, 7$ . The purple line with triangles denotes the estimator based on the true propensity score, while the blue line with squares represent the estimators based on the estimated propensity scores. The shaded region indicates the 0.025 and 0.975 quantile range of the moderator values.



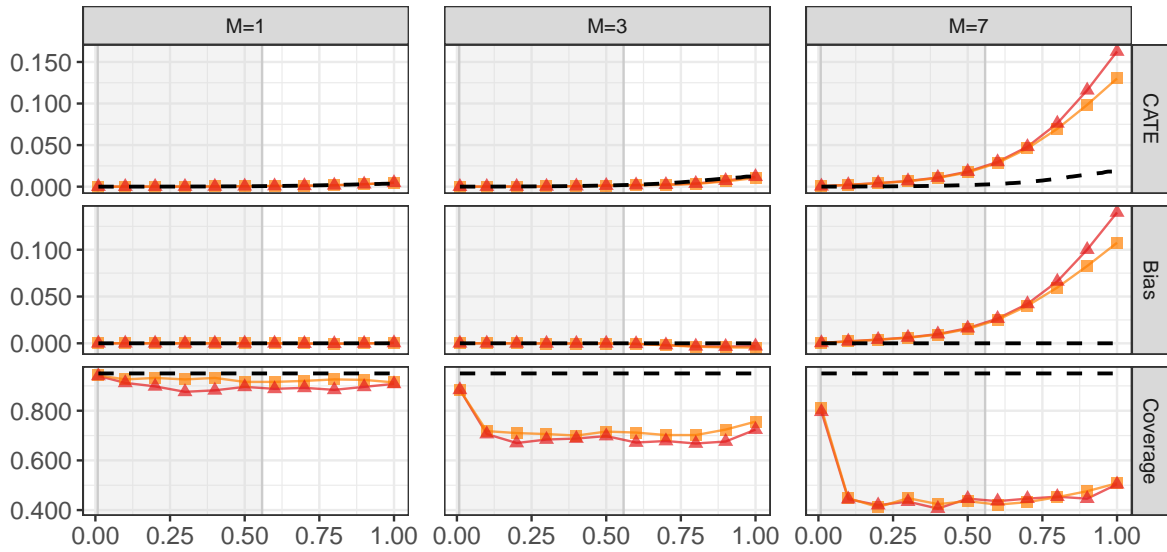
(a) Spatial moderator

—▲ IPW —■ IPW with estimated PS



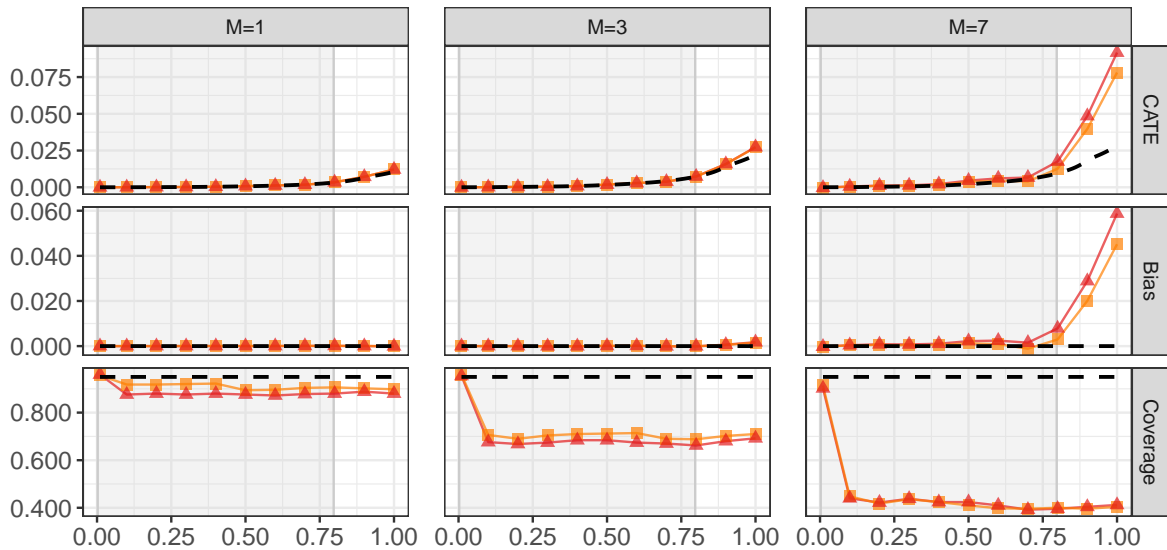
(b) Spatio-temporal moderator

Figure A.9: The average of estimated CATE (first row), bias (second row) and coverage (third row) based on IPW estimators for  $F_{h_1}^M$  versus  $F_{h_3}^M$  across 500 simulations. Dashed lines in the first, second, and third rows represent the true CATE, zero bias, and the theoretical minimum coverage, respectively. Plot (a) corresponds to the spatial moderator, while plot (b) pertains to the spatio-temporal moderator, both for various values of  $M = 1, 3, 7$ . The purple line with triangles denotes the estimator based on the true propensity score, while the blue line with squares represent the estimators based on the estimated propensity scores. The shaded region indicates the 0.025 and 0.975 quantile range of the moderator values.



(a) Spatial moderator

—▲ IPW —■ IPW with estimated PS



(b) Spatio-temporal moderator

Figure A.10: The average of estimated CATE (first row), bias (second row) and coverage (third row) based on IPW estimators for  $F_{h_2}^M$  versus  $F_{h_3}^M$  across 500 simulations. Dashed lines in the first, second, and third rows represent the true CATE, zero bias, and the theoretical minimum coverage, respectively. Plot (a) corresponds to the spatial moderator, while plot (b) pertains to the spatio-temporal moderator, both for various values of  $M = 1, 3, 7$ . The purple line with triangles denotes the estimator based on the true propensity score, while the blue line with squares represent the estimators based on the estimated propensity scores. The shaded region indicates the 0.025 and 0.975 quantile range of the moderator values.

## J.4 Efficiency due to the use of the estimated propensity score

We examine the relative efficiency of the IPW and Hájek estimators when using the estimated propensity score rather than the true propensity score. In particular, we computed the Monte Carlo standard deviation of the estimators across 500 simulations and present the ratio of standard deviation for the proposed estimator based on the true propensity score over that based on the estimated propensity score. If the ratio is greater than 1, the estimated propensity score makes the Hájek and IPW estimators more efficient than the true propensity score. According to Theorem 2 and Theorem A.3, these ratios should be no less than 1 asymptotically.

The results are shown in Figure A.11. We find that the estimated propensity score yields a significant efficiency gain for the IPW estimator for  $M = 1$  and  $M = 3$ , while the variance ratio for the Hájek estimator remains close to 1 in all scenarios. Occasionally, the variance ratio falls below 1, especially in high-variability scenarios with  $M = 7$ . This may be because the Monte Carlo variance does not sufficiently approximate the true asymptotic variances for the sample sizes considered.

## J.5 Efficiency comparison of IPW and Hájek estimators

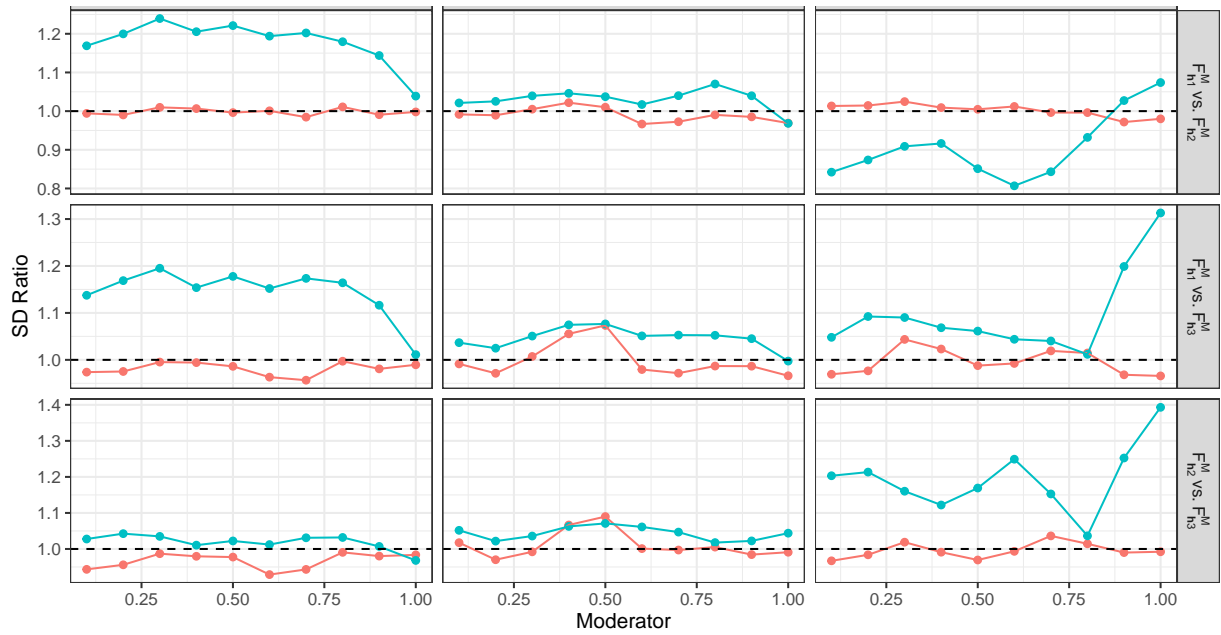
Finally, we compare the variance of the IPW estimator with that of the Hájek estimator. We compute the Monte Carlo standard deviation of the IPW and Hájek estimators based on the estimated propensity score across 500 simulations with  $T = 500$  under several scenarios. Figure A.12 presents the ratio of these estimated variances. We find that the Hájek estimator is consistently more efficient than the IPW estimator in all scenarios considered here.

# K Additional results for the empirical application

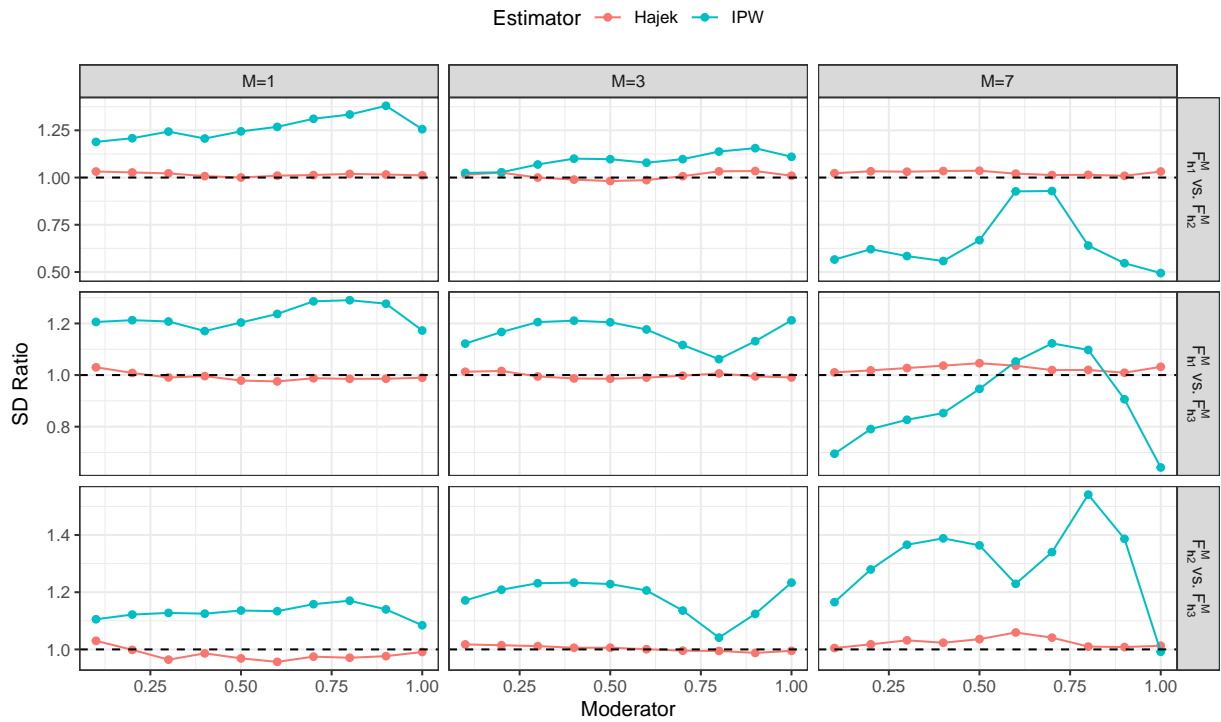
In this section, we present the results of an additional empirical analysis. We first evaluate the quality of the propensity score model using out-of-sample prediction. We then conduct two additional analyses: one with different moderator definitions and the other with different ways of truncating the estimated propensity score. Finally, we use an additional model specification with the binary aid moderator.

## K.1 Out-of-sample prediction for propensity scores

To evaluate the appropriateness of the propensity score model, we compare the predicted number of airstrikes with the observed number of airstrikes in the following four governorates in Iraq: Baghdad, Diyala, Salah al-Din, and Anbar. We assess both out-of-sample

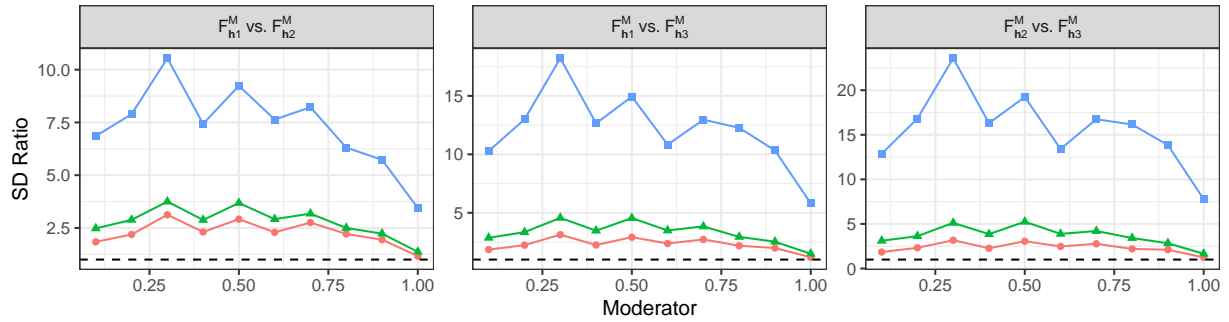


(a) Spatial moderator

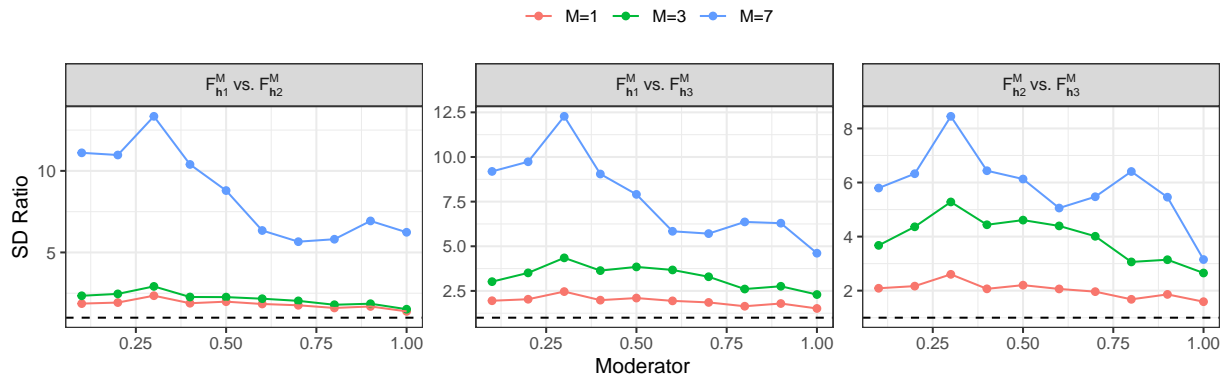


(b) Spatio-temporal moderator

Figure A.11: Standard deviation ratio of the proposed estimator based on the true propensity score over the proposed estimator based on the estimated propensity score. The results are based on Monte Carlo approximation with  $T = 1000$  and 500 simulations. The estimated propensity score is obtained from the correctly specified model. We compare interventions that are over different time periods:  $M = 1, 3, 7$ . In one time period, the expected number of outcome events yielded by  $F_{h_1}^M$ ,  $F_{h_2}^M$  and  $F_{h_3}^M$  are 3, 5, 7 respectively.



(a) Spatial moderator



(b) Spatio-temporal moderator

Figure A.12: Standard deviation ratio of the Hájek estimator based on the true propensity score over the IPW estimator based on the true propensity score. The results are based on Monte Carlo approximation with  $T = 500$  and 500 simulations. We compare interventions that are over different time periods:  $M = 1, 3, 7$ . In one time period, the expected number of outcome events yielded by  $F_{h_1}^M$ ,  $F_{h_2}^M$  and  $F_{h_3}^M$  are 3, 5, 7 respectively.

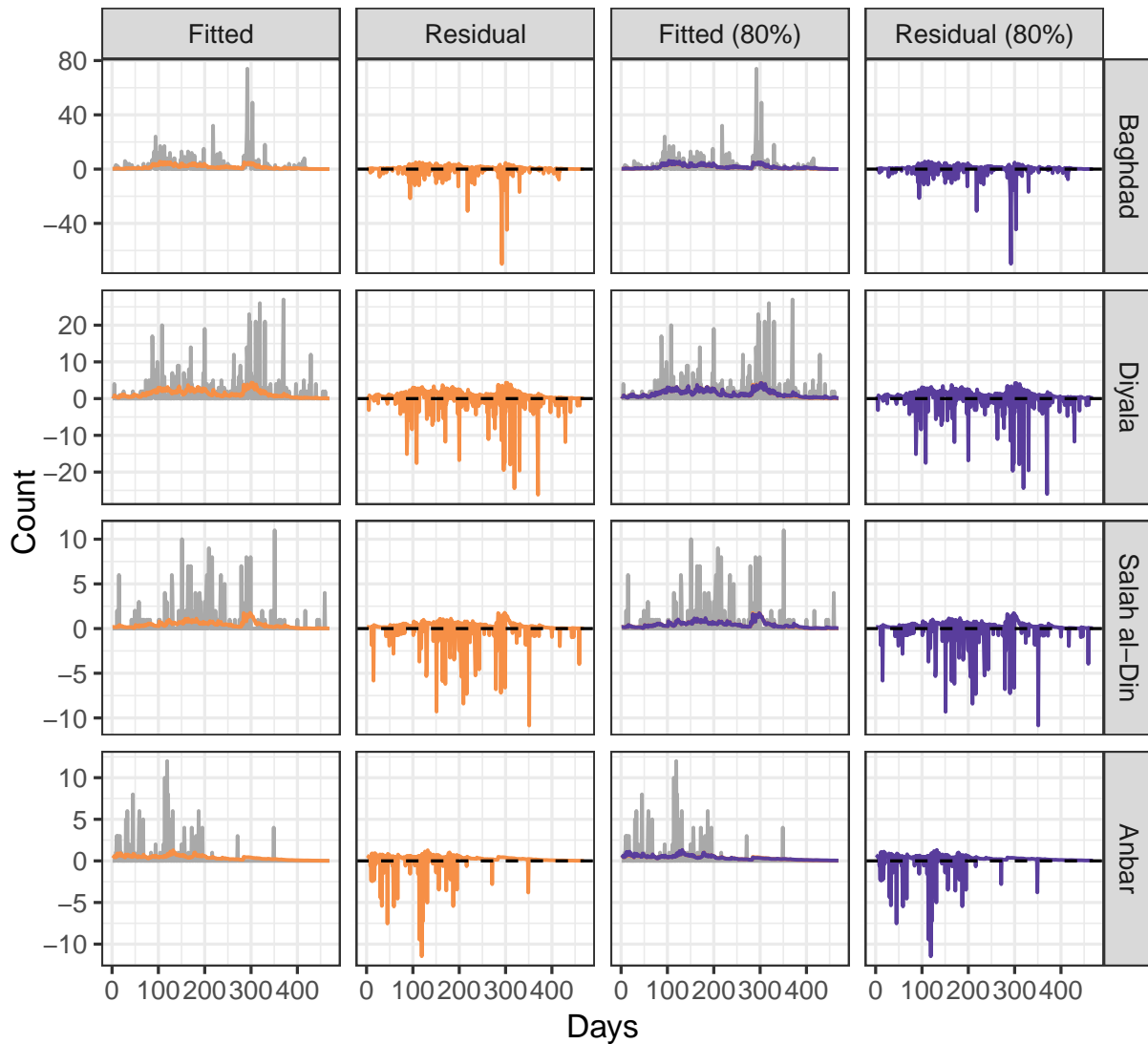


Figure A.13: Actual and predicted counts of airstrikes for four governorate in Iraq (rows). In the first column, the orange and gray lines indicate the fitted and actual counts, respectively. The second column shows the residual plot. In the third and fourth columns, the blue line indicates the results of out-of-sample prediction employing the first 80% of observations.

predictions, where the model is trained on the first 80% of the observations, and in-sample predictions, where the model is trained using the entire dataset.

Figure A.13 presents the results. The estimated propensity score model captures the general trend of airstrikes in these governorates, although it misses some spikes. The discrepancies are likely due to the large variance in the outcome that is inherent in any point process. Furthermore, the model trained on the first 80% of the data performs similarly to the estimated model using all observations, suggesting that the propensity score model is not overfit.

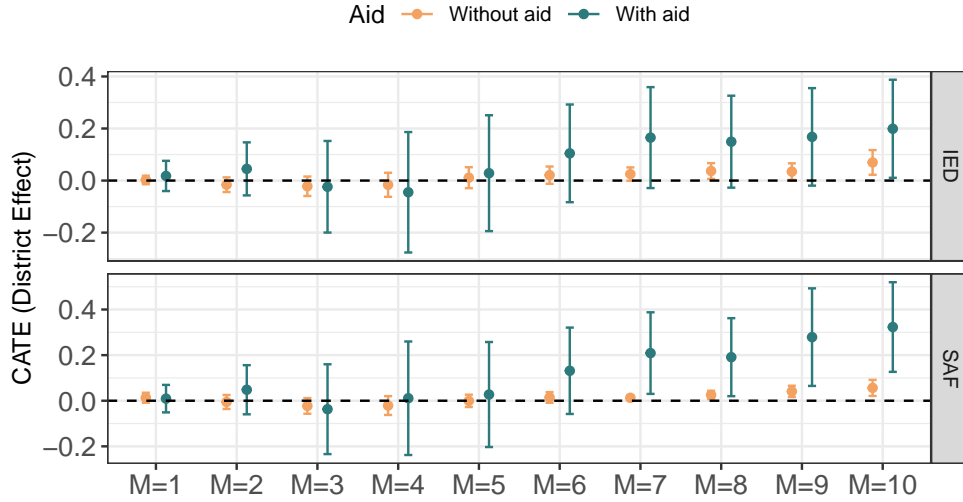
## K.2 Different moderator definitions

We conduct an analysis similar to the one presented in Section 4 but define the aid moderator using different lag lengths. Specifically, for the binary moderator, we consider the indicators of aid provision during the previous two weeks and two months. For the continuous moderator, we use the aid per capita received in the previous two weeks and two months. The results for the binary aid moderator are presented in Figures A.14 and A.15, while Figures A.16 and A.17 show the corresponding results for the continuous aid moderator.

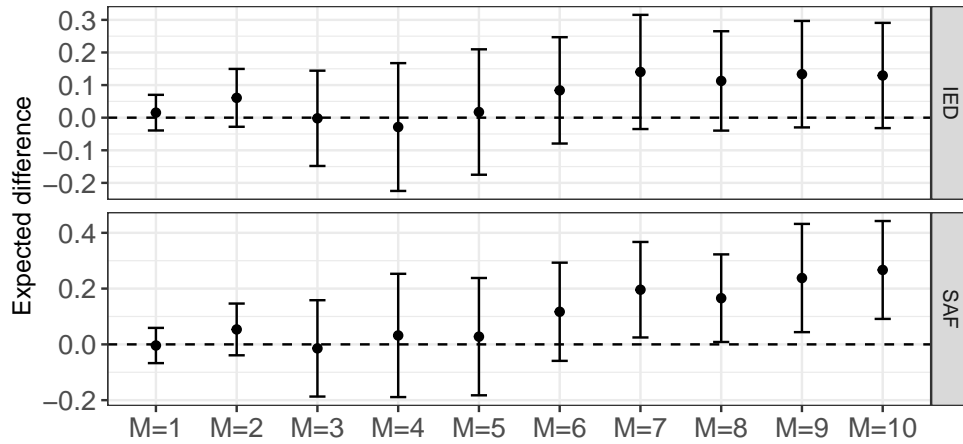
For the binary moderator, the results are largely consistent across the two lag lengths. As seen in Figures A.14 and A.15, the estimated CATEs remain stable across all intervention lengths  $M = 1, \dots, 10$ , with confidence intervals overlapping between the two-week and two-month definitions of aid. For SAF, the CATEs become statistically significant when the intervention lasts at least seven days, regardless of the lag length. Similarly, for IED, the results remain inconclusive, consistent with the findings in the main analysis. Although the overall patterns remain similar across the lag lengths, the magnitude of the estimated CATEs tends to be larger when the moderator is the provision of aid over the previous two weeks compared to the previous two months. For example, for IED attacks with  $M = 10$ , the estimated CATE is 0.20 for districts that received aid during the previous two weeks, compared to 0.15 for those who received aid during the previous two months. This difference reflects the more immediate effect of the recent aid provision.

For the continuous moderator, shown in Figures A.16 and A.17, the results show some sensitivity to the lag length, particularly for longer intervention periods. Across all durations of the intervention  $M$ , confidence intervals tend to be wider when using aid in the previous two weeks, particularly for SAF. This increased uncertainty is likely due to greater variability in the short-term aid measure, which may capture more noise relative to the more stable two-month lag. For shorter intervention lengths ( $M = 3$  and  $M = 7$ ), the differences in the estimated CATEs between the two lag lengths are minor, and overall trends remain consistent. Specifically, CATEs exhibit a flat pattern for small  $M$ , increase for moderate  $M$ , and decrease as  $M$  becomes large, regardless of the lag length.

In summary, while the choice of lag length affects the magnitude and precision of the estimated CATEs, the overall patterns observed in the main analysis are preserved. Aid provision during the previous two weeks tends to produce slightly larger estimated effects and wider confidence intervals compared to aid measured over the previous two months, particularly for longer intervention.



(a) Estimated CATE

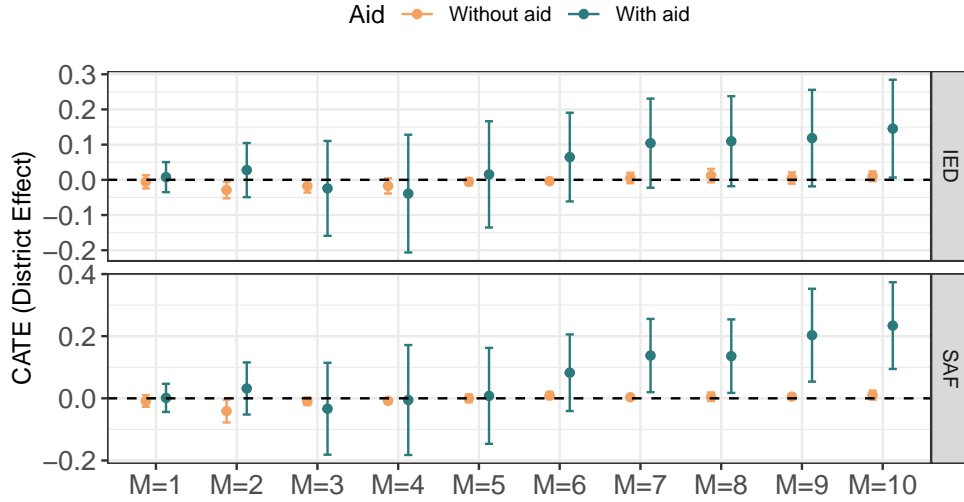


(b) Expected difference

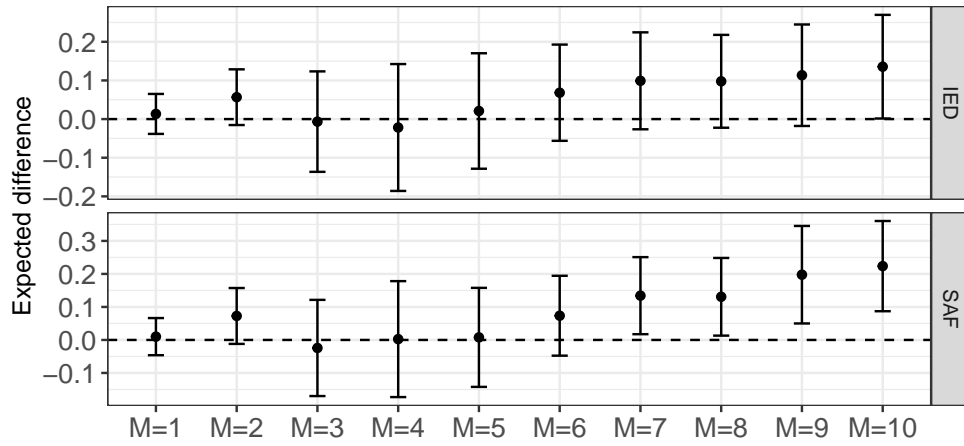
Figure A.14: Results for the binary aid moderator. Plot (a) shows the estimated CATEs of increasing airstrike intensity on the number of insurgency attacks (Improvised Explosive Device or IED in the top panel, and Small Arms Fire or SAF in the bottom panel) a district with or without aid in the previous *two weeks*. Plot (b) shows the estimated difference in the CATEs between a district that received aid in the previous *two weeks* and those that did not. The corresponding 95% confidence intervals are also shown for all estimators.

### K.3 Sensitivity to truncation levels of the estimated propensity scores

To evaluate the sensitivity of our results to the level of truncation of the estimated propensity scores, we compare the results using truncation at the 90% and 98% quantiles. Figures A.18 and A.19 show the results for the binary aid moderator, while Figures A.20 and A.21 present the corresponding results for the continuous aid moderator.



(a) Estimated CATE



(b) Expected difference

Figure A.15: Results for the binary aid moderator. Plot (a) shows the estimated CATEs of increasing airstrike intensity on the number of insurgency attacks (Improvised Explosive Device or IED in the top panel, and Small Arms Fire or SAF in the bottom panel) a district with or without aid in the previous *two months*. Plot (b) shows the estimated difference in the CATEs between a district that received aid in the previous *two months* and those that did not. The corresponding 95% confidence intervals are also shown for all estimators.

For the binary aid moderator, truncating the propensity scores at higher quantiles, such as 98%, tends to produce larger estimates of the CATEs with wider confidence intervals compared to truncation at the 90% quantile. As shown in Figure A.18 and Figure A.19, general patterns remain consistent across truncation levels. For SAF, the estimated difference in CATEs between districts with and without aid becomes positive and statistically significant for intervention periods of at least 7 days. However, for IED, the estimation uncertainty is substantial, and the results remain inconclusive regardless of the truncation

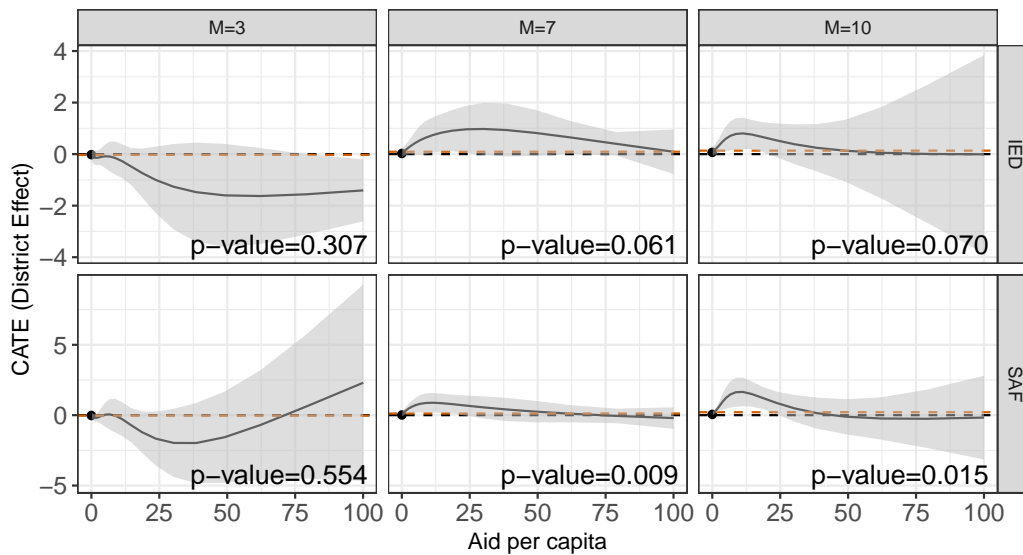


Figure A.16: Estimated CATEs of increasing airstrike intensity on the number of insurgency attacks (Improvised Explosive Device or IED in the top panel, and Small Arms Fire or SAF in the bottom panel) for different values of aid per capita received in the previous *two weeks* with the shaded region indicating the 95% confidence intervals. The red lines represent the estimated average treatment effects. The p-values correspond to tests for the overall heterogeneity effect.

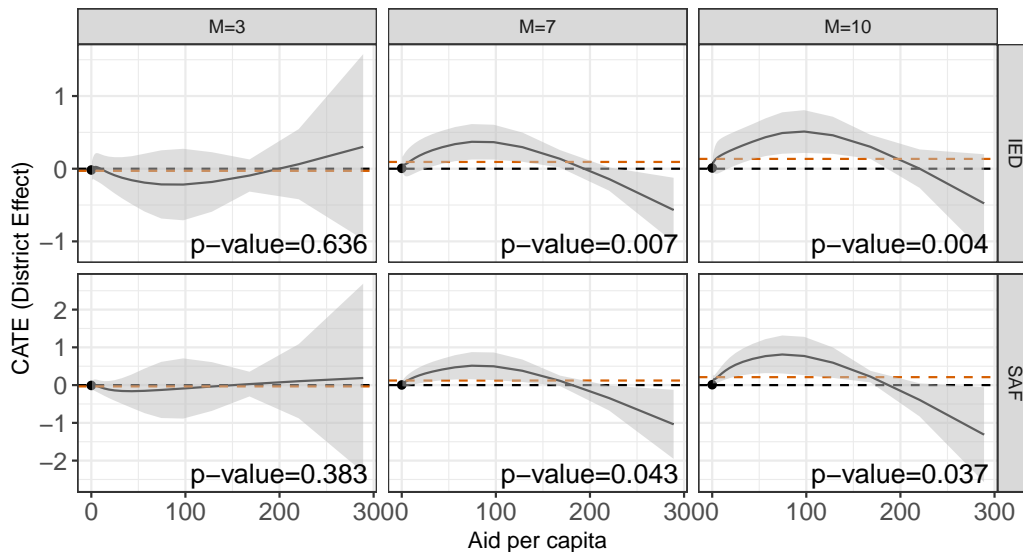


Figure A.17: Estimated CATEs of increasing airstrike intensity on the number of insurgency attacks (Improvised Explosive Device or IED in the top panel, and Small Arms Fire or SAF in the bottom panel) for different values of aid per capita received in the previous *two months* with the shaded region indicating the 95% confidence intervals. The red lines represent the estimated average treatment effects. The p-values correspond to tests for the overall heterogeneity effect.

level.

For the continuous aid moderator, results are shown in Figure A.20 and Figure A.21. Here, we observe greater sensitivity to the choice of truncation level. Higher truncation levels, such as the 98% quantile, lead to larger estimated CATEs and wider confidence intervals, reflecting the increased variability of the estimates. For instance, in Figure A.16, the estimated CATE for SAF at  $M = 10$  decreases substantially when moving from the 90% to the 98% truncation level. Although the magnitude of the estimates changes, the overall patterns are preserved at all truncation levels, with CATE estimates exhibiting little change for small values of  $M$ , increasing for moderate values, and decreasing as  $M$  becomes large.

The p-values corresponding to tests of no heterogeneity effect are also reported in the figures. For the continuous aid moderator, the p-values tend to decrease as  $M$  increases, suggesting stronger evidence of heterogeneity for longer intervention periods. However, there are cases where the significance depends on the truncation level. For example, in Figure A.20, the p-values for SAF at  $M = 10$  are significant when truncated at the level 90%, while the same results are not significant under the 98% truncation level (Figure A.21).

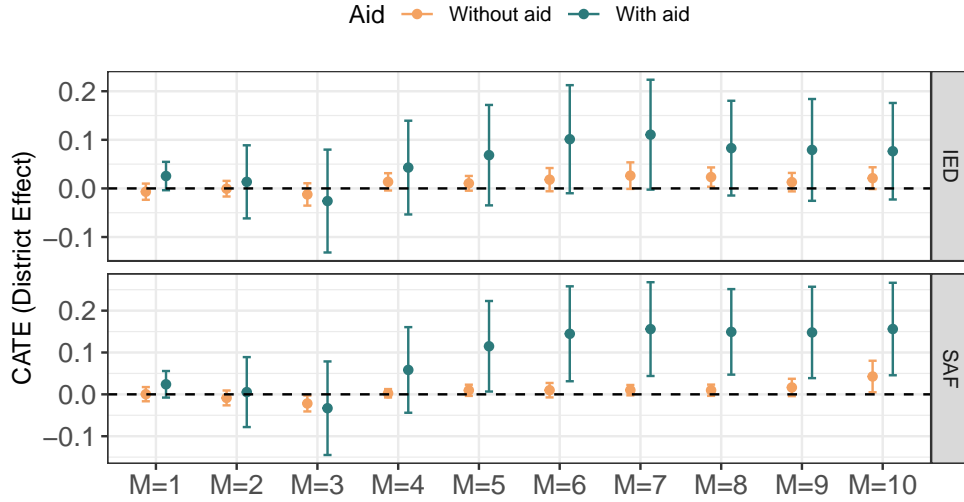
Overall, while the choice of truncation level affects the magnitude of the estimated effects, it does not alter the general trends observed in the main analysis. For the binary aid moderator, the estimated CATEs for SAF remain positive and significant for intervention periods of at least seven days, while the results for IED remain inconclusive. For the continuous aid moderator, the results are more sensitive to truncation, but the observed patterns are robust, with evidence of heterogeneity increasing as the intervention period grows longer.

## K.4 Additional analysis for the binary moderator

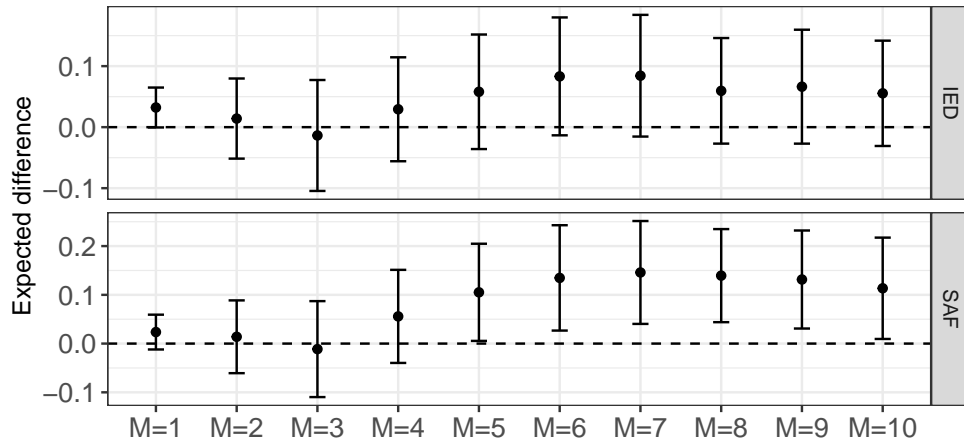
As discussed in Section 4, the baseline distribution of airstrikes is not uniform across space, which means that increasing airstrike intensity relative to baseline causes some regions to experience a greater increase in airstrikes than others. To account for this variation, we study how the treatment effect varies with the binary moderator, defined as the indicator of receiving aid during the previous month, while controlling for expected changes in the number of airstrikes.

Specifically, we include the expected change in airstrike numbers and its interaction with the aid indicator in the regression model. The model is given by:

$$\tau_{t,h_1,h_2}^{\text{Proj.}}(r; \boldsymbol{\beta}_t) = \beta_{t,0} + \beta_{t,1}r + \beta_{t,2}q + \beta_{t,3}r \times q,$$



(a) Estimated CATE

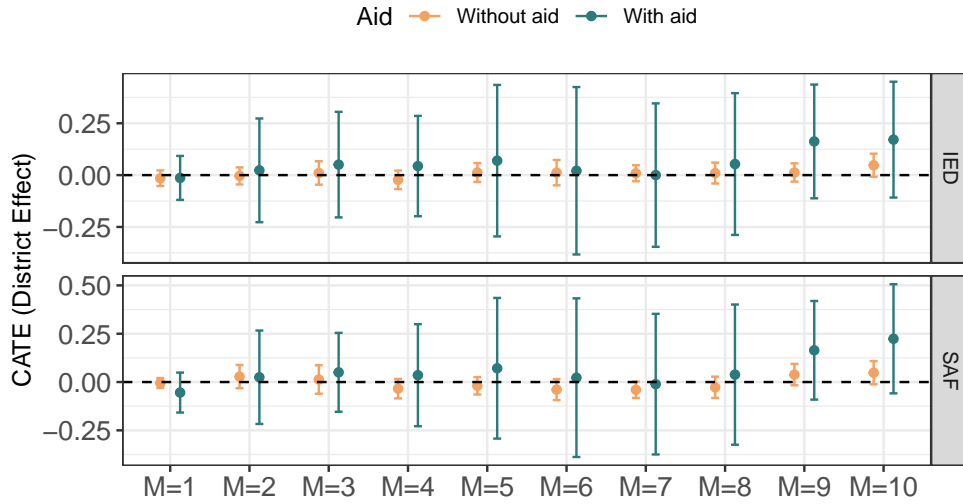


(b) Expected difference

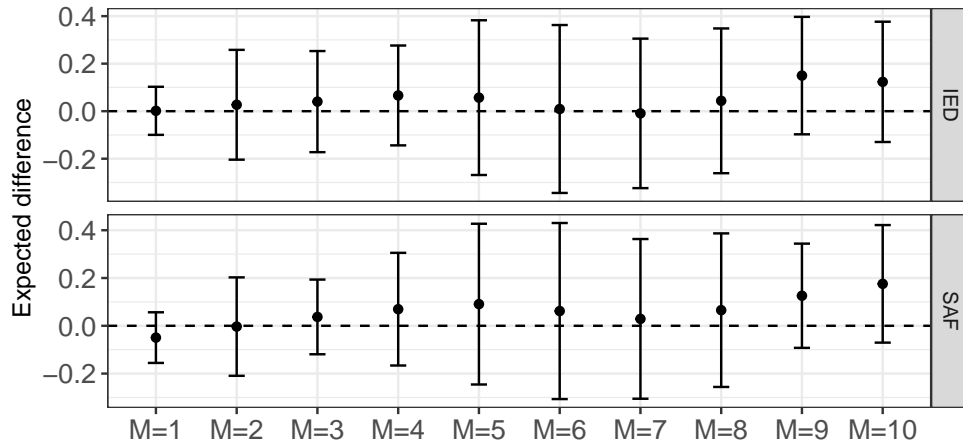
Figure A.18: Results for the binary aid moderator based on propensity scores truncated at the 90<sup>th</sup> percentile. Plot (a) shows the estimated CATEs of increasing airstrike intensity on the number of insurgency attacks (Improvised Explosive Device or IED in the top panel, and Small Arms Fire or SAF in the bottom panel) a district with or without aid in the previous one months. Plot (b) shows the estimated difference in the CATEs between a district that received aid in the previous one months and those that did not. The corresponding 95% confidence intervals are also shown for all estimators.

where  $r$  is the binary aid moderator, and  $q$  is the expected change in the number of airstrikes in a district. After estimating the coefficients, we plug in the median value of  $q$  to represent the expected airstrike intensity and compare the CATEs for areas with and without aid.

Figure A.22 presents the results for both IED and SAF attacks. Plot (a) shows the estimated CATEs for intervention windows ranging from  $M = 1$  to  $M = 10$ , while Plot (b) displays the estimated difference in the CATEs between districts with and without aid.



(a) Estimated CATE



(b) Expected difference

Figure A.19: Results for the binary aid moderator based on propensity scores truncated at the 98<sup>th</sup> percentile. Plot (a) shows the estimated CATEs of increasing airstrike intensity on the number of insurgency attacks (Improvised Explosive Device or IED in the top panel, and Small Arms Fire or SAF in the bottom panel) a district with or without aid in the previous one months. Plot (b) shows the estimated difference in the CATEs between a district that received aid in the previous one months and those that did not. The corresponding 95% confidence intervals are also shown for all estimators.

The findings generally align with the results in Section 4, where the expected intensity of airstrikes was not included in the model. For SAF attacks, districts that received aid in the previous month continue to show a stronger reaction to airstrikes, particularly when the intervention spans at least seven days. Importantly, for IED attacks, the estimated differences in CATEs now become statistically significant, suggesting a stronger effect in regions with prior aid.

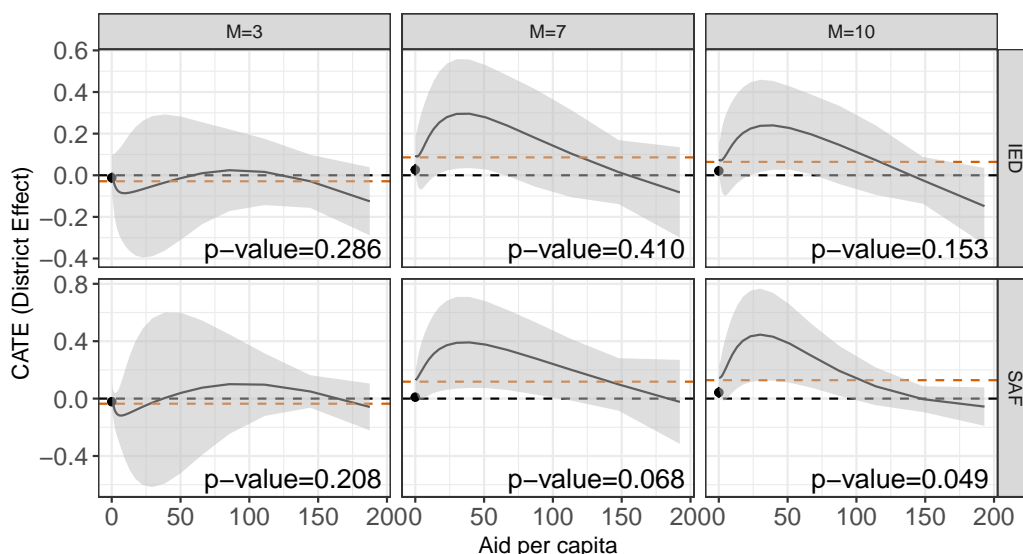


Figure A.20: Estimated CATEs of increasing airstrike intensity on the number of insurgency attacks (Improvised Explosive Device or IED in the top panel, and Small Arms Fire or SAF in the bottom panel) for different values of aid per capita received in the previous two weeks with the shaded region indicating the 95% confidence intervals. The results are using propensity scores truncated at the 90<sup>th</sup> percentile.

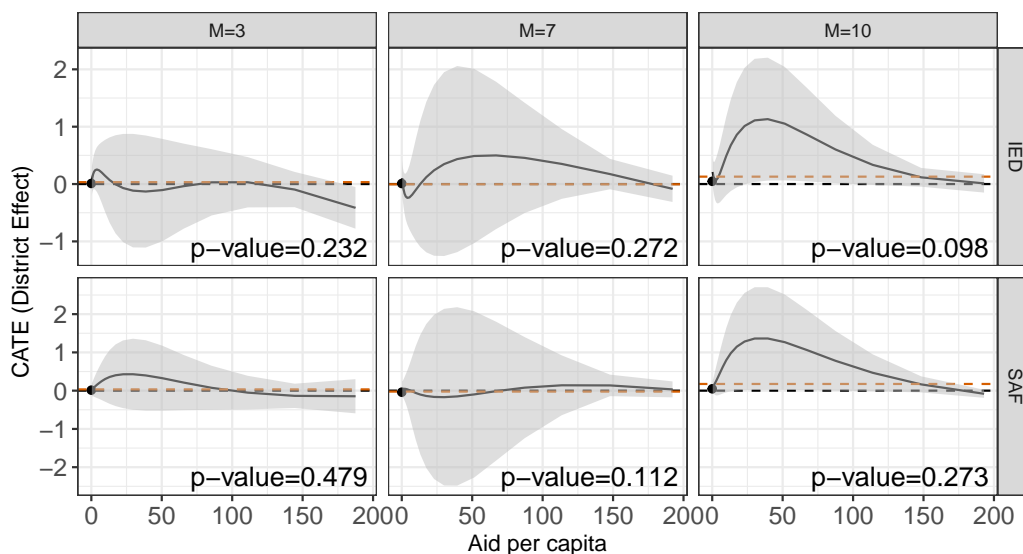
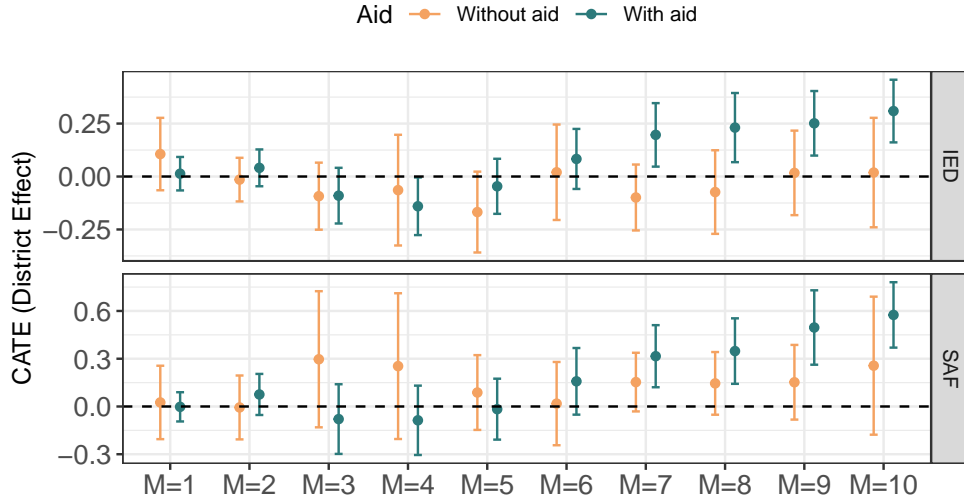
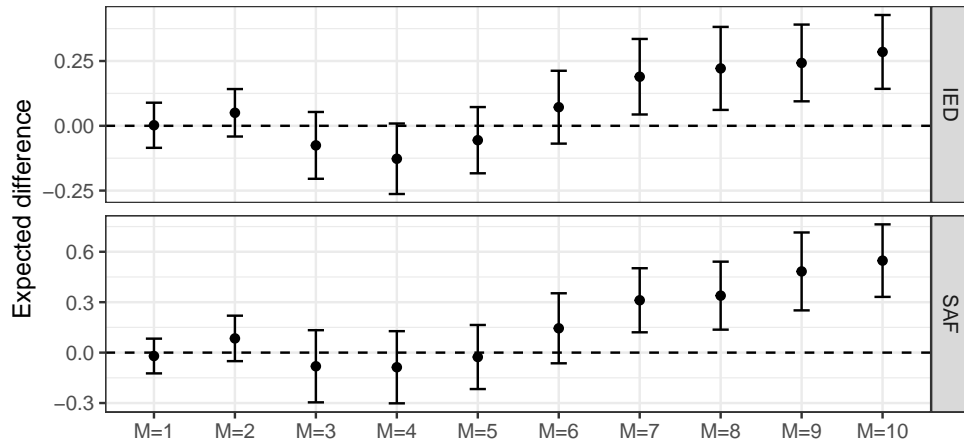


Figure A.21: Estimated CATEs of increasing airstrike intensity on the number of insurgency attacks (Improvised Explosive Device or IED in the top panel, and Small Arms Fire or SAF in the bottom panel) for different values of aid per capita received in the previous two months with the shaded region indicating the 95% confidence intervals. The red lines represent the estimated average treatment effects. The results are using propensity scores truncated at the 98<sup>th</sup> percentile. The p-values correspond to tests for the overall heterogeneity effect.



(a) Estimated CATE



(b) Expected difference

Figure A.22: Results for the binary aid moderator for regions with *median level* of increased airstrike intensity. Plot (a) shows the estimated CATEs of increasing airstrike intensity on the number of insurgency attacks (Improvised Explosive Device or IED in the top panel, and Small Arms Fire or SAF in the bottom panel) a district with or without aid in the previous one months controlling the expected changes in the airstrike intensity. Plot (b) shows the estimated difference in the CATEs between a district that received aid in the previous one months and those that did not. The corresponding 95% confidence intervals are also shown for all estimators.

Overall, controlling for expected airstrike intensity does not alter the main conclusion that regions receiving aid in the previous month exhibit a stronger response to increased airstrike intensity. These results indicate that the observed heterogeneity in treatment effects is not driven by differences in the intensity of airstrikes across regions with and without aid.

## K.5 Additional analysis for adaptive interventions

This section extends the main application from static interventions, where the counterfactual treatment distribution remains fixed across  $M$  consecutive days and across time, to adaptive interventions, in which the counterfactual treatment distribution may depend on the observed history.

In all other respects, the analysis follows the same structure as in Section 4. The treatment variable (airstrikes), the outcome variables (SAF and IED), the spatial resolution, the moderators (whether a district received any aid and the amount of aid per capita in the previous month) and the propensity score model remain unchanged. The main difference lies in the construction of the baseline distribution of airstrikes and the definition of the counterfactual interventions. To obtain the baseline intensity, we fit a non-homogeneous Poisson point process using historical data from 2006. The specification of this model is similar to the propensity score model described in Section 4.2, except that the covariate vector  $\mathbf{X}_t$  excludes time splines, the surge indicator, and prior airstrikes. The exclusion of prior airstrikes is intentional. If the current airstrike intensity were modeled as explicitly dependent on past airstrikes, then under an adaptive intervention spanning multiple periods, such dependence could artificially amplify or attenuate changes in the expected airstrike intensity at later time points, making the interpretation of the estimated effects more complicated.

We define two counterfactual treatment distributions by halving and doubling the baseline intensity, denoted  $h'_t(\omega) = 0.5 \lambda_t^{\text{Base}}(\omega)$  and  $h''_t(\omega) = 2 \lambda_t^{\text{Base}}(\omega)$ , where  $\lambda_t^{\text{Base}}(\omega)$  is the estimated baseline intensity. The corresponding counterfactual interventions over  $M$  time periods are defined as  $F_{h'_t} = (F_{h'_t}, F_{h'_{t-1}}, \dots, F_{h'_{t-M+1}})$  and  $F_{h''_t} = (F_{h''_t}, F_{h''_{t-1}}, \dots, F_{h''_{t-M+1}})$ .

For an adaptive intervention lasting one period ( $M = 1$ ), the observed history remains unchanged, and the contrast between  $F_{h'_t}$  and  $F_{h''_t}$  represents how the expected outcomes would differ if the expected number of airstrikes were shifted from one-half to twice the estimated baseline intensity. When the adaptive intervention extends over multiple periods ( $M > 1$ ), the intensity is halved or doubled at each period conditional on the observed history up to that time. For later periods, however, the observed history itself is modified because the distribution of airstrikes in earlier periods differs under the two intervention rules. Consequently, when  $M > 1$ , the comparison should be interpreted as contrasting two adaptive assignment strategies that update sequentially according to past realizations, rather than comparing two fixed sequences of airstrike intensities based on the estimated baseline intensity.

We first examine the binary moderator indicating whether a district received any U.S.

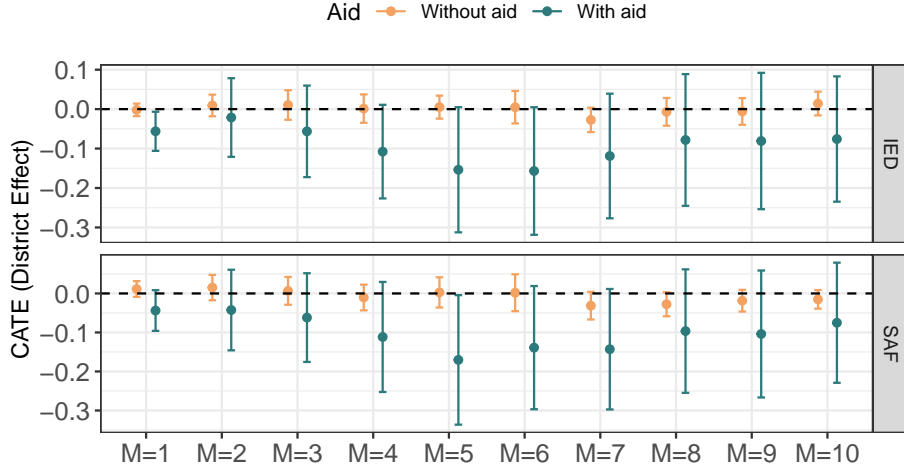


Figure A.23: Estimated district-level CATEs of changing the adaptive intervention rule from halving to doubling the baseline airstrike intensity, by intervention length ( $M = 1, \dots, 10$ ). The top and bottom panels show IED and SAF outcomes, respectively. Error bars represent 95% confidence intervals.

aid spending in the previous month. For each  $M$  ranging from one to ten, we estimate district-level conditional average treatment effects (CATEs) for districts with and without aid, using the same model specification as in the main text. The estimated CATEs with 95% confidence intervals are presented in Figure A.23, and the corresponding differences are shown in Figure A.24.

For SAF, districts that received aid consistently experienced fewer attacks than those without aid. The estimated reduction is largest when the airstrike strategy shifts from  $F_{h'_t}$  to  $F_{h''_t}$  over a five-day period and gradually diminishes as the duration of the intervention increases. The decrease in SAF attacks is statistically significant when the adaptive intervention is maintained for approximately five to six days. For other values of  $M$ , the estimation uncertainty is substantial, making it difficult to draw firm conclusions about whether districts with and without aid respond differently to the change in airstrike strategy from  $F_{h'_t}$  to  $F_{h''_t}$ . The results for IED display similar patterns to those observed for SAF.

We next examine heterogeneity in the adaptive intervention effects as a function of aid per capita in the previous month. The working model is identical to the one in Section 4.3, using four natural cubic spline basis functions for strictly positive aid and an indicator for zero aid. Figure A.25 presents the estimated CATEs for varying levels of prior aid  $r$ , along with the average treatment effect when the treatment strategy shifts from  $F_{h'_t}$  to  $F_{h''_t}$ . The p-values shown in the figure correspond to tests for the overall heterogeneity effect described in Section 2.6.

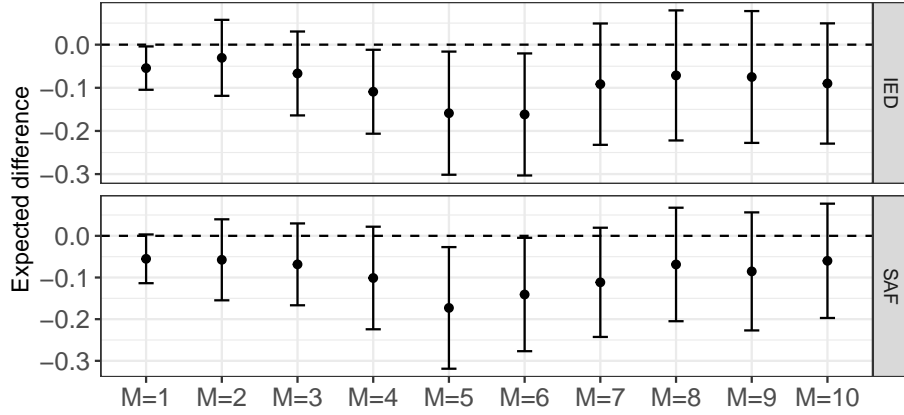


Figure A.24: Estimated difference in district-level CATEs between districts with and without aid in the previous month ( $r = 1$  minus  $r = 0$ ) for adaptive interventions of different durations ( $M = 1, \dots, 10$ ). Error bars represent 95% confidence intervals.

The patterns for SAF and IED are broadly similar. For IED attacks, the estimated effects display consistent behavior across intervention horizons  $M = 3, 7, 10$ , with the evidence for heterogeneity becoming stronger as  $M$  increases. The estimated CATEs show an initial decrease as prior aid rises from \$0 to approximately \$25 per capita, followed by an increase between \$25 and \$125, after which the effect gradually declines as aid becomes larger. These results indicate that districts respond differently to the change in airstrike strategy from  $F_{h'_t}$  to  $F_{h''_t}$  depending on the amount of aid previously received, and that such heterogeneity becomes more pronounced when the adaptive intervention spans multiple time periods.

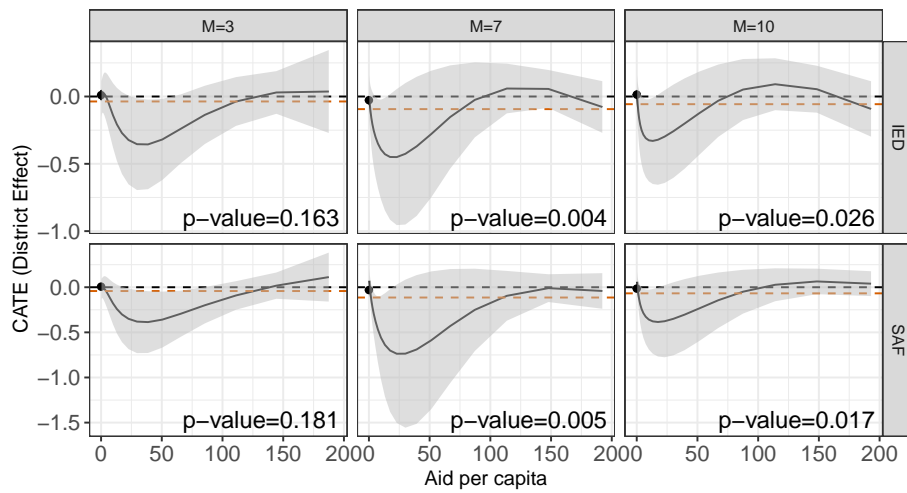


Figure A.25: Estimated district-level CATEs of changing the adaptive intervention rule from halving to doubling the baseline airstrike intensity, as a function of aid per capita in the previous month. The top and bottom panels correspond to IED and SAF outcomes, respectively. Shaded regions represent 95% confidence intervals. The red lines represent the estimated average treatment effects. The p-values correspond to tests for the overall heterogeneity effect.